USE OF DYNAMIC PHASE ANGLE AND COMPLEX MODULUS FOR THE LOW TEMPERATURE PERFORMANCE GRADING OF ASPHALT CEMENTS

by

Abdolrasoul Soleimani

A thesis submitted to the Department of Chemistry

In conformity with the requirements for

the degree of Master of Science in Engineering

Queen's University

Kingston, Ontario, Canada

(August, 2009)

Abstract

This thesis discusses and documents the validation efforts related to Ontario's LS-299 and LS-308 test methods which are two new test methods developed for the performance-based specification grading of asphalt cement. In addition, this report presents the field validation of a simple performance indicator, loss tangent, for specification grading of asphalt cement for thermal cracking. Furthermore, another objective of this study is to investigate and compare the low temperature fracture and rheological behavior of engineered asphalt materials from field and laboratory-aged test sections on Highway 655 in northern Ontario.

Extracted asphalt cements from 20 contract sites in eastern and northeastern Ontario were tested according to Ontario's LS-299 and LS-308 test methods. It was found that all good performing contracts that showed little or no distress showed low grade losses in LS-308 and retained high strain tolerances as measured in LS-299 compared to the poor performing contracts.

Asphalt cements recovered from these 20 contract sites in eastern and northeastern Ontario were also tested in torsion bar geometry to determine their viscoelastic properties. It was decided to focus on the phase angle, as a more direct measure for low temperature performance. Phase angle is a very sensitive parameter to small changes in rheology as the phase angle is approximately equal to the derivative of the logarithm of the stiffness with respect to frequency.

It was found that tan(δ) was able to distinguish good from poor performers with 95% accuracy after only a short period of conditioning prior to testing. This is a considerable improvement over the current low temperature bending beam rheometer protocol.

Black space diagrams, frequency sweeps, Cole-Cole plots, and master curves were generated for comparison of field and laboratory aged materials from the Highway 655 trial in northern Ontario. The findings show that chemical hardening occurs much faster in the field than through laboratory ageing methods. Also, reversible ageing of binders may occur at low

temperatures and could be linked to field performance. Furthermore, a high low temperature phase angle appears to be a reasonable indicator for thermal cracking resistance.

Acknowledgements

I am grateful to my supervisor, Dr. Simon Hesp, for providing me with the opportunity to work on this project. His guidance and encouragement has been a great help in finishing this research project. A portion of this thesis has been written up by Professor Hesp in the form of two scientific publications.[1,2]

I also wish to thank undergraduate students Shanan Walsh, Lisa Whitelaw, Irsan Kodrat, David Scafe, and Kevin Houlihan for their assistance with collecting part of the data in this thesis. Furthermore, Sathish Subramani was always there for help and suggestions in my work. Staff of the Ministry of Transportation of Ontario Eastern Region Office is specifically thanked for providing the materials and distress surveys for the various trial sections and regular contracts.

Finally, financial support for this research was kindly provided by the National Sciences and Engineering Research Council of Canada (NSERC), the Highway Infrastructure Innovations Funding Program of the Ministry of Transportation of Ontario (HIIFP MTO), and the Charitable Foundation of Imperial Oil of Canada.

Table of Contents

Appendices

List of Figures

List of Tables

Abbreviations, Acronyms and Symbols

AADT	Average Annual Daily Traffic Count
AASHTO	American Association of State and Highway Transportation Officials
AC	Asphalt Cement
ASTM	American Society for Testing and Materials
BBR	Bending Beam Rheometer
CTOD	Crack Tip Opening Displacement, m
DENT	Double-Edge-Notched Tension
DSR	Dynamic Shear Rheometer
HMA	Hot Mix Asphalt
LS	Laboratory Standard Test Method
LTPPBind®	Long Term Pavement Performance Binder Selection Software
m(t)	Slope of the Creep Stiffness Master Curve (m-value)
MTO	Ministry of Transportation of Ontario
PG (PGAC)	Performance Grade (Performance Graded Asphalt Cement)
SBS	Styrene-Butadiene-Styrene Block Copolymer
SHRP	Strategic Highway Research Program
S(t)	Creep Stiffness, Pa

Chapter 1
Introduction

1.1 Introduction

Road and highway systems play a crucial role in the modern economy. The United States' 4 million mile highway system carried 65 percent of that nation's $15 trillion in shipment traffic and 88% percent of family trade occurred by private car in 2001.[3] In Canada the numbers are similar. One thing to keep in mind is that the highway system is a network between other sources of transportations.

Road maintenance and construction is a large industry, particularly in cold climates such as the northern US and Canada where road life is seriously reduced due to exposure to temperature extremes. In the United States, $45 billion was spent on asphalt in 2006. In Canada, expenditures reached $11 billion, with a very small percentage allotted to expansion of the transportation system. In Ontario, $300 million is spent annually for construction, repair and resurfacing.[4] Because of the wide variation in geographical and climatic conditions a careful selection of asphalt materials is required to increase the useful life of the pavement and reduce the huge cost of road maintenance.

The following failure modes have been identified for asphalt pavement: rutting, fatigue, moisture damage, and thermal cracking. Rutting is the term used for the permanent deformation of a pavement surface which happens at high temperatures during summer when the asphalt is softer. Fatigue cracking is caused by many load repetitions (heavy trucks) over time that cause the pavement to deflect until cracked. The environment and climatic condition along with the pavement structure, mixture composition and construction play important roles for the failure of the pavement in this mode. Thermal cracking in asphalt pavement is a serious problem in a cold climate such as that of the northern U.S. and Canada. Thermal cracking is attributed to tensile

stress, which results from temperatures falling to extreme lows. When the temperature goes down, tensile stresses develop as the pavement tries to contract. When the tensile stress induced in the pavement equals the strength of the asphalt concrete mixture at low temperatures, a micro-crack grows at the edge and surface of the pavement. At colder temperatures, or after repeated temperature cycles, the crack penetrates the full depth and width of the asphalt concrete layer. Figure 1 represents the comparison of different forms of failure modes.

Figure 1a. Fatigue crack caused by repeated traffic loading

Figure 1 b. Longitudinal and transverse cracks caused by thermal effects

Figure 1c. Ruts on the wheel path

Figure 1d. Alligator-type fatigue cracks caused by load (traffic) distress

Figure 1. Comparison of different forms of failure modes.[5]

Many researchers have sought to identify methods which can predict cracking prior to construction of the pavement. This thesis deals with a new specification test for asphalt binders and aims to bring a new perspective to select appropriate asphalt binders for a given temperature.

1.2 Scope

Many researches have attempted to develop a specification test to reduce low temperature cracking problems in asphalt concrete pavement by selecting the correct material for a given set of climatic conditions. The first objective of this study is to develop a fast test to evaluate resistance of asphalts to low temperature cracking. A simple test is proposed based on rheological properties of asphalt binders that measure their ability to relax stress at low temperatures. As such, it can serve as a better indicator in asphalt selection than the more empirical test used at present. The second objective of this study is to correlate the rheological properties of asphalt binders to their observed field performance. It was decided to focus on the phase angle as a more direct measure for low temperature performance. Phase angle is a very sensitive parameter to small change in rheology as the phase angle is approximately equal to the derivative of the logarithm of the stiffness with respect to frequency according to the following equation[6]:

$$\delta(\omega,T) \approx \frac{\pi}{2}\left[\frac{d(\ln G^*(\omega,T)}{d\ln\omega}\right] \qquad (1\text{-}1)$$

Chapter 2
Literature Review

2.1 Asphalt Literature Review

2.1.1 Definition of Asphalt

The word "asphalt" comes from the Greek word ""asphaltos," meaning "secure". In the US asphalt industry, the word “asphalt” or “asphalt cement” is used for the residue material which is obtained during the distillation process of crude oils. However, outside North America this material is typically called bitumen.

Asphalt is defined by ASTM as a “dark brown to black cementitious materials in which the predominant constituents are bitumens that occur in petroleum processing”.[7] The Dictionary of Geological Terms (1962) defines asphalt as “brown to black solid and semi-solid bituminous substances”. However, there exists no standard definition for natural asphalt.

2.1.2 Application of Asphalt

In the ancient world, asphalt was used as an adhesive. Its viscosity decreases at warm temperatures while on cooling it quickly turns hard. Thus, it was used to glue together various utensils. In the Gilgal Site, located 20 km north of the Dead Sea and dated to the Pre-Ceramic Neolithic period (8500 BC), a stone axe head was found which was covered asphalt to glue it to a wooden handle.[8] Recently, with the advent of new natural and synthetic glues this use of asphalt has dramatically decreased.

Asphalt was used for making small decorated utensils such as bowls, for coating statues for making ornaments and so on.[9,10]

The Persian traveler, Nasir-i-Khusran, describes how asphalt was also used to coat the roots of fruit trees and thus protect them against "worms and things that creep below the surface" when he visited the area near Egypt in 1047 AD. It is possible that the aromatic compounds and sulfur content in the asphalt explain this beneficial effect.[11]

The use of asphalt as a waterproofing engineering material goes back to 3500 B.C. as it was used in the shipping industry by Sumerians. Ancient Phoenicians, Egyptians, and Romans used asphalt to waterproof temples and baths and water tanks. They also used asphalt as a binding material for bricks. It is interesting to know that asphalt was used as a medicine in the ancient Middle East[12] Galen, 2nd century A.D., the most famous doctor of medicine in the Roman and Medieval word, used the dead sea asphalt for medical purposes. Recently, Professor A. Docstrovsky from Hasassah Medical School in Jerusalem found a valuable material called "bitupal" which was very effective for curing certain skin diseases.[13] This material still is in use and has been produced by the Teva Pharmaceutical Company in Israel. [14]

Besides the above applications in the ancient world, asphalt has also been used for mummification,[14] photography,[15] waterproofing and in oil exploration.[14]

In the late 18th century, the first use of asphalt as a material for road building was reported in Newark, N.J.[16] During the 19th and 20th centuries, the use of asphalt as a road-building material increased exponentially together with the development of the automobile industry.

2.1.3 Sources of Asphalt

Natural Asphalt

The total amount of asphalt (including tar sands) has been estimated at 2.7×10^{12} barrels.[17] About 95 % of natural asphalt cement (referred to as tar sand) is in Canada. In fact, there is a huge deposit of Athabasca tar sands in northern Alberta. The major sources of natural asphalt are in Pit

Lake, Trinidad; Gard, Auvergne, Ain and Haute Savoie in France; Central Iraq; Latakia, Syria; Maestu, Spain; Butin Island, Indonesia; and the Dead Sea area in Israel and Jordan.[17]

Petroleum Asphalt

Petroleum asphalt is obtained from the refinery of petroleum. Most asphalt in the United States and Canada is produced through the refining of crude oil. Atmospheric and vacuum distillation is the basic unit of operation. However, blending, air blowing, solvent deasphalting, solvent extraction, emulsification and modification are available to produce various grades of asphalt depending on the crude sources. Table 1 represents the methods used to produce and process asphalt materials.

Table 1. Methods Used to Produce and Process Asphalt Materials.[18]

Production/Process	Base Material	Product
Atmospheric and Vacuum Distillation	Asphalt-based Crude or Crude Mix	Asphalt Cement
Blending	Hard and Soft Asphalt Asphalt Cements and Petroleum Distillates	Asphalt Cements of Intermediate Consistency Cutback Asphalts
Air-Blowing	Asphalt Flux	Asphalt Cements, Roofing Asphalt, Pipe Coating, Special Membranes
Solvent Deasphalting	Vacuum Residuum	Hard Asphalt
Solvent Extraction	Vacuum Residuum	Asphalt Components (Asphaltenes, Resin, Oils)
Emulsification	Asphalt, Emulsifying Agent, and Water	Emulsified Asphalts
Modification	Asphalt and Modifiers (Polymers, Chemicals, etc.)	Modified Asphalts

2.1.4 Asphalt Chemical Characterization

Asphalt is an extremely complex mixture of largely organic and organo-metallic compounds. It is composed saturated hydrocarbons with a small amount of heteroatoms and trace amounts of metals.

A standard sample of asphalt consist of about 82-88 % carbon, 8-11 % hydrogen, 0-6 % sulphur, 0-1.5 % oxygen and 0-1 % nitrogen. Asphalt also contains trace quantities of certain metal atoms (e.g. Fe, Ni, V), which act as a fingerprint for the point of origin of the asphalt.[19]

Asphalt can be separated into two chemical groups, called asphaltenes and maltenes by precipitation in n-heptane.[20-22] Asphaltenes are polar compounds with a fairly high molecular weight and hence they do not dissolve in a linear hydrocarbon such as n-heptane. Depending on the method used to determine their molecular weight, it ranges from 1,000 to as high as 100,000 g/mol. The size of a typical asphaltene molecule is typically between 5 and 30 nm and the ratio of hydrogen to carbon is close to 1:1. The amount of asphaltene present in asphalt cement has a strong effect on its rheological properties. They are responsible for the high viscosity. For example, asphalts with a high amount of asphaltenes are harder and have a higher viscosity whereas asphalts with less asphaltenes are softer and have a lower viscosity.

Maltenes can be divided into three further groups: saturates, aromatics and resins. Saturated compounds are largely composed of straight and branched-chain aliphatic hydrocarbons along with alkyl-naphthenes and some alkyl-aromatics. Saturates constitute approximately 5 to 20 % of the asphalt cement. Resins, which are dark brown in color and which are strongly adhesive to the aggregate in a pavement mixture, are composed of hydrogen and carbon together with small amounts of oxygen, sulphur and nitrogen. The main function for the resins is to disperse the asphaltenes in the oils (saturates and aromatics). Aromatics, which are dark brown viscous liquids, constitute approximately 30 to 50 % of the total amount of bitumen. Aromatics are

composed of unsaturated ring systems and they act as a solvent for the other higher molecular weight hydrocarbons (resins and asphaltenes).[23]

Figure 2. Aromatic structures.[23]

Figure 3. Saturated structures.[23]

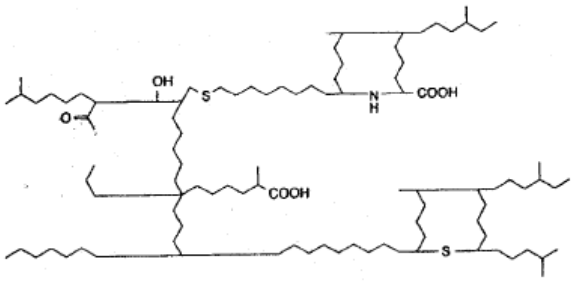

Figure 4. Asphaltene structure.[23]

2.1.5 Asphalt Physical Characterization

Asphalt is considered to be a viscoelastic material.[23] The binder is a viscous liquid at high temperatures that flows easily. At relatively low temperatures it behaves like an elastic solid. Therefore, asphalt is able to return to its original shape under the removal of certain amount of loads (elastic behaviour). However, some of the input energy may dissipate in the asphalt which leads to permanent deformation (viscous behaviour).

The molecular compounds in asphalt can further be divided into two general categories: polar and non-polar. Polar compounds in the asphalt are responsible for the elastic properties and an example of a polar compound would be an asphaltene. Non-polar compounds such as the maltene fractions contribute to the viscous behavior. As temperature or load increases, the long chains tend to align and flow and that will make the asphalt behave like a viscous liquid and not like an elastic solid. However, upon cooling or removal of the stress, these same molecules will move back to their original shape (elastic response), but not in the exact same conformation as before the disturbance (viscous response).

2.1.6 Traditional Asphalt Testing

The oldest asphalt cement grading test as invented by Brown of the Baber Asphalt Paving Company in 1888,[24] is the penetration test. The penetration test measures the depth of a sewing needle pushed into a sample of asphalt under a specific condition of loading time and temperature. Since 1959, the penetration test has been measured according to an ASTM standard. A 100 gram standard load is applied on top of a needle which is allowed to penetrate the asphalt binder for 5 seconds at 25ºC. The depth of penetration is measured in units of 0.1 mm and is reported in penetration units of 0.1 mm. Another test that was used for grading asphalt binders is the viscosity test. Viscosity tests measure the time required for the asphalt cement to flow through a calibrated glass tube. Viscosity values are obtained at 60ºC and 135ºC.

Unfortunately, both of these tests only measure the asphalt sample at a specific temperature and they do not give an accurate indication of how the materials would perform at a wide spectrum of temperatures which is what the asphalt pavement normally experiences in service. Furthermore, both of these tests are empirical tests, meaning that their results are correlated with pavement performance over the years.[25]

2.2 Superpave Specification Tests

In the United States, highway agencies appropriated significant funds during the late 1980's and early 1990's for a series of research programs to develop new methods for the specification grading of asphalt cements and mixtures. This was due to the failure of conventional grading tests that provided binder properties with little or no correlation to pavement performance. The Strategic Highway Research Program (SHRP) ran for a period of five years and spent close to $150 million for the development of a range of asphalt cement and mixture tests to better design pavements to last for the requisite amount of time. These new test methods have led to a new

specification known as Superpave® (Superior Performing Asphalt Pavements).[25,26] In these new specification methods, the binders are being tested under conditions which better simulate the critical conditions during the asphalt life in service. Test results under Superpave® are based on a measurement of the asphalt's fundamental physical properties that are supposed to be directly related to field performance through sound engineering principles. Unfortunately, recent experiences have shown that the Superpave® specification, while an improvement over historical penetration and viscosity methods, still leaves significant room for improvement. Asphalt cements graded the same can shows significant performance variations while the performance grade (PG grade) does not protect a pavement against typical distress.

2.2.1 Dynamic Shear Rheometer Testing

The dynamic shear rheometer (DSR) is used to evaluate rheological (flow) properties of asphalt binders from low to high temperatures. An understanding of the rheological properties of asphalt binders is essential for predicting the end-use performance of these materials. The DSR measures the complex shear modulus (stiffness) G* and phase angle δ over a wide range of temperatures and frequencies. This test will be discussed in detail in the next chapter however the complex modulus and phase angle are both used in the Superpave® specification for the grading of asphalt cements for fatigue and rutting.

2.2.2 Bending Beam Rheometer Testing

The bending beam rheometer (BBR) was also developed under the Strategic Highway Research Program. It measures two important parameters of asphalt cement. First, it measures the creep stiffness S(t) and second it measures the m-value of the asphalt cement as defined by the slope of the creep stiffness master curve. Both S(t) and m(t) are supposed to be related to low temperature thermal cracking performances of the asphalt pavement. The BBR also determines the limiting

temperature of the binders and gives an indication of how the asphalt binders should be able to resist low-temperature cracking.

The S(t) provides a measure of the creep stiffness for asphalt binders, and it is calculated using the following equation:

$$S(t) = \frac{PL^3}{4bh^3\delta(t)} \qquad (2\text{-}1)$$

$S(t)$ = asphalt binder stiffness at a specific time;

P = applied constant load (100 g or 0.98 N);

L = distance between beam supports (102 mm);

b = beam width (12.5 mm);

h = beam thickness (6.25 mm); and

$\delta(t)$ = deflection at a specific time.

In order to determine the master creep stiffness curve, the stiffness of the specimen is measured at loading times of 8, 15, 30, 60, 120 and 240 seconds. The slope of this master curve is known as the m-value, which is a measure of the binder's ability to relax stress due to viscous flow. Thus, the lower the m-value the less ability to relax stress. Accordingly, the minimum value for the m-value was set by the SHRP researchers at 0.3. [27]

2.2.3 Extended Bending Beam Rheometer Testing (MTO method LS-308)

Under the extended BBR protocol, specimens are stored for one hour, 24 hours, and 72 hours at -10ºC and -20ºC and tested for their limiting stiffness and m-value temperatures. Both pass and fail temperatures are selected in order to determine an exact grade according to AASHTO M320 criteria by interpolation. The grade is plotted on a semi-logarithmic scale, and the worst grade loss is recorded for each binder.[27]

2.2.4 Double Edge Notched Tension Testing (MTO method LS 299)

The double-edge-notched tension test (DENT) for asphalt cements was recently developed at Queen's University [28,29,30] and is now commonly used to determine the essential (w_e) and plastic works (w_p) of fracture in the ductile regime at 15ºC and at a rate of loading of 50 mm/min. This set of conditions provides a reasonably fast test and is targeted at measuring the resistance to ductile failure under low strain conditions at and around freeze-thaw temperatures where the pavement experiences a lot of movement due to water freezing and thawing in the foundation.

The essential work of fracture (W_e) is proportional to the ligament cross sectional area (i.e. ligament length (L) multiplied by thickness (B)), while the plastic work (W_p) is proportional to the volume of the plastic zone. The plastic zone simply refers to the fracture area (L x B) multiplied by ligament length and a β-factor which depends on the shape of the zone (circular, elliptical, diamond shapes, etc.). A mathematical expression for the total work of fracture, W_t , is given by equation (2-2):

$$W_t = W_e + W_p = LBw_e + \beta L^2 Bw_p \qquad (2\text{-}2)$$

where W_e is the total essential work of fracture (J), W_p is the total plastic work of fracture (J), L is the ligament length (m), B is the sample thickness (m), β is a geometry factor to account for the shape of the plastic zone around the fracture zone, w_e is the specific essential work of fracture (J/m^2), and w_p is the specific plastic work of fracture (J/m^3). The w_e and w_p terms, determined under plane stress or mixed mode (plane stress-plane strain) conditions, represent material properties for a given thickness of material.[31,32] Under plane strain conditions (thick specimens compared to the size of the fracture zone), the specific essential work w_e is a material property independent of the thickness of the material. Furthermore, total specific work of fracture can be written in following equation,

$$w_t = \frac{W_t}{LB} = w_e + \beta w_p L \qquad (2\text{-}3)$$

Where w_e is the specific essential work of fracture (J/m^2), and w_p is the specific plastic work of fracture (J/m^3).The plot of the total specific work of fracture (w_t) against the ligament length (l) results in a straight line, having an intercept equal to the essential work of fracture (w_e) and slope equal to the specific multiplied by the shape factor (βw_p).

It should be noted that specific essential work of fracture (w_e) can be estimated from the crack tip opening displacement (CTOD) using the following relationship:

$$w_e = M\sigma_y CTOD \qquad (2\text{-}4)$$

M = plastic constraint factor for DENT = 1.15;

CTOD = crack tip opening displacement (m); and

σ_y = net section stress or yield stress (N/m^2).

where CTOD is the approximate critical crack opening displacement (m), providing a measure of strain tolerance in the ductile state under near plane strain conditions (high confinement). Then, the fracture behavior of asphalt binders can be determined via crack tip opening displacement (CTOD).[33]

It was revealed that the crack tip opening displacement parameter could be used as a property that correctly ranks performance and provides a high correlation with cracking distress. The procedures followed are now outlined in a laboratory standard LS 299 *Method of Test for Asphalt Cement Grading for Fracture Performance Using Double-Edge-Notched Tension (DENT) Geometry*, in the Laboratory Testing Manual of the Ministry of Transportation of Ontario.[33]

2.3 Asphalt Modification

The modification of asphalt binders to enhance performances goes back as far as 1843. During the 1930s in Europe, polymer-modified asphalts were used to build test trials to investigate these new materials. This new European technology began to be used in the U.S. in the mid 1980's, but before this European technology, neoprene latex was used in North America as early as 1950.[35,36]

In a survey from the Department of Transportation in the United States, among eighteen states and twenty experts, seventy percent responded that there was a benefit in using polymer modified asphalt mixture in terms of performances during asphalt service life. Using polymer modified asphalt mixture also increases the resistance of asphalt to thermal cracking and durability of the asphalt. The survey also indicated that an increase in the rutting resistance of asphalt pavement is one of the primary reasons of why companies choose to use polymer modified asphalt.[18]

2.3.1 Types of Modifiers and Additives

A wide variety of materials is used to modify asphalt binders. These are produced in a number of ways but in fact, polymer modification is the most prevalent. One group of polymeric materials used as asphalt modifiers are plastomers. These materials, when they are stretched, will largely remain in the stretched position if the load is released. Examples of these polymers are: polyethylene (often the low density polyethylene, which is identified as LDPE), ethylene-vinyl-acetate (EVA), and ethylene-acrylate (EA). The above polymers are used to decrease permanent deformation or rutting in asphalt pavements.

Another group of modifiers for asphalt binders are called elastomers. Elastomers unlike plastomers will largely return to their original shape after the load is removed. Examples of these polymers are styrene-butadiene rubber latex (SBR), diblock styrene-butadiene (SB) and triblock styrene-butadiene-styrene (SBS). The benefits of using these polymers in asphalt binders is again the mitigation of permanent deformation or rutting of asphalt binders and further a reduction in fatigue and thermal cracking distress.

Anti-stripping additives such as polyamines and fatty amidoamines are used to reduce moisture susceptibility of an asphalt mixture by increasing the adhesion between the asphalt binder and aggregate surfaces. Asphalt binder extender material such as sulphur and wood lignin and oxidants like manganese compounds were used to increase high temperature stiffness in the 1980s. [18]

Acid modification such as polyphosphoric acid (PPA) has recently been a common approach to modify asphalt. It is used to increase the softening point of a binder without lowering the penetration value. PPA has also found increasing use to raise the grading range typically at high temperature, but depending on the source of crude oil, it may have a negative effect on long term fatigue performance.[37]

2.4 Chemical and Physical Ageing

As asphalt is composed of organic substances, it is affected by the presence of oxygen, ultraviolet radiation, and by changes in the temperature. These external influences result in changes in structure and composition of the asphalt molecules. For example, oxidation will result in the asphalt becoming hard and brittle. Thus, it increases the stiffness of the asphalt. Consequently, oxidized asphalt is far more likely to crack from an applied load. This hardening is known as "chemical aging". In the surface of the asphalt, where the material is exposed to the environment, hardening phenomena can have deleterious effects and result in cracking. This effect can decrease the service life of the pavement dramatically.

Physical aging occurs when the asphalt is kept at a low temperature over a period of time. Petersen[38] has stated the reasons of why physical aging occurs and he found three important factors:

1. Loss of oily compounds by adsorption or volatilization
2. Changes of composition by reaction in the air.
3. Reorientation of asphalt molecules and slow crystallization of waxes.

In 1999, Anderson and Marasteanu concluded that physical aging rate is a strong function of wax content.[39] However, Bahia argued that physical aging was largely due to free volume collapse.[40] Lu and co-workers have reported "there is no simple relation between asphalt cracking and bitumen wax content".[41]More recently Hesp and co-workers have stated that in the asphalt binders, wax content can contribute to the physical aging process but that some asphalt cements with low wax contents still exhibit physical hardening. They also concluded that asphaltene clusters and small amount of asphaltene sheet size are two factors which contribute to physical aging process.[42]

Given the above review of the recent literature, it can be concluded that it is still unclear what morphological and chemical changes occurs in the asphalt binders during the physical hardening process.

Chapter 3
Dynamic Shear Rheometer Testing

3.1 Rheology

Rheology is a branch of science dealing with the flow and deformation of material. The word rheology is derived from the Greek word rho, which means literally “to flow”. In the case of asphalt cement, the rheological behavior of the asphalt is controlled by the molecular structure, the crystallinity, the associated cross-linking in the asphalt and additive types and amount. Additionally, physical hardening, oxidation of asphalt and chemical association of the asphalt causes change in the asphalt binder’s rheological properties. Understanding the rheology of asphalt cement can bridge the gap between the molecular structure and the ultimate performance of the asphalt.

3.2 Visco-elastic Behavior of Asphalt

The stress-strain behavior defines the response of materials to a load. When stress or strain is applied on a material, rearrangement take place inside the material as the response to that stimulus. Materials which are able to return to their original shape after the removal of stress are known as elastic materials. The stress-strain behavior of these material are time-independent and can be characterized by an elastic modulus. On the contrary, some materials dissipate the input energy which leads to permanent deformation. The stress-strain behavior of these materials are time-dependent and are characterized by their elastic and viscous moduli. Asphalt binders exhibit aspects of both elastic and viscous behavior and are thus called visco-elastic materials. Figure 5 represents these three types of stress-strain behavior.

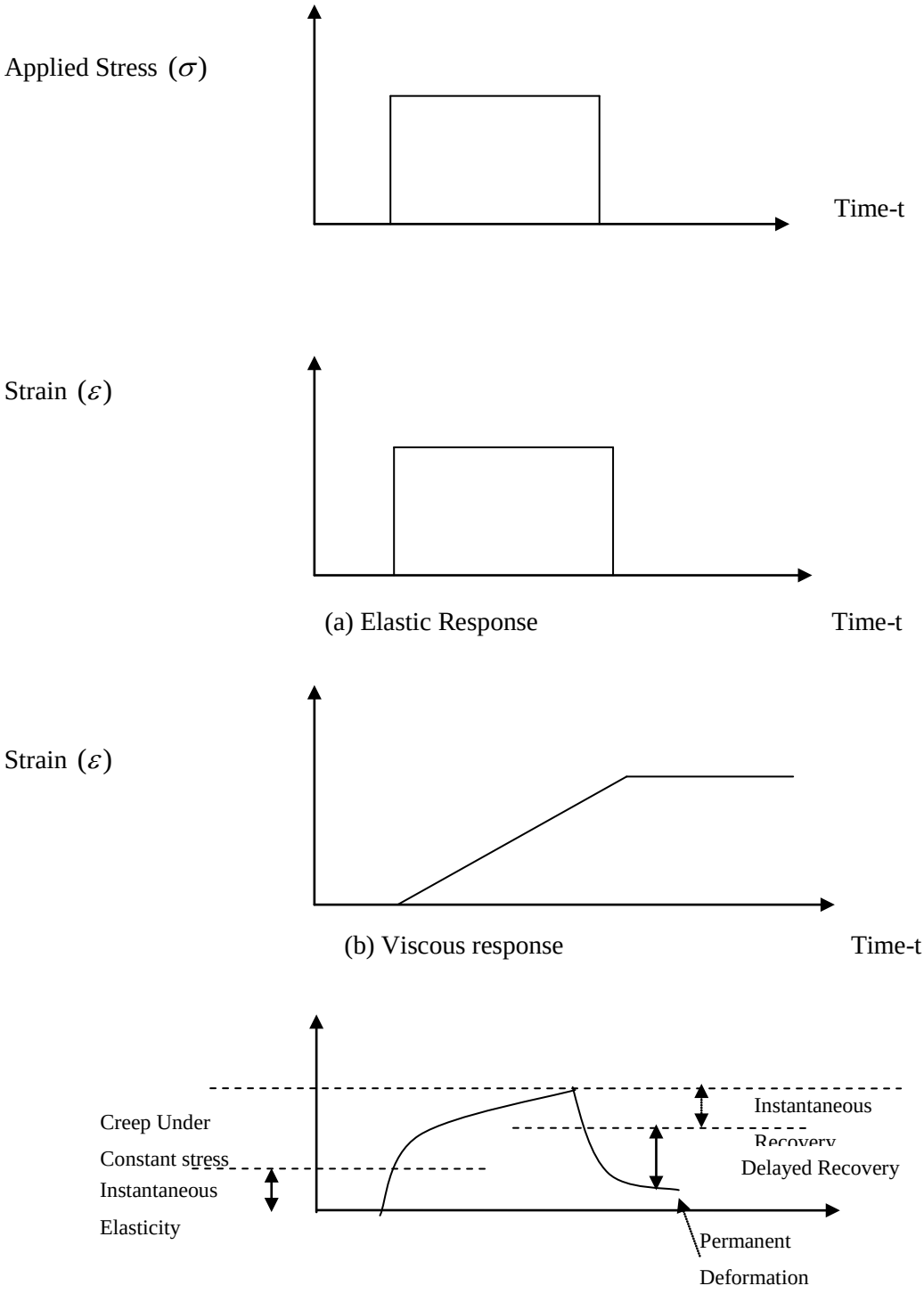

Figure 5. Idealized response of elastic, viscous and viscoelastoc material under constant stress loading.[43]

3.3 Dynamic Shear Rheometer Testing

The dynamic shear rheometer is a common tool used to study the rheology of asphalt binders at high and intermediate temperatures. The operation of a DSR is fairly basic. A sample of asphalt binder is sandwiched between two parallel plates, one standing and one oscillatory. The oscillating plate is rotated accordingly with the sample and the resulting shear stress is measured.

Two important parameters are obtained from the dynamic shear rheometer test on asphalt: G* the complex modulus and δ the phase angle. These parameters can be used to characterize both viscous and elastic behavior of the material. The complex modulus can be defined as a ratio between the maximum and minimum strain and stress as shown in figure 6 and equation 3-1, respectively.

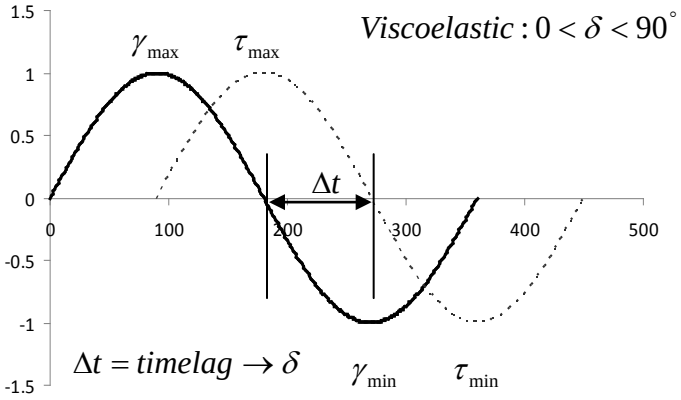

Figure 6. Demonstration of the definition of phase angle.

$$G^* = \frac{\tau_{max} - \tau_{min}}{\gamma_{max} - \gamma_{min}} \quad (3\text{-}1)$$

The complex modulus is a measure of a binder's total resistance to deformation. The complex modulus can be divided into two components, a real part and imaginary part. The simple relation is shown in equation (3-2) below:[23]

$$G^*(\omega) = G'(\omega) + iG''(\omega) \quad (3\text{-}2)$$

$$\left|G^*(\omega)\right| = \sqrt{G'(\omega)^2 + G''(\omega)^2} \quad (3\text{-}3)$$

$$G'(\omega) = G^*(\omega)\cos(\delta(\omega)) \quad (3.4)$$

$$G''(\omega) = G^*(\omega)\sin(\delta(\omega)) \quad (3\text{-}5)$$

Where,

$G^*(\omega)$ = complex shear modulus at frequency ω,

$G''(\omega)$ = dynamic storage modulus at frequency ω,

$G'(\omega)$ = dynamic loss modulus at frequency ω,

$\delta(\omega)$ = phase angle at frequency ω.

i = complex number (equal to $\sqrt{-1}$).

Additionally, the phase angle can be represented by the following equation:

$$\delta = \tan^{-1}\left(\frac{G''(\omega)}{G'(\omega)}\right) \quad (3\text{-}6)$$

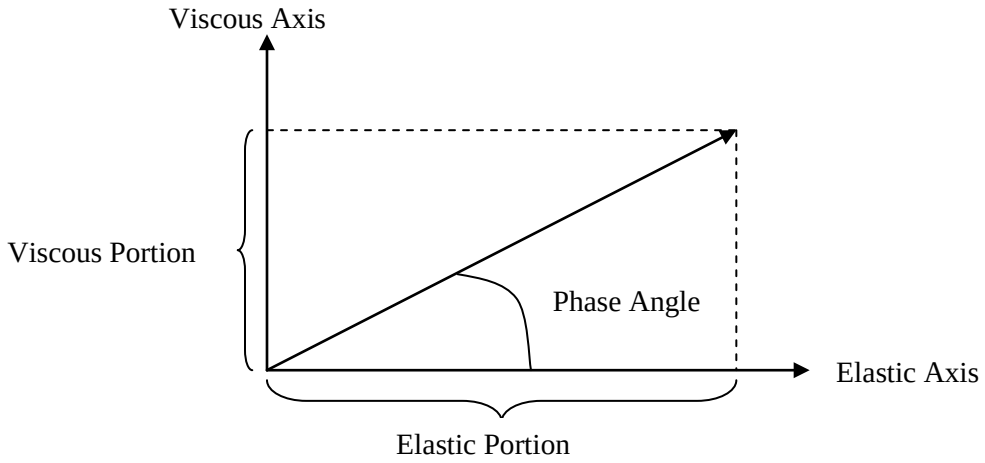

Figure 7. The relation between viscosity and elasticity in asphalt.

At high temperatures or low frequencies, the asphalt behavior is like a viscous fluid with no capacity for recovery. In this case, seen in figure 7, the asphalt could be represented by the vertical axis. There would be no elastic component of G*, since $\delta = 90^{o}$. At very low temperatures or high frequencies, the asphalt binder behaves like an elastic solid, which regains its original shape after deformation completely. This condition is represented by the horizontal axis. In this case there is no viscous component of G* since $\delta = 0$. G' and G'' are related to each other through the phase angle as shown in equation 3-6. As discussed earlier, as the temperature increases or frequency decreases, asphalt begins to lose the majority of its G' behaviour and starts to behave as a viscous fluid. As such, δ will approach 90 degrees and G'' becomes dominant. As the temperature decreases or the frequency is increased, the asphalt will behave like an elastic solid and then δ will approach 0 and G' will be dominant. Therefore, materials with higher storage moduli have greater ability to recover from deformation, and material with higher loss moduli have greater ability to resist deformation at prescribed frequency.

3.4 Booji and Thoone Approximation: Interrelation between Viscoelastic Functions

The integral transform functions that relate the real and the imaginary parts of the response to a harmonic excitation are known among physicists as the Kramers-Kronig function after worked reported by Kronig and Kramers in studies on the theory of electromagnetic radiation.[44] These relations are valid for function meeting the Bolzman superposition principle which means that "a system's total response to all components of an excitation history is linear and therefore independent and additive" and casuality principle which means "the system response follows the cause" can be applied for complex modulus.

Booij and Thoone described that the real and imaginary parts of functions with the above characteristics and without singularities on the real frequency axis are interrelated according to Kronig-Kramers functions.[6] They showed that for shear complex modulus defined as:

$$G^*(i\omega) = G'(\omega) + iG''(\omega) = |G^*|e^{i\delta(\omega)} \qquad (3\text{-}7)$$

Kramers-Kroning gives the following equations:

$$\log|G^*(\omega)| - \log|G^*(\infty)| = -\frac{2}{\pi}\int_0^\infty \frac{u.\delta(u) - \omega.\delta(\omega)}{u^2 - \omega^2}du \qquad (3\text{-}8)$$

$$\delta(\omega) = \frac{2\omega}{\pi}\int_0^\infty \frac{\log|G^*(u)| - \log|G^*(\omega)|}{u^2 - \omega^2}du \qquad (3\text{-}9)$$

By simplifying equations (3-8), (3-9) and under certain conditions, Booij and Thoone reported that, the Kramers-Kronig relation give the following equations for the linear viscoelastic materials:

$$G'(\omega) \approx \frac{\pi}{2}\left[\frac{dG''(u)}{d\ln(u)}\right]_{u=\omega} \qquad (3\text{-}10)$$

$$G'(\omega) - G'(0) \approx -\frac{\omega\pi}{2}\left\{\frac{d\left[G''(u)/u\right]}{d\ln(u)}\right\}_{u=w} \qquad (3\text{-}11)$$

where G' and G'' are the storage and loss modulus, respectively, and u is a dummy variable. Equation (3-10) was published long ago by Staverman and Schwarzel and it is useful over a broad frequency range.[45] Booji and Thoone stated that Equation (3-11) is most general in form and also better supported by experiment for a variety of linear viscoelastic materials.[3] Equation (3-11) can be rewritten ,

$$\frac{\delta(\omega)}{90} \approx \frac{d\log|G^*|}{d\log\omega} \qquad (3\text{-}12)$$

where G^* is the shear complex modulus and delta is frequency dependent phase angle. This equation states that the slope of the master curve is approximately equal to the phase angle in degrees divided by 90. Thus, the phase angle can be interpreted as an approximation of the frequency or time dependency of the bitumen.

3.5 Similarity between m-Value and Phase Angle

As discussed earlier, the BBR test is used to determine an asphalt binder's creep stiffness as a function of time. According to AASHTO M-320, the asphalt cement is loaded in three-point bending, and the creep stiffness (S(t)) and slope of the creep stiffness master curve (m(t)) are measured. The m-value is the slope of the plot of S(t) versus time on a double logarithmic scale. Binders with low m-values are slow to relax their stress as the temperature decreases, resulting in a thermal stress that builds more rapidly than that of those having a higher m-value. AASHTO standard TP1 describe the test method used to obtain the S and the m-value. Furthermore, creep stiffness is calculated using standard beam theory. The stiffness master curve is typically fitted to a second order polynomial function of an entirely empirical nature:

$$S(t) = a + b\log(t) + c[\log(t)]^2 \qquad (3\text{-}13)$$

Where:

$S(t)$ = asphalt binder stiffness

t = time

a, b, c = empirically determined constants.

The m-value is calculated as the first derivative of the above relationship, which results in the following equation:

$$m(t) = \frac{d(\log(S(t))}{d(\log(t))} = b + 2c\log(t) \qquad (3\text{-}14)$$

which represents a straight line on a semi-logarithmic plot of m(t) versus log(t).

Similarly, the DSR machine measures two important parameters, the dynamic shear modulus and phase angle. As discussed above, Booij and Thoone reported that phase angle can be proportional to the slope of the logG* master curve as follows:[3]

$$\delta(\omega, T) \approx \frac{\pi}{2}\left[\frac{d(\ln G^*(\omega, T)}{d\ln\omega}\right] \qquad (3\text{-}15)$$

Hence, because phase angle is approximately equal to the derivative of the logarithm of the stiffness with respect to frequency, it provides a much more sensitive measure of changes in rheology compared to stiffness alone. It gives an indication of stiffness at long loading times, in excess of those used for the measurement, and as such provides a sensitive measure of the sol/gel nature of the asphalt material. Small decreases in phase angle will result in significant increases in stiffness at long loading times, which would reflect reversible hardening caused by a sol-gel transition. For these reasons we decided to focus our investigation on the phase angle as a more

direct measure for low temperature performance. Furthermore, the phase angle is analogous to the m-value and it can be measured on a significantly smaller amount of material. Hence, this is at least one benefit for using it rather than the m-value.

3.6 DSR Test Result

3.6.1 Master Curve

In constructing master curves for the asphalt binders, dynamic shear rheometer data are collected over a range of temperatures and frequencies. A standard reference temperature must be selected. Then, the data at all other temperatures are shifted relative to this reference temperature until a smooth curve is generated. The master curves of the complex modulus, storage modulus, loss modulus and phase angle with the change in frequency can be constructed in this manner. Shift factors can be used to compare the rheological complexity of the sample. For instance, a rheologically simple material exhibits the same shift factor for both the complex modulus and phase angle master curve, while for a rheologically complex material these are expected to be different.

3.6.2 Time – Temperature Superposition Principle and Shift Factor

Time-temperature superposition (TTS) is a well known method to observe the dependence of the temperature on the change of viscoelastic properties of polymers. In accordance with TTS, viscoelastic properties measured at two different temperatures will have the same value if the frequency of measurement is also shifted appropriately. The shift factor a_t is used to characterize this required shift in frequency or time. Ferry discussed that in order to have a valid time-temperature superposition principle, the shift factor for all other derived viscoelastic functions

such as G', G'', G^*, etc should be the same.[46] Many studies of the rheological properties of unmodified binders have confirmed their thermo-rheological simplicity[44-4647-49] and, furthermore, the SHRP performance criteria for low temperature,[25,50] rutting and fatigue were proposed based on the time-temperature superposition principle.[25,5022,47] Many researchers have criticized the validity of the time-temperature superposition principle for polymer-modified binders, especially in the high strain regime,[51-53] while others have reported that time-temperature superposition holds neither for polymer-modified asphalt[54] nor unmodified asphalt.[55]

The Williams-Landel-Ferry (WLF) equation is commonly used to describe shift factors as a function of temperature:

$$\log a(T)_R = -\frac{C_1(T - T_R)}{(C_2 + T - T_R)} \qquad (3\text{-}16)$$

where

T = The selected temperature, °C or K;

T_R = The reference temperature, °C or K;

$a(T)_R$ = The shift factor at temperature T relative to the reference temperature;

T , C_1, C_2 = empirically determined coefficients.

However, Anderson et al.[25] found that for paving asphalt, the appropriate form for the WLF equation was as follows:

$$\log_{10} a(T)_d = -\frac{C_1(T - T_d)}{(C_2 + T - T_d)} \qquad (3\text{-}17)$$

where

$a(T)_d$ is the shift factor at temperature T relative to the defining temperature T_d ;

and

T_d is the defining temperature, in °C or °K, which is a characteristic parameter for each asphalt cement.

After anal**y**zing the shift factor data for the SHRP asphalts, the researchers found that the values of C_1 and C_2 for use in the WLF equation can be fixed for all asphalts to 19 and 92, respectively. Then, they calculated the defining temperature T_d for SHRP asphalt which are shown in table 2.

Table 2. Defining Temperature T_d for PAV-Condition SHRP Asphalts

Sample	T_d ° C
AAA-1	-14.5
AAB-1	-6
AAC-1	3.5
AAD-1	-8.7
AAF-1	5.2
AAG-1	2.7
AAK-1	-9.2
AAM-1	6

However, they found that for the temperature below T_d a better fit is provided by an Arhennius equation:

$$\log_{10} a(T)_d = -\frac{2.303E_a}{R}\left(\frac{1}{T} - \frac{1}{T_d}\right) \qquad (3\text{-}18)$$

where

E_a = the activation energy for flow below T_d; and

R = the ideal gas constant, 8.34 J/mol. K.

The activation energy for flow below T_d, E_a can be fixed at 261 kJ/mol.

When a full dynamic characterization has been performed, nonlinear least squares analyses can be used to determine the value of T_d, with the suggested constant values for the various coefficients. Thus, equations (3-17) and (3-18) are functions of T and T_d which simplify this aspect of the viscoelastic behavior to a single parameter, T_d.

3.6.3 Black Space Diagrams

A Black space diagram is a plot of log G* versus δ over all test temperatures and frequencies. This plot is very sensitive to morphology.[56] Unlike the master curve, the Black space diagram does not require any shifting, thus temperature- independent curves can be constructed when the material obeys time-temperature superposition.[57] Typically, expected viscoelastic behavior describes a decreasing phase angle and increasing complex modulus as the temperature decreases. The Black space diagram will appear discontinuous for the following reasons:

1- The sample is tested in the non-linear region;
2- The sample is not rheologically simple (i.e., phase transitions occur over the studied temperature and frequency range); and
3- The sample is tested outside of the testing machine resolution.

3.6.4 Han Diagrams

Han plots or modified Cole-Cole plots, represent changes between the elastic and viscous components of the complex modulus.[58] Such graphs are useful for interpreting the relative elasticity or viscosity of a particular asphalt over a range of temperatures. As expected, at high temperatures the asphalts are predominantly viscous, while as the temperature decrease the asphalt becomes more elastic and less viscous. Figure 8 shows Han plots for a polymer-modified asphalt at different temperatures. If a straight line is plotted such that G' = G", its intercept with the Han curve shows the crossover frequency between G' and G". Data on the right and under the

straight line represents a behavior dominated by the viscous or loss modulus while data on the left or above the line indicate that the elastic modulus dominates the behavior of the sample under the given testing condition.[59]

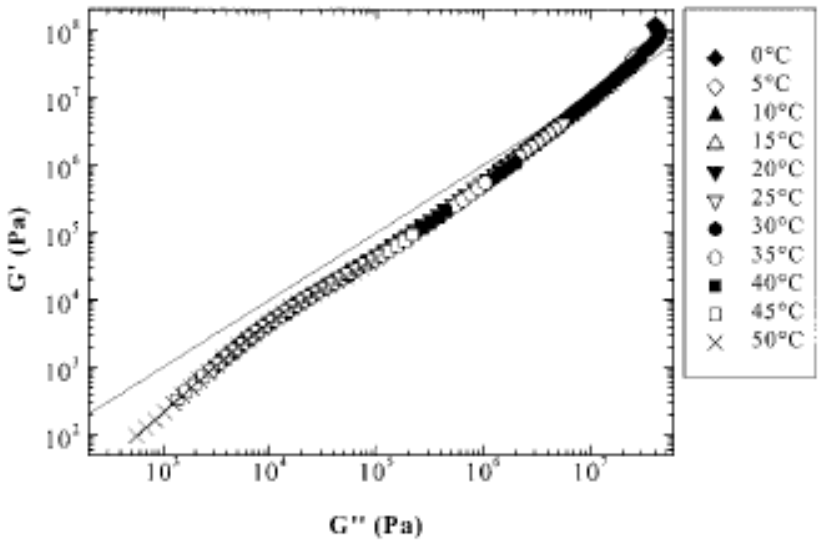

Figure 8. Han plots for asphalt modified with 4% Styrene-Butadiene-Styrene elastomer at different temperatures.[59]

Chapter 4

Materials and Experimental Procedures

4.1 Materials

4.1.1 Eastern and Northeastern Ontario Contracts

In this study, twenty recovered asphalt binders from contracts in eastern and northeastern Ontario were tested. In order to recover the asphalt from the field core samples, about 4 kg of the cores were cut into smaller sizes and soaked in tetrahydrofuran (THF) for about 24 hours. The asphalt was rinsed with enough THF to remove nearly all asphalt cement from the aggregate. Subsequently, a 4 L solvent bottle was used for the sedimentation of the fine aggregate before evaporation of the solvent. A rotary evaporator at high vacuum was used to remove the solvent. At the end of the recovery process, asphalt binders were heated at 150ºC for an addition one hour under a vacuum of 20-40 mm Hg in order to remove the solvent completely from the recovered binders. All contracts investigated in eastern and northeastern Ontario are listed in Table 3. Furthermore, a map of all contract locations is given in Figure 9.

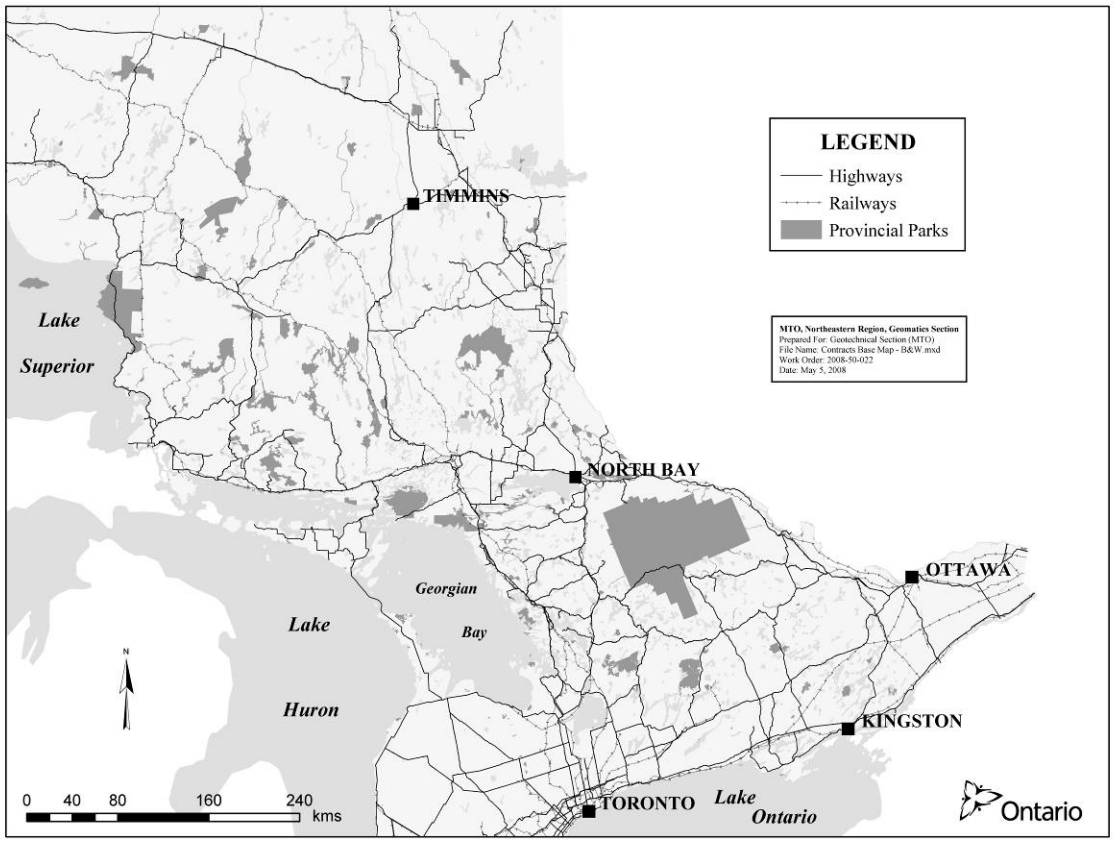

Figure 9. Contract locations for eastern and northeastern Ontario sites investigated.

Table 3. Eastern Ontario Contract Details

Site	Hwy	Location	Age	LTPPBind® Temperatures (98%, ºC)	Specification Grades, ºC/Pen	
					Binder Course	Surface Course
A	6	Little Current	2000	-29.3	58-34	58-34
B	11	Cochrane	1999	-37.8	52-34	52-34
C	11	Smooth Rock	1998	-36.8	52-34	52-34
D	17	Petawawa	1996	-32.5	85/100	85/100
E	28	Burleigh Falls	1993	-29.2	300/400 (30)	150/200
F	28	Lakefield	97/98	-29.2	52-34(25)+ 64-34	58-28
G	33	Conway	1998	-25.9	-	58-28
H	35	Lindsay	1997	-31.0	85/100	85/100
I	41	Dacre	2000	-31.7	58-34	58-34 PMA
J	41	Denbigh	1996	-33.6	300/400 (35)	150/200
K	41	Kaladar	1999	-33.7	58-34	58-34
L	41	Northbrook	2000	-33.6	58-34 M	58-34 M
M	41	Vennachar	97/98	-33.6	58-34 PMA	58-34 PMA
N	60	Bat lake	1998	-34.8	58-34	58-34
O	60	Wilno	1994	-34.4	-	-
P	62	Bannockburn	1997	-33.6	300/400 (30)	300/400 (30)
Q	62	Bloomfield	1993	-27.7	150/200 (20)	150/200 (20)
R	138	Cornwall	00/01	-28.7	58-34 PMA	58-34 M
S	138	Monkland	1998	-31.5	58-34	58-34
T	416	Spencerville	1999	-29.0	64-34	64-34

4.1.2 Highway 655 Trial Sections

The asphalt cement details for the Highway 655 pavement trial are given in Table 4. At the time of paving, all tested samples were aged in the rolling thin film oven (RTFO) and pressure aging vessel (PAV) (100ºC for 20 hours) according to American Association of State Highway and Transportation Officials (AASHTO) standard T-240, R-28. Five years later, field-aged sample from each test section were extracted and recovered through rotary evaporation.

Table 4. Highway 655 Trial Section Details

Section	Modifier	Base AC	PGAC Grade, ºC	G*sinδ (16ºC), kPa	$T_{G^*\sin\delta = 5\ MPa}$, ºC
1	RET+PPA	Lloydminister	65-36	2218	9.8
2	Ox + SBS	Unknown	65-36	2588	10.1
3	SBS	Unknown	65-36	1954	7.8
4	SBS + P[31]	Unknown	67-35	2226	9.1
5	SBS	Western Canadian	66-35	2273	9.7
6	Ox + P[31]	Unknown	59-35	1820	7.1
7	P[31]	Unknown	54-35	1542	6.7

Note: RET = reactive ethylene terpolymer; PPA = polyphosphoric acid; Ox = oxidized; SBS = styrene-butadiene-styrene; P[31] = additive containing phosphorous (likely polyphosphoric acid). Continuous grades are rounded to the nearest degree, are averages from three laboratories, and varied by less than 1.9ºC between laboratories. The base asphalt for Section 5 was from a Bow River, Cold Lake or Lloydminster source, or a mixture thereof.

4.2 Distress Surveys

Distress surveys were all conducted in the fall of 2007.[60] Detailed cracking locations were recorded, and photographs were taken of typical cracks. Crack lengths were calculated from the average of three locations (beginning, middle, and end) in each contract.

(A) Highway 6 north of Little Current

The contract covered 16 km through varied terrain with a relatively low volume of commercial traffic (Annual Average Daily Traffic Count (AADT) = 3560 with 11.2% commercial for 2007). This stretch of highway was reconstructed in 2000 and cracked prematurely and excessively in the first few years of service. The distress was so pervasive that crack sealing was never an option. The pavement condition index, the pavement condition index is a numerical index between 0 and 100 and 100 represents an ex excellent pavement, had fallen to 79 in 2007 and is expected to deteriorate rapidly in years to come due to the extensive low temperature cracking.[37]

(B) Highway 11 west of Cochrane

This 30 km section of Highway 11 was reconstructed in 1999 and has performed remarkably well given that it is one of the most northerly contracts investigated. Joints, shoulders, and areas over culverts have remained free of serious cracking distress. The area is exposed on regular occasions to air temperatures below –40ºC and experienced a record low of nearly –50ºC as logged on a nearby pavement trial in early 2004. [33]

(C) Highway 11 east of Smooth Rock Falls

The 26 km stretch of Highway 11 to the west of the previous contract is also in relatively good condition. It was reconstructed in 1998 and has very good ride and pavement condition ratings in spite of its slightly older age but this may be due to a slightly lower traffic level. The asphalt cement came from the same supplier as that used for Site B, so was likely from the same source.

(D) Highway 17 near Petawawa

This stretch of Highway 17 was reconstructed in 1996 and is now in serious need of rehabilitation. The centreline joint and shoulders are riddled with extensive low temperature cracking distress. Full width transverse cracking is pervasive throughout and numerous cracks are starting to spall. The asphalt cement used for this contract was an 85/100 penetration grade that would likely have graded short of the required –34ºC in this area. However, the site was included in this study since the recovered asphalt cement still grades at a level that is reasonable compared to the lowest calculated pavement temperatures. Weather data from a nearby station (Canadian Forces Base Petawawa) suggests that the pavement surface temperature has never fallen below –27ºC.[61]

(E) Highway 28 north of Burleigh Falls

The stretch of Highway 28 investigated was reconstructed in 1993 and is virtually free of low temperature cracks today. If the mix designs are correct, then both binder courses contained 30% recycled asphalt pavement (RAP), whereas the surface course contained no RAP. Hence, for this study the asphalt cement from both binder courses was recovered for analysis. However, it should be noted that Ontario contractors have an option to use RAP in hot mix with adjustments to the high temperature grade if the RAP content exceeds 20%. There is no indication in the documentation available for this contract whether this actually happened.

The entire 18.5 km section showed only sporadic cracking distress. Hence, only three locations of 250 m were surveyed. The first survey was conducted just south of Eel's Creek at the northerly end of the contract. Three minor transverse cracks were noted (one full lane and two quarter lane width) in addition to approximately 11 m of very minor mid-lane cracking. The second survey was conducted approximately 8 km north of Burleigh Falls near the junction with Highway 56. This 250 m stretch was free of cracking distress. A third survey conducted

approximately 2 km north of Burleigh Falls had approximately 10 m of mid-lane cracking in a swampy area. Figures 10 (a) and (b) show the general state of the pavement and the cracking distress in the swamp area.

A ~0.5 cm thick microsurfacing overlay was applied in 2004 to correct a problem with inadequate friction. Note that the overlay may have covered up some minor cracking distress but that major transverse cracks would likely have resurfaced after three winters if they had been present.

(a) (b)

Figure 10. Surface condition of Highway 28.

Note: Arrow indicates minor wheel path cracking in a swamp area.

(F) Highway 28 south of Lakefield

This stretch of Highway 28 was reconstructed with PG 58-28 asphalt cement in 1997 and 1998. The binder used in this contract fails the required PG –34 for the area, but the surface condition is still excellent today, which may be due to the thick design of the road (120 mm) and moderate traffic volume (AADT = 5740 with only 9.3 % commercial vehicles).

(G) Highway 33 east of Conway

This stretch of Highway 33 was reconstructed in 1998 with a PG 58-28 grade asphalt cement, which is appropriate for the area. It is totally free of cracking distress today even though the pavement is only 50 mm in thickness. The ride condition index stands at 7.2 and the pavement condition index at 81, likely due to surface unevenness resulting in part from the thin design.

(H) Highway 35 south of Lindsay

This stretch of Highway 35 was reconstructed in 1997 with an 85/100 penetration grade asphalt cement, which likely would not have made the required –34ºC Superpave® grade for this area. However, the pavement is in very good condition today, which may be due to the design (three lifts totalling 130 mm), the low commercial traffic component (AADT = 8062 with 9% commercial vehicles), or the recent mild weather for the area.

(I) Highway 41 from Dacre to Egansville

This stretch of Highway 41 was reconstructed in 2000 with two different PG 58-34 grade asphalt cements. The material used in the surface course was categorized as “polymer-modified,” but that in the binder course, while of the same grade, was not categorized as such. The pavement surface

is in excellent condition today with only minor cold temperature cracking localized in the northern half near Egansville.

(J) Highway 41 near Denbigh

The stretch of Highway 41 investigated was reconstructed in 1996. Total hot mix asphalt for this contract amounted to nearly 24,000 tonnes. An additional 93,000 tonnes of granular material was used for the rehabilitation of the pavement foundation. The binder course contained 35 % RAP, whereas the surface course contained none. The asphalt binder from both courses was recovered for analysis since it was difficult to decide which lift was most susceptible to cold temperature cracking. The contract covered 13 km through mainly forested area with good drainage on either side of the pavement.

The contract showed early and extensive cracking distress from beginning to end. Hence, three stretches of only 100 m each were surveyed. The first stretch was severely damaged, with the shoulders and part of the lane showing significant freeze-thaw distress. Figure 11 (a) and (b) provide a representative image. In addition, 18 additional transverse cracks in total were counted. Ten of these cracks reached the width of a single lane, while the remainder all covered the entire width of the pavement.

The second and third surveys had 43 and 29 transverse cracks, respectively, most of which covered the full width of the pavement and were of intermediate severity.

(a) (b)

Figure 11. Surface condition of Highway 41.

Note: Arrow indicates major thermal cracking sprouting out of wheel path distress.

(K) Highway 41 from Kaladar to Northbrook

The stretch of Highway 41 investigated was reconstructed over 12.4 km in 1998 and 1999. The pavement design consisted of a 40 mm binder course constructed on pulverized grade and a 40 mm surface course. The contract covered 12.4 km through mainly forested areas with reasonable drainage on either side of the pavement. Total hot mix asphalt for this contract amounted to nearly 24,000 tonnes. An additional 52,000 tonnes of granular material was used for the rehabilitation of the pavement foundation. No recycled material was used in this contract, and the binder grade specified was a PG 58-34.

During the 2007 survey the cracking was considered to be severe throughout the contract. Figures 12 and 13 provide representative images. Over 40,000 m of cracks were sealed in this contract in 2003, but at the time of the survey in 2007 many additional cracks had already appeared.

Figure 12. Surface condition for Highway 41 north of Kaladar.

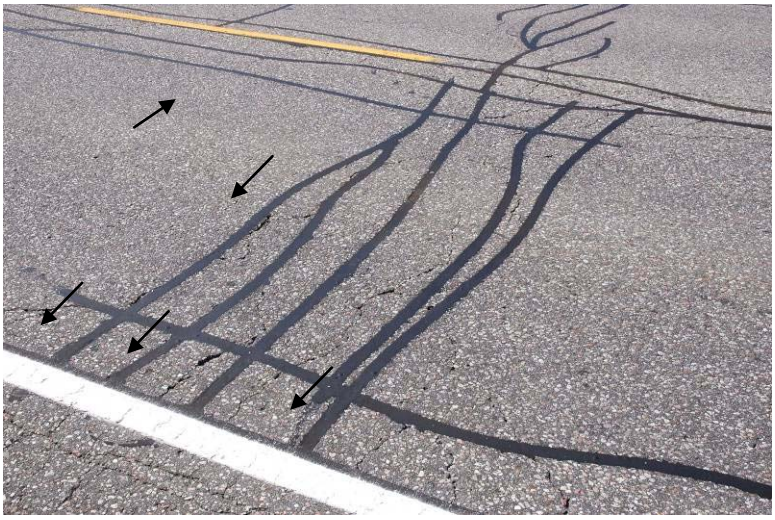

Figure 13. Condition for Highway 41 north of Kaladar. Note: Arrows indicate thermal cracks that have appeared after the original crack sealing.

(L) Highway 41 from Northbrook to Cloyne

The stretch of highway investigated was reconstructed in 2000. The design consisted of a two-lift asphalt concrete pavement on top of a pulverized grade. Total hot mix asphalt for this contract amounted to 13,000 tonnes. Transverse cracking commenced shortly after construction and was considered excessive throughout within a few years, with cracks spaced approximately 3 m apart. The contract covered 8.7 km over mainly forested terrain with good drainage on either side of the pavement.

(M) Highway 41 near Vennachar

The stretch of highway investigated was reconstructed in 1997 and 1998. The design consisted of a two-lift asphalt concrete pavement on top of a pulverized grade. Distress in this contract was judged to be minimal at the time of the survey in 2007, with transverse cracks spaced approximately 43 m apart. The contract covered approximately 20 km over mainly forested terrain with good drainage on either side of the pavement. The asphalt cement used in this contract was listed as “polymer modified”, which may explain some of the improved performance.

(N) Highway 60 near Bat Lake

The stretch of Highway 60 investigated was reconstructed in 1998. Total hot mix asphalt for this contract amounted to 21,000 tonnes. The asphalt was placed on a minimum of 150 mm of freshly pulverized and compacted granular material throughout the contract. No recycled materials were used in the hot mix asphalt; hence the binder grade specified was a PG 58-34. The contract covered 13.1 km over mainly forested terrain with good drainage on either side of the pavement.

After only five years of service a total of 29,000 m of cracks had to be sealed in this contract. During the 2007 survey the cracking was considered to be severe throughout the contract, with many areas showing additional deterioration.

(O) Highway 60 east of Wilno

The stretch of Highway 60 investigated was reconstructed in 1994. Little if any information was available about construction details except that the pavement consisted of two lifts on a pulverized grade. The road is now in very poor condition, with pervasive transverse and longitudinal cracking throughout. Cracking started early in the life of the pavement, and total crack sealing in 2004 amounted to 50 km over 8 km of pavement, with approximately half of this for transverse cracking alone.

(P) Highway 62 near Bannockburn

The stretch of Highway 62 investigated was reconstructed in 1997. The pavement design consisted of two lifts of asphalt concrete on top of a pulverized grade. Total hot mix asphalt for this contract amounted to nearly 23,000 tonnes. Nearly 16,000 tonnes of granular material was used for the rehabilitation of the pavement foundation and shoulders. As both binder and surface courses contained 30% RAP the asphalt binder from both courses was recovered for analysis. The contract covered 15 km through mainly swampy and forested area with somewhat poor drainage on either side of the pavement.

The road was severely cracked from beginning to end after only a few years of service. Hence, three stretches of 100 m were surveyed for cracking distress. The crack counts for the three sections were 57, 86, and 73, respectively, with a mixture of quarter lane, half lane, and full lane, most of minor or very minor severity.

(Q) Highway 62 north of Bloomfield. This stretch of Highway 62 was reconstructed in 1993. The pavement design consisted of two lifts of asphalt concrete on top of a pulverized grade. Total hot mix asphalt for this contract amounted to nearly 20,000 tonnes. As both asphalt courses contained 20% RAP the asphalt cement from both was recovered for analysis. The terrain is mainly farmland with good drainage on either side of the pavement.

The entire 11.4 km length of this site showed only sporadic distress. Hence, three stretches of 250 m were surveyed in detail. The first survey was conducted approximately 1 km north of the junction with Highway 33. A total of four very minor transverse cracks were noted in addition to approximately 49 m of very minor inner wheel-path cracking. Figures 14 (a) and (b) show typical cracking patterns.

(a) (b)

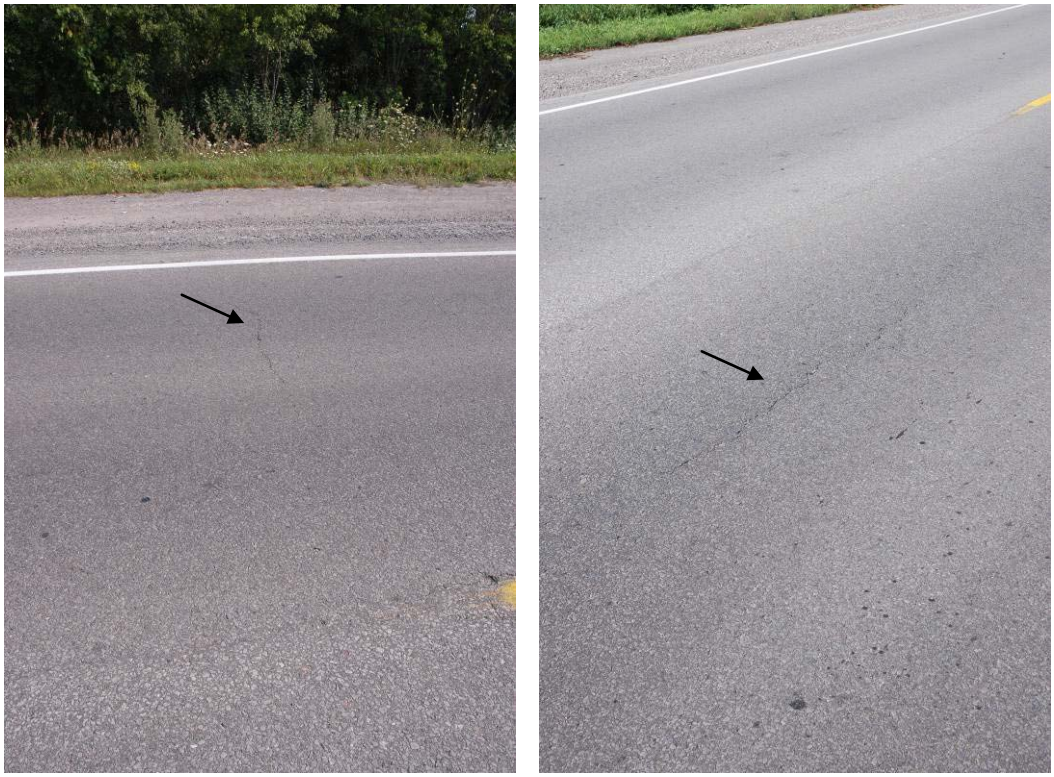

Figure 14. Typical surface condition for Highway 62.

The second survey was conducted approximately 4.6 km north of the junction with Highway 33. It showed only very minor cracking associated with a traffic loop in this area and minor cracking in the shoulders (neither of which was included for this analysis). The third survey was done approximately 9.5 km north of Highway 33. This section had two transverse cracks both a quarter lane wide in addition to some 19.8 m of very minor wheel path cracking.

(R) Highway 138 from Cornwall to Monkland.

This stretch of Highway 138 was reconstructed in 2000 and 2001. The pavement design consisted of three lifts of asphalt concrete (130 mm) on top of a pulverized grade. No recycled material was used and the asphalt cement specified was a PG 58-34. Hence, for this study the asphalt cement from all three courses was recovered for analysis. The contract covered 17.0 km through varying terrain (mainly agricultural areas) with good drainage on either side of the pavement. The entire length of the contract was largely free of distress.

(S) Highway 138 north of Monkland.

This stretch of Highway 138 was reconstructed in 1998. The pavement design consisted of three lifts of asphalt concrete on top of a pulverized grade. Total hot mix asphalt for this contract amounted to nearly 44,000 tonnes. An additional 45,000 tonnes of granular material was used for the rehabilitation of the pavement foundation. No recycled material was used, and a PG 58-34 grade of asphalt cement was specified. Hence, for this study material from all three courses was recovered for analysis. The contract covered 17.2 km through varying terrain (swamps, forests, and agricultural areas) with good drainage on either side.

The pavement was surveyed in three locations. A total of 66,667 m of cracks in this contract had been sealed after only six years of service. However, at the time of the survey for this study,

additional cracks had appeared in many areas that had not yet failed at the time of the repairs three years before. During the 2007 survey the cracking was considered to be severe throughout the contract. Figures 15 (a) and (b) show typical distress levels for this location.

(a)

(b)

Figure 15. Surface condition of Highway 138.

(T) Highway 416 near Spencerville.

This stretch of the southbound lanes of Highway 416 was newly constructed in 1999 as part of the twinning of the highway between Ottawa and Highway 401. The pavement design consisted of three lifts of asphalt concrete (140 mm) on top of a pulverized grade. No recycled asphalt pavement was used in this contract, and the binder specified was a PG 64-34 in both the surface and two heavy-duty binder courses. The asphalt from the surface course was recovered for analysis. The contract covered 17.9 km through varying terrain with excellent drainage on either side of the pavement. The entire length of the contract was largely free of distress.

The summary of approximate crack lengths for each of the 20 contracts is provided in Figure 16 note that the total crack length does not say much about the severity of the distress. The superior pavements also showed the least severe cracking, while the others had a mixture of mild to extremely severe cracking as shown in the various photographs in Figures 11 to 15.

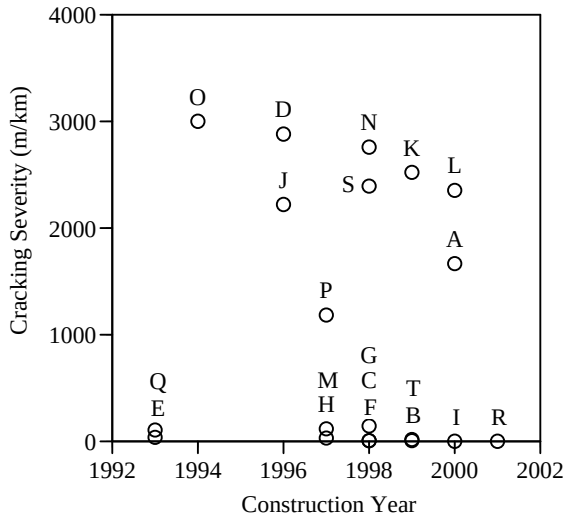

Figure 16. Cracking distress versus construction year for 20 eastern and northeastern Ontario pavement contracts constructed between 1993 and 2000.

4.3 Experimental Procedures

4.3.1 Regular BBR Testing According to AASHTO Method M320

The sample was heated in the oven for approximately 1 hour at 160 ºC in order to be fluid enough to easily pour. After heating, the sample was poured into aluminum molds greased with vaseline™ while Teflon strips were placed against the greased face of dimension. Once, the sample was poured, it was cooled for additional 1 hour. Figure 17 provide a schematic of the aluminum mold and the dimension of the asphalt beam. Furthermore, the end pieces of the mold were treated with glycerin and talc mixed to achieve paste-like consistency. After one hour, excess asphalt was trimmed from the top of each mold using a hot spatula. The beam specimen is supported at two points 102 mm apart in a controlled temperature fluid bath. The beam is then loaded at mid point with a load of approximately 1000 mN for a period of 240s.

Beam stiffness, often called "creep stiffness" (S (t)) and the slope of creep stiffness master curve(m(t)) were calculated at a loading time of 60s. According to the AASHTO M320 the creep stiffness should not go over 300 MPa at 60 second loading and m-value less than 0.3 at 60 second loading time. All samples were tested in duplicate and the reproducibility was found to be excellent. Figure 18 shows a schematic of the bending beam rheometer.

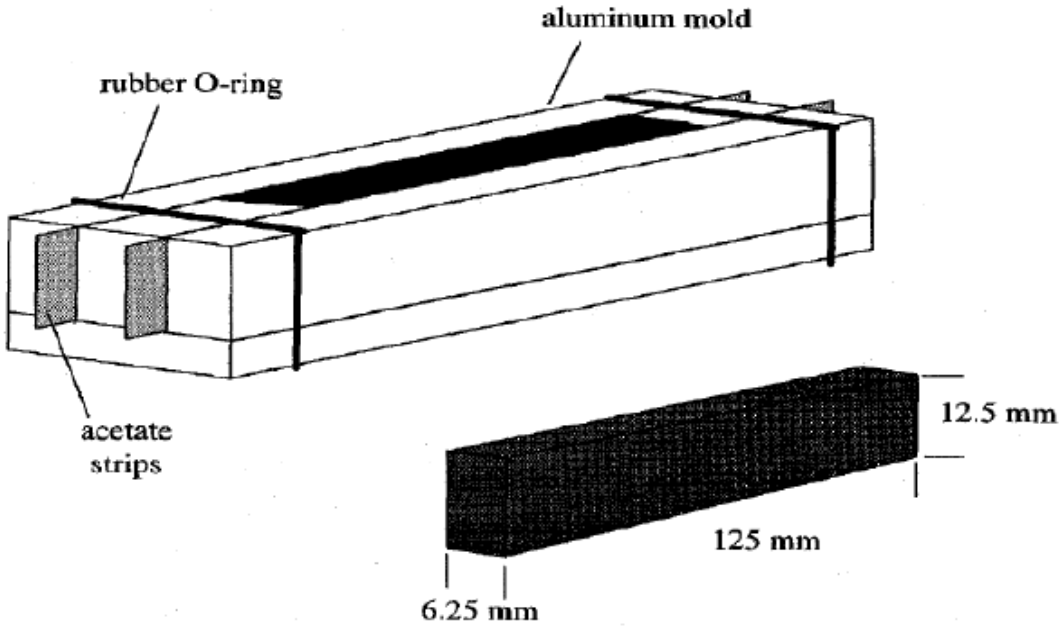

Figure 17. BBR test mould assembly and sample dimensions.[62]

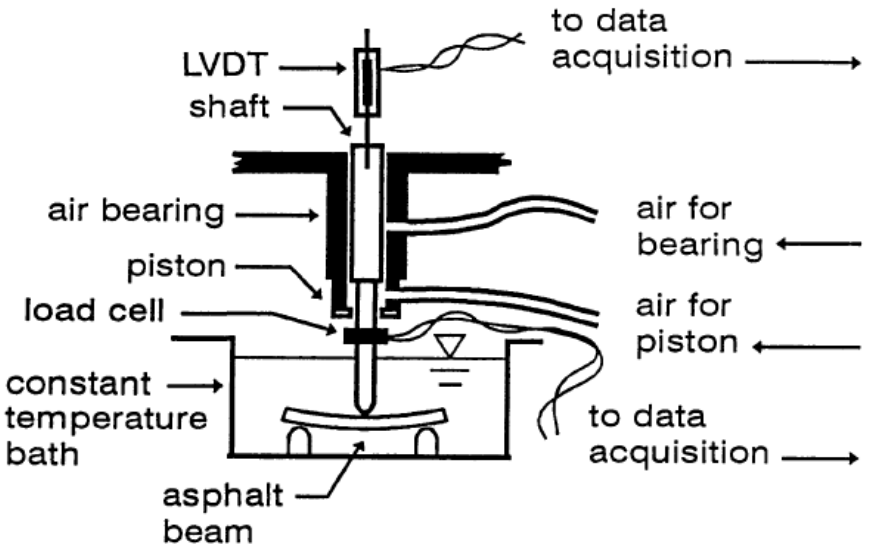

Figure 18. Schematic diagram of bending beam rheometer.[25]

4.3.2 Extended BBR Testing According to MTO Method LS-308

A total of 12 BBR beams were prepared according AASHTO M320. Asphalt beams were subsequently conditioned at both 10ºC and 20ºC above the pavement design temperature for one, 24 and 72 hours. Six beams were used at each conditioning temperature.

The samples for the test were run at two different temperatures. Those were tested between pass and fail temperature according to AASHTO M320 critical properties (S = 300 MPa and m-value = 0.3). From the resultant temperature obtained, the maximum grade loss is calculated. Both the worst grade temperature and grade loss are calculated after three days. The 10ºC shift is the application of the time-temperature superposition principle.

4.3.3 Ductile Failure Testing According to MTO Method LS-299

The asphalt binders were heated for about one hour in oven at 160. The samples were poured into prepared silicon (DENT) moulds having two aluminum end pieces inserted into each of the molds.

Each silicon mold includes three different notch depths (ligaments between notch tips include 5, 10 and 15 mm). Figure 19 below shows a photograph of how the molds are filled.

The samples were conditioned at ambient temperature for 24 hours before they were removed from the silicon mold and were loaded into tensile machine. Subsequently, the samples were conditioned 30 min at 15 ºC prior to test in the bath of the tensile machine. In this study, Samples were tested at a speed of 50 mm/min. Figure 20 shows a photograph of DENT test set-up.

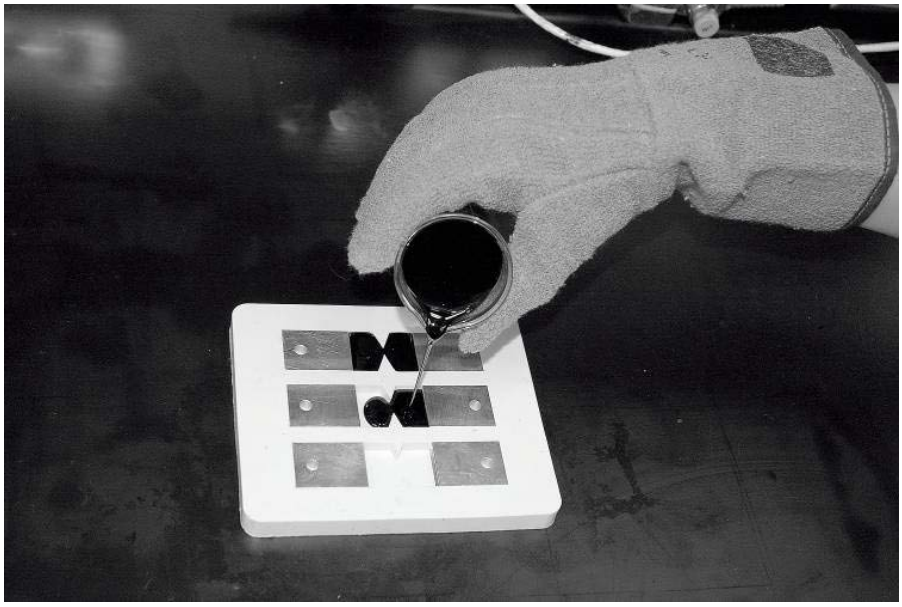

Figure 19. Pouring of sample in silicon mould.

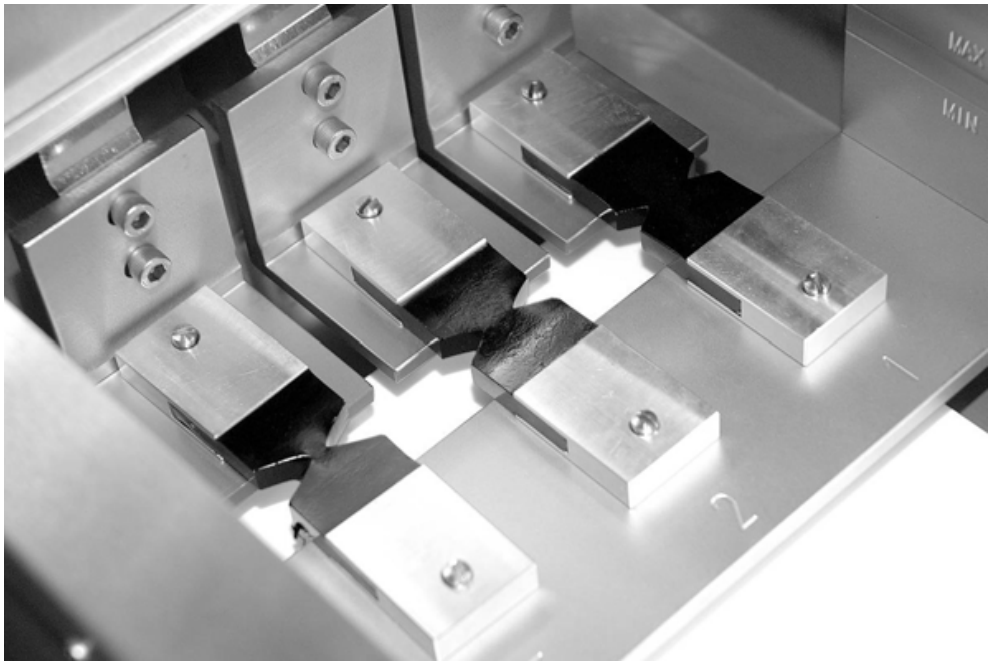

Figure 20. Double Edge Notched Tension (DENT) test set up.

4.3.4 Dynamic Shear Rheometry

To prepare a sample for the test, an oven was preheated to 340 ºF, at which point the samples were placed in the oven and allowed to melt. The average melting time of the sample was approximately 20 minutes. A small amount of the melt was poured into three small rectangular molds. It should be noted that Teflon strips and Vaseline™ were used to facilitate their removal, and rubber bands were used to hold the assembly together as the sample solidified. All samples were cooled for an additional hour prior to the test.

The report is based on data obtained through use of a Rheometrics® RDA-II model with a liquid nitrogen controlled environmental chamber. A picture of the dynamic shear rheometer can be seen in figure 21.

RSI Orchestrator® software was used to determine the complex modulus (G*), storage modulus (G'), loss modulus (G"), and phase angle (δ) or loss tangent (tan (δ) = G"/G'). For the tests presented within this report, the parameters were set as outlined in table 5

Table 5. Basic Test Parameters

Test Parameter	Value
Total Test Time	2 hours
Soak Period at Each Temperature	10 min
Measurement Period	10 sec
Temperatures	-10°C
Oscillation Frequency	0.1 rad/s
Shear Strain	0.1 %

Specimens were placed in the rheometer and secured through the tightening of the two clamps at each end using a screw. A diagram of the torsion bar apparatus can be seen in figure 22.

In the second part of the experiment, the limiting temperature at which tan(δ) reach 0.3 was determined. The samples were conditioned in a freezer at –10 ºC for 72 hours prior the test. All specimens were tested at -6, –12, –18, –24 and –30 ºC with soak times of 30 minutes prior to testing.

At the last part of the experiment the samples were conditioned in a freezer at -20 ºC for 1 and 24 hour. Reading was recorded for 0, -6, -12 and -24ºC. Furthermore, two parallel plate dimensions (diameters of 8mm and 25mm) were used to run a test at 0, 25, 38, and 50ºC. the smaller plate (8mm) was used for lower temperature 0ºC , while the larger plate (25mm) was used for higher temperature 25, 35 and 50ºC . The small plate can not be used at higher temperature because the stress is below the minimum torque which is detected by instrument. It should be noted that the mould for parallel plate samples consisted of silicon rubber mould with wells. The wells of the mold are 5 mm deep, with a diameter of 25 and 8 mm. the sample were then left to cool at room temperature for 1 hour. Before conducting a new test, the digital gauge was zero with the empty plates so that the separation of the plate once the sample had been added would be known. The sample was held between two plates. The upper plate is fixed and the lower plate is oscillated. The upper plate was gently lowered as the contact and compression of the sample was now exerting a tensile force on the rheometer. Once the gap between two plates was approximately 2.1 mm, the excess asphalt that had been compressed out side the diameter of the plate was trimmed with a razor blade. Finally, the upper plate was then lowered until a final 2mm gap between two plates was achieved.

Figure 21. Dynamic Shear Rheometer

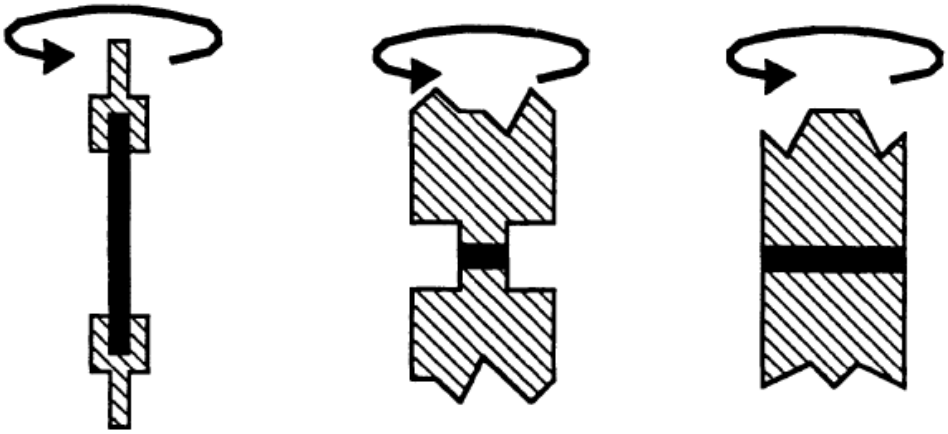

Rectangular Torsion 8 mm Parallel Plate 25 mm Parallel Plate

Figure 22. Parallel plate and torsion bar geometries used for dynamic shear rheometer.[25]

Chapter 5
Results and Discussion

5.1 Regular BBR Testing According to AASHTO Method M320

The results of the regular BBR for all 20 contracts are shown in figure 23. The cracking distress is plotted versus the grade deficit or surplus according to the difference between the required LTPPBind® and obtained AASHTO M320 grade temperature.[63] This figure shows that AASHTO M320 does not properly distinguish the good and poor performing asphalts.

Specifically, contracts pertaining to S, L, O, K and D all passed the test while they exhibit poor performance in the field. Moreover, several contracts such as P, A, J and N are on the boundary line of pass or fail. Furthermore, given that the Ministry of Transportation accepts a 3ºC margin of error when grading the asphalts, it is likely that all tested binders would have ultimately passed the grade requirements for the respective contracts. Thus, it represents unreliability within the test. Therefore, the total accuracy of this analysis is just 55%, with the nine failing contracts in service but all passing the current specification limits.

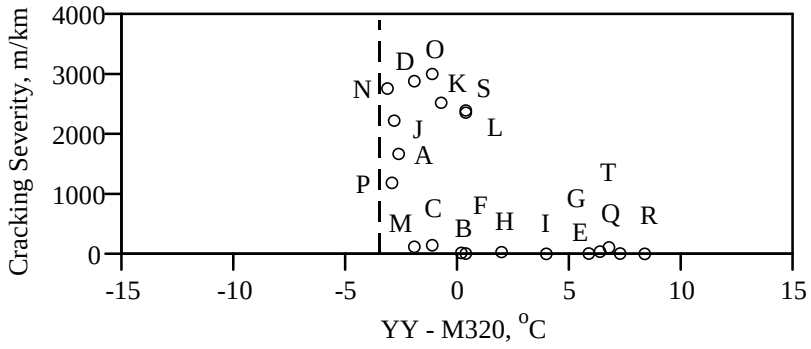

Figure 23. Regular BBR grading results according to AASHTO M320 criteria for 20 eastern and northeastern Ontario contracts.

5.2 Extended BBR Testing According to MTO Method LS-308

Figure 24, in this graph cracking severity is plotted against the grade deficit/surplus. As can be seen the M, C out of 20 samples are outliers. The accuracy of this test is 90%. The range increases over 20ºC due to three days conditioning which is twice the range obtained in AASHTO M320. The physical hardening aspect, which is totally missed out in AASHTO M320 is captured in this test method. Thus the poor performing samples, which are more elastic, retain thermal stresses within them showing high grade losses.

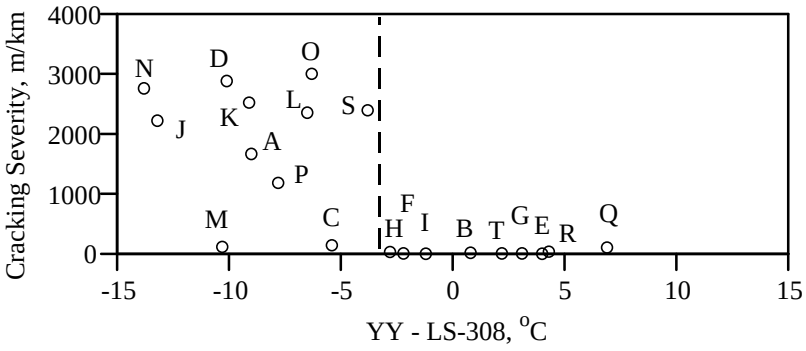

Figure 24. Grading results according to MTO LS-308. Note: The dotted line is placed in a somewhat arbitrary position yet with the aim of obtaining the highest accuracy of 90 %.

In figure 25**,** three-day grade loss in LS-308 versus the cracking severity in 20 eastern and northeastern Ontario contracts is plotted. This figure demonstrate the strong correlation between the grade loss for the samples after three days of conditioning at -10^{o}C and their associated cracking severity as noted from the field. The accuracy of these results is 95 %. Just the sample M is the only outlier. The reason for the sample M behavior can be traced to the fact that this sample is polymer modified asphalt and the polymer gives it more flexibility at low temperature. This graph also demonstrates that the poor performance asphalt lost more grade than the good performers.

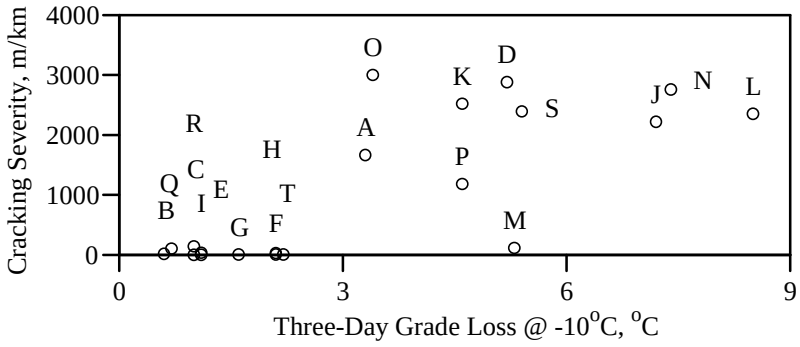

Figure 25. Three-day grade loss in LS-308 versus the cracking severity in 20 eastern and northeastern Ontario contracts.

5.3 Dynamic Torsion Testing on Contract Samples

The samples were tested at –10ºC, 0.1 % strain, and 0.1 rad/s and the tan delta measured at 10 minute intervals for a total two hours. By plotting the value of tan delta after 10 minutes and two hours against the cracking severity for each site in Figure 26, it can be clearly seen that there is a strong relationship between the cracking distress and tan (δ) at –10ºC. The two hours test can separate the well- and poor-performing asphalt. It may be related to this fact that the 10 minute test does not provide enough time for samples to reach their equilibrium condition.

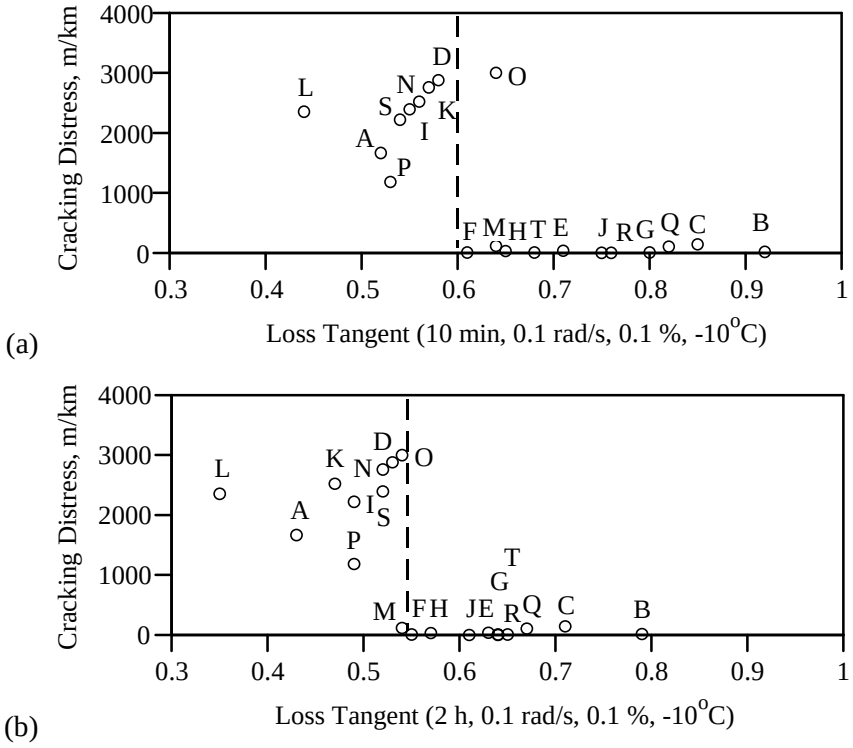

Figure 26. Cracking distress versus loss tangent at –10ºC:

(a) 10 minutes; and (b) 2 hours conditioning.

As expected, the asphalt cements with high tan (δ) (sol type) are able to relax stresses prior to the melting of pavement during spring. Thus, those are expected to show less thermal cracking. On the other hand, asphalt cements with low tan (δ) tend to form gel and expected to suffer reversible aging (asphaltene structuring/gelation, wax crystallization, free volume collapse, etc.), resulting in high thermal stresses with subsequent increased tendencies to crack. These effect are most noticeable at low deformations and rate of strain (i.e., in the pavement at long loading time in areas away from fracture zone).

Baskin of Imperial Oil in Toronto, as early as 1935 stated that “the fact that most damage occurs during the period when frost is coming out of the ground would lead one to suspect that

the slow and gradual strains caused by the movement of subsoil may well be the most potent cause of cracking. All this would reduce our problem largely to pliability of paving mixtures at 32º F (0ºC)."[64]Similarly, Shieds and Anderson in 1964 proposed that it is not clear whether the cracking happens when the temperature goes down or a rapid increase of temperature cause visible transverse cracking distress.[65] Rader and Ochalek in 1971 reported that a combination of low temperature and freeze-thaw distress causes visible transverse cracking distress. They went to say that to decrease low temperature cracking, a low modulus of elasticity and a high modulus of rupture are desirable.[66] In recent publications, researchers have concluded that at low temperature viscous behaviour is preferred over elastic behaviour.[67,68]

As can be seen in figure 26a tan (δ) can predict the well- and poor- performing asphalt after 10 minutes. It can be due to the fact that tan(δ) was measured at –10º C, where the asphalt cements are more fluid and so reach their equilibrium gel structure more quickly. The second reason could be that tan (δ) represents a value of elastic modulus of a material, and is a good indicator of the tendency of asphalt cement to physically age at low temperatures.[69] Finally the third reason could be that tan (δ) is a better indicator than both the BBR specification parameters, S(60) and m(60), due to the fact that tan (δ) is a factor of ability of the material to relax stress in the free-thaw regimes.

5.3.1 Low Temperature Regime

As suggested by earlier research on low temperature cracking,[66] it is also important to consider the low temperature regime. The data as presented in Figure 26 were obtained on a set of recovered binders from current paving contracts for which the asphalt cements had already been specified for the particular climatic condition. Hence, it is conceivable that asphalt cements exist that have good freeze-thaw performance yet still fail due to their low temperature rheological properties being out of the acceptable range (differences in complex moduli (G*, G', and G") for binders of approximately equal tan(δ) were found to be significant).

To understand better the relation between the low temperature rheological properties and the degree of cracking, the temperature at which tan(δ) reaches a lower limit of 0.3 was measured. Since the torsion bars are unlikely to fail in a brittle manner, which could happen at a lower temperature, a limit tan(δ) of 0.3 chosen. The determination of a limiting tan(δ) was done after pouring and after 72 hours of condition at -10º C.

The torsion bar specimens were tested at –6, –12, –18, –24 and –30º C with soak times of 30 minutes at each temperature. Figures 27 demonstrates the correlation between cracking severity and the low temperature grading according to limiting tan(δ) of 0.3, relative to the required grade temperature based on the LTTPBind© software specifications (LTPPBind, v. 2.1, 1999) for each sample.[63] As expected, all contracts that have a high level of grade loss perform poorly, while those with a surplus are supposed to perform well. Comparison between figure 27a and figure 27 b show that the ability of the limiting temperature at which tan (δ) reaches 0.3 to predict failure increase from 30 minutes to three days of conditions. This result is in agreement with the result given in figure 23 and 24.

Besides, in agreement with the results of BBR in figure 24, the spread in limiting temperature increase after three days of conditioning. A larger spread will present more accurate

grading results provided the standard deviation (random error) in the measurement is not affected by the increased conditioning time.

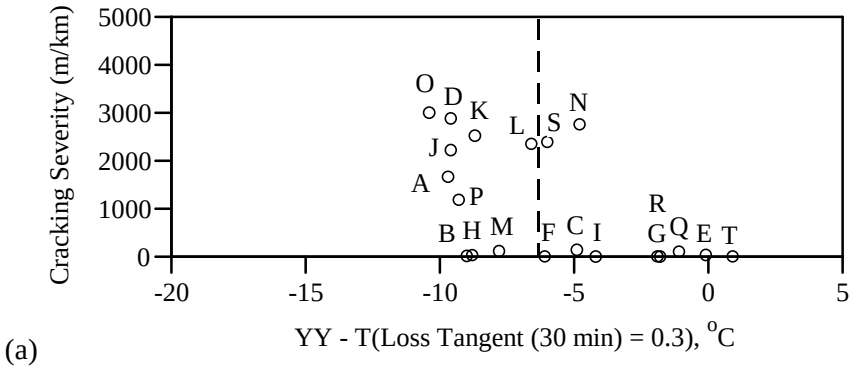

(a)

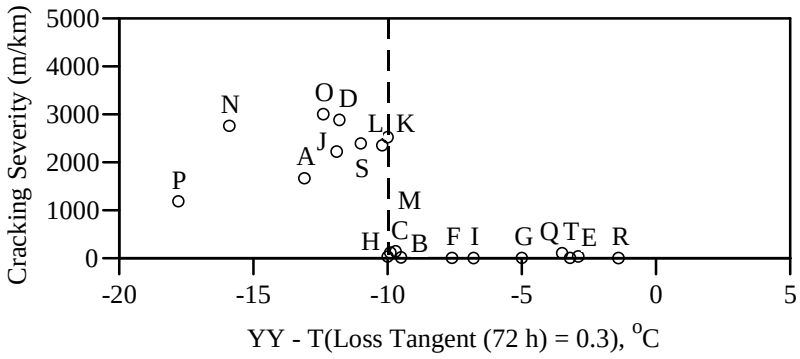

(b)

Figure 27. Comparison of tan(δ) grading results: (a) Temperature where tan(δ) reaches 0.3 after conditioning at test temperature; and (b) Temperature where tan(δ) reaches 0.3 after 72 h of conditioning at –10ºC.

A graph of three day grade loss at -10°C, according to DSR procedures, versus the distress in pavements is plotted in figure 28. A comparison between this graph and figure 25 demonstrates that the DSR grading temperature result differs from the extended BBR grading results in that there is no correlation between the loss in tan (δ) grade temperature over three days

of conditioning in the DSR. However, in the extended BBR there is strong relation between the grade losses for each sample after three days of conditioning. The importance of this difference in the DSR is still unclear and the issue needs to be further investigated.

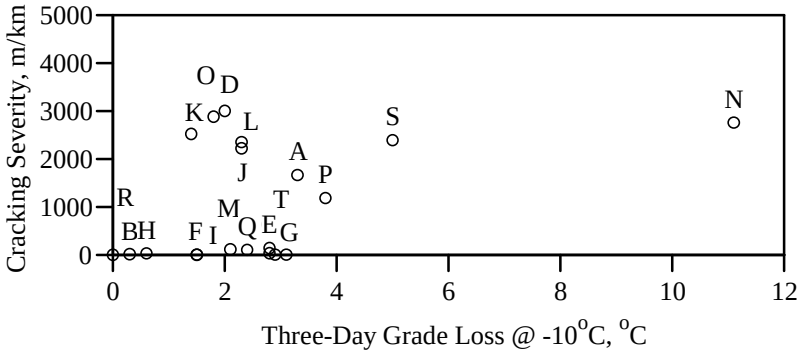

Figure 28. Three days grade loss for limiting tan (δ) reaches 0.3 after 72 h of conditioning at –10ºC.

5.3.2 Source of Errors

Error should be taken into consideration for all tests performed for the purpose of this thesis. In terms of sample preparation, in particular, the removal of the sample from the mold required the careful use of a razor. In doing this, unseen deformation may have been occurred. Furthermore, small notches could have been created along the edges of the sample when the teflon from the surface has been removed. Moreover, sample handling, equipment calibration, temperature control and mesurement are another source of uncontroled errors.

5.3.3 Analysis of Accuracy and Precision

Numerous new test methods for specifying asphalt binders have been proposed in the past few years. Ideally for a test method to be widely accepted, the results of the method have to be not only accurate but also precise. The accuracy is defined by the number of times that a measurement is able to correctly predict a certain outcome (i.e., in this study good or poor pavement performance). The precision is the way in which the individual grading results can be reproduced. The precision in this work is influenced by uncontrolled variables such as errors in sample preparation/handling, equipment calibration, temperature control, and measurement.

A summary of the accuracy and errors of all grading methods is given in Table 6. For all measurements, the accuracy is defined by the number of times the method was able to correctly predict either good or poor performance. The table also lists the ability of each method to predict either good or poor performance independently. The standard deviations given are those obtained by pooling different sets of data where n is the total number of test results used and k is the total number of data sets that are pooled in each instance. Individual results that were at least three pooled standard deviations away from the average for the other data in a given data set were deemed ‘obvious outliers’ and were not included in the determination of the pooled standard deviation.

Pooled standard deviation has been calculated from the following equation where n is Number of individual tests and k is the Number of data sets.

$$s_p = \sqrt{\frac{(n_1 - 1)s_1^2 + (n_2 - 1)s_2^2 + \cdots + (n_k - 1)s_k^2}{n_1 + n_2 + \cdots + n_k - k}}$$

The analysis shows that the pooled standard deviation is not significantly different for any of the grading methods. This suggests that those methods that are done after three days of conditioning

are preferred given that they spread out the grading results more widely in a manner that is consistent with the observed performance in service. Also, the accuracy of the tests after three days is definitely much improved in LS-308 and for the limiting temperature where tan(δ) reaches 0.3 while the spread increases significantly for all tests utilizing an extended conditioning period prior to testing.

Table 6. Analysis of Accuracy and Precision for Regular BBR (AASHTO M320), Extended BBR (LS-308) and Torsion Bar Method

	AASHTO M320	LS-308	Limiting T(tan(δ) = 0.3)	
Conditioning time, h	1	72	0	72
Accuracy, %	55	90	75	90
Ability to predict poor performance, %	0	100	66	78
Ability to predict good performance, %	100	82	82	100
Range, ºC	11.3	20.0	11.3	14.5
Pooled standard deviation, ºC	0.3	0.5	1.0	1.0
Number of individual tests (n)	51	61	33	41
Number of data sets (k)	14	29	13	17
Pooled Standard Deviation/Range	0.03	0.02	0.09	0.07

5.4 Ductile Failure Testing

The ductile failure properties according to Ontario's recently developed double-edge-notched tension method[31] LS-299 were determined and the LS-299 DENT results are provided Figure 29. The BBR and DSR results as provided in Figures 24-27 show that for binders of nearly the same

limiting temperatures there can still be significant differences in cracking distress. It is believed that this is due to differences in strain tolerance as already suggested by Rader and Ochalek.[66] LS-299 measures the strain tolerance by extrapolating the specific total work of fracture to a small ligament length and dividing the essential work so obtained by the net section stress at a 5 mm ligament.[33] The property obtained is an approximate critical crack tip opening displacement (CTOD) and it is believed to add a second layer of protection given the fact that it excludes materials that are exceptionally strain intolerant in the presence of severe constraint (i.e., in asphalt mixtures). Certain asphalt cements that are modified with gelling agents can pass a low strain rheological test but will most certainly fail a high strain failure test such as described in LS-299. The results within the dashed line in Figure 29 show that all binders made with problematic modification technology perform very poorly in the DENT test. Asphalt cements recovered from all sites were tested for phosphorous in a nuclear magnetic resonance spectrometer, with those obtained from Sites A, J, K, P and S testing positive, suggesting that these were modified with polyphosphoric acid. This additive is known to seriously limit the strain tolerance in the ductile state,[37] which showed up as premature and excessive cracking. The same asphalts are penalized under a specification that would be based on a limit in tan(δ) equal to 0.5.

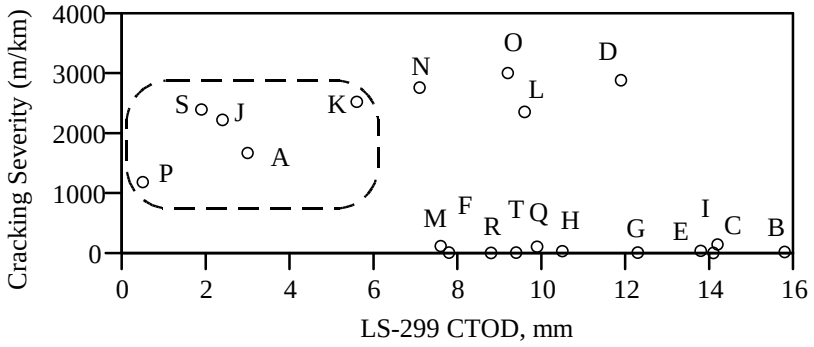

Figure 29. Ductile failure properties as measured in double-edge-notched tension test and approximated by critical crack tip opening displacement (LS-299 CTOD).[1]

Chapter 6
Characterization of Modified Asphalt by Dynamic Shear Rheology

6.1 Results and Analysis

6.1.1 Torsion Bar Results

The Black space diagram and Cole-Cole plots for each section after 1 hour and 24 hours of cooling at -20ºC can be seen in figures 30-41 and appendices 1-5. The results are also summarized in table 7.

As can be seen from the Black Space Diagram figures 20-37, smaller phase angle are observed for section 655-2 and 655-5 after 24 hours of cooling. On the other hand, sections 655-1 and 655-5 show greater phase angle after 24 hours of cooling shown in figures 35-37 compare to 1h of cooling shown in figure 34 and figure 36.The phase angles remained relatively the same after 1 hour of cooling and 24 hour of cooling for the remaining the test sections.

For the test section 655-1 and 655-5 the results from Cole- Cole plots show an increase in loss modulus from 1 hour of cooling to 24 hour of cooling figure 38 and figure 39. The loss modulus observed in the Cole-Cole plot in appendices 3-5 remained the same for Sections 655-2, 655-3, 655-5, 655-6, 655-7, However, decreased for section 655-2 shown in figures 1,2 of appendix 3.

Table 7. Change in Phase Angle and Loss Modulus Between 1 h and 24 h Conditioning Time.

Highway	The change in phase angle between 1 h and 24 h conditioning at -20ºC	The change in loss modulus between 1 h and 24 h conditioning at -20ºC
655-1	Increase	Increase
655-2	Decrease	No change
655-3	Decrease	No change
655-4	No change	Decrease
655-5	Increase	Increase
655-6	No change	No change
655-7	No change	No change

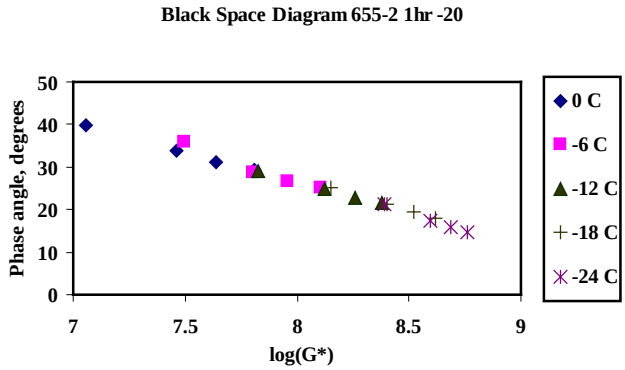

Figure 30. Black space diagram 655-2 1 h -20ºC

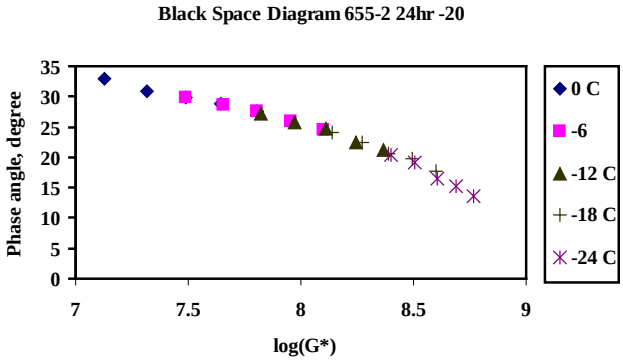

Figure 31. Black space diagram 655-2 24 h -20ºC

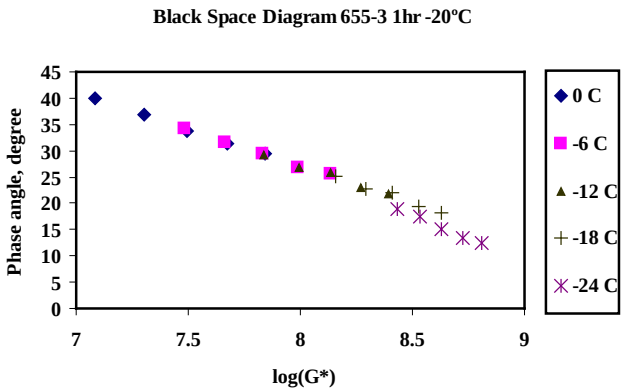

Figure 32. Black space diagram 655-3 1 h -20ºC

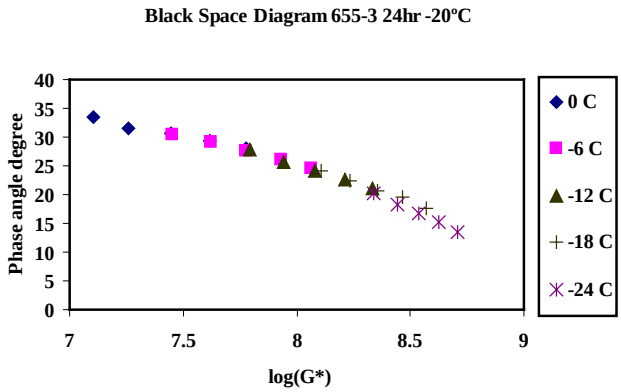

Figure 33. Black space diagram 655-3 24 h -20ºC

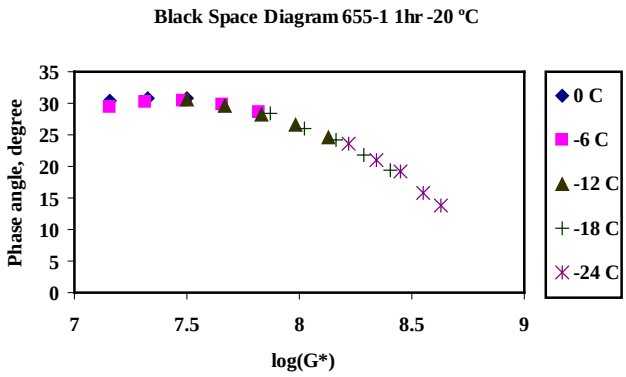

Figure 34. Black space diagram 655-1 1 h -20ºC

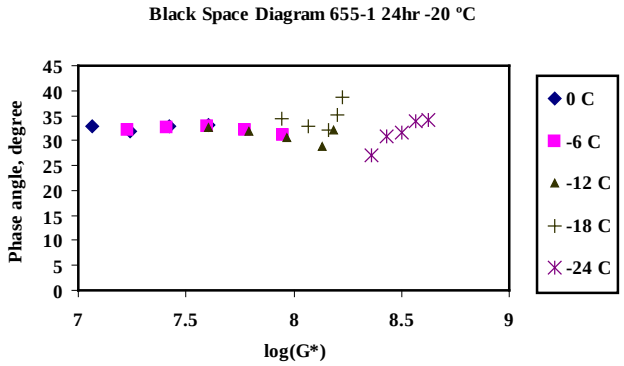

Figure 35. Black space diagram 655-1 24 h -20ºC

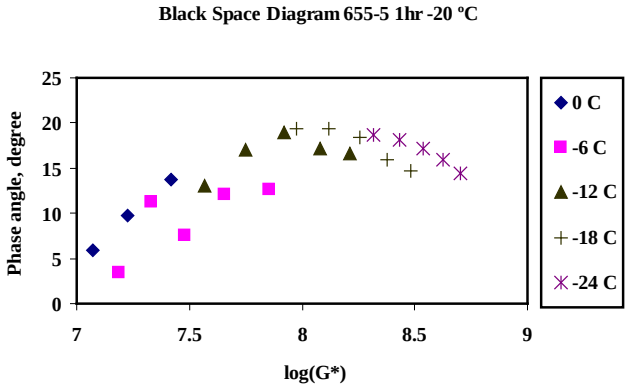

Figure 36. Black space diagram 655-5 1 h -20ºC

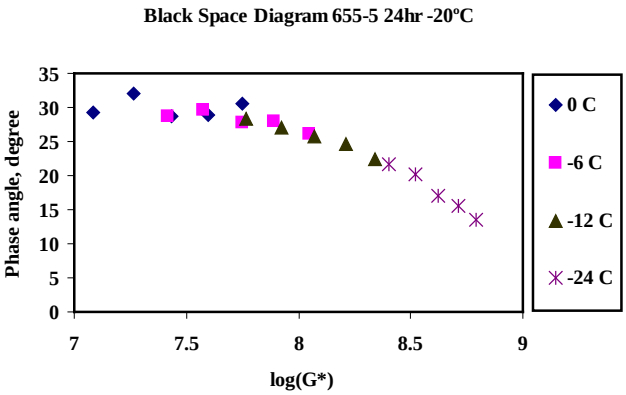

Figure 37. Black space diagram 655-5 24 h -20ºC

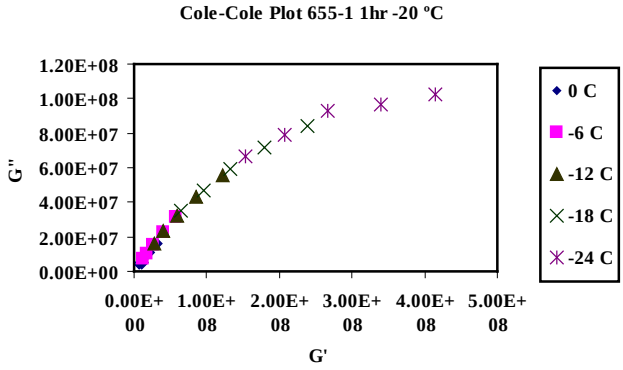

Figure 38. Cole-Cole plot 655-1 1 h -20ºC

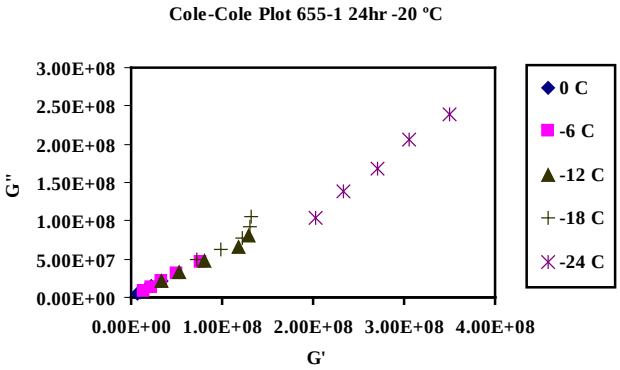

Figure 39. Cole-Cole plot 655-1 24 h -20ºC

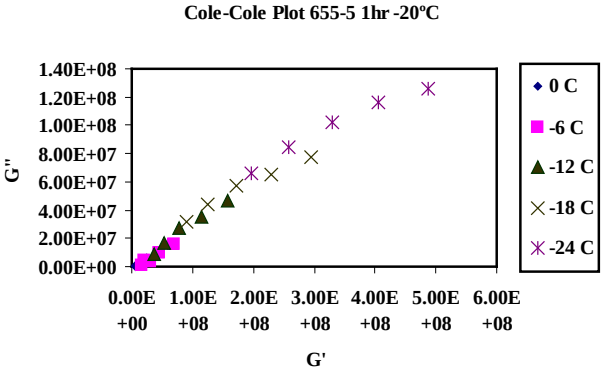

Figure 40. Cole-Cole plot 655-5 1 h -20ºC

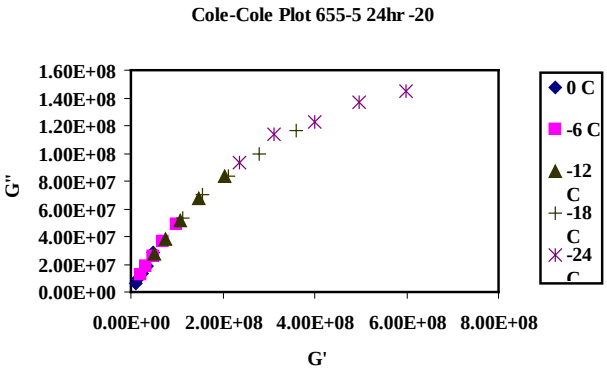

Figure 41. Cole-Cole plot 655-5 24 h -20ºC

6.1.2 Parallel Plate Results

The parallel plate results and torsion bar results after 24 hours of cooling were plotted together for each of the test sections shown in Appendices 6-16. The higher temperature data from parallel plate analysis followed the same trend as the lower temperature data from torsion bar analysis in the Black space diagrams, Cole-Cole plots and master curves for all test sections. As the temperature increased, the phase angle increased and the complex modulus decreased. Using Section 655-6 as an example, it can be seen that the high temperature plots are in high correlation with the low temperature plots such that a line could be accurately drawn through all of the data points. The compiled torsion bar and parallel plate Black space diagram, Cole-Cole plot, master curve frequency sweep and master curve phase angle for Section 655-6 are illustrated in Figures 1, 2, 3 and 4 of Appendix 14, respectively.

6.1.3 Overlaid Result

In order to compare the different test sections, overlaid Black space diagrams, Cole-Cole plots and master curves were generated shown in figures 42-45. From the overlaid Black space diagram shown in Figure 42, it can be seen that Section 655-1 has the greatest phase angle. Section 655-5 also shows relatively greater phase angle compared to the other test sections. On the other hand, Section 655-4 is seen to have a smaller phase angle in the Black space diagram. Section 655-2 shows the smallest phase angle in the Black space diagram.The order of phase angle can be summarized as follows:

655-1>655-5>655-3=655-6=655-7>655-4>655-2

From the overlaid Cole-Cole plot shown in Figure 43, it can be seen that Section 655-1 has the greatest loss modulus (G") exhibiting greater viscosity. Section 655-5 also shows relatively greater loss modulus compared to the other test sections. On the other hand, Section

655-4 lowest loss modulus compared to the other asphalt test sections in the Cole-Cole plot. Section 655-2, 655-3 shows mid-range loss modulus compared to the other test sections, but lower loss modulus for Sections 655-6 and 655-7 are seen in the Cole-Cole plot. According figure 43 the order of loss modulus can be summarized as follows:

655-1>655-5>655-3=655-6=655-7>655-4>655-2

The differences in phase angle and complex modulus can be seen more clearly in the overlaid master curves. The overlaid master curve frequency sweep is shown in Figure 44 and the overlaid master curve phase angle is shown in Figure 45.

Sections 655-1 and 655-5 have the lowest complex modulus observed in the graph of overlaid master curve frequency sweep Sections 655-2 and 655-3 show high and mid-range complex modulus in the graph of overlaid master curve frequency sweep. Section 655-3 demonstrates moderate complex modulus in the graph of overlaid master curve frequency sweep. Mid-range complex modulus is observed for Sections 655-6 and 655-7 relative to the other test sections in the graph of overlaid master curve frequency sweep. According figure 44, the order of complex modulus can be summarized as follows:

655-2>655-3=655-4=655-6=655-7>655-5>655-1

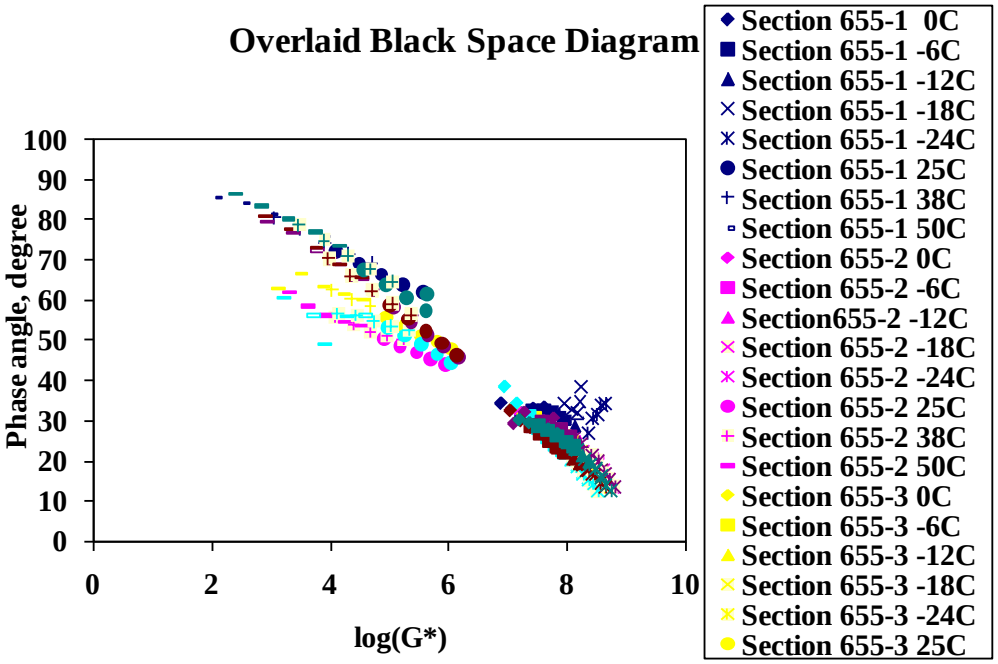

Figure 42. Overlaid black space diagram 655 field aged.

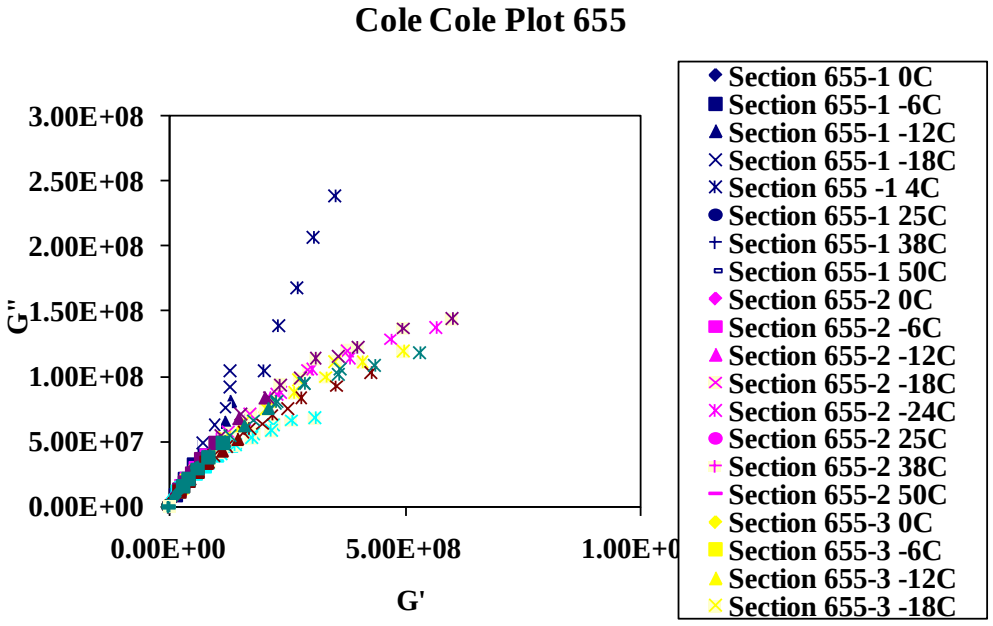

Figure 43. Overlaid Cole-Cole plot 655 field aged.

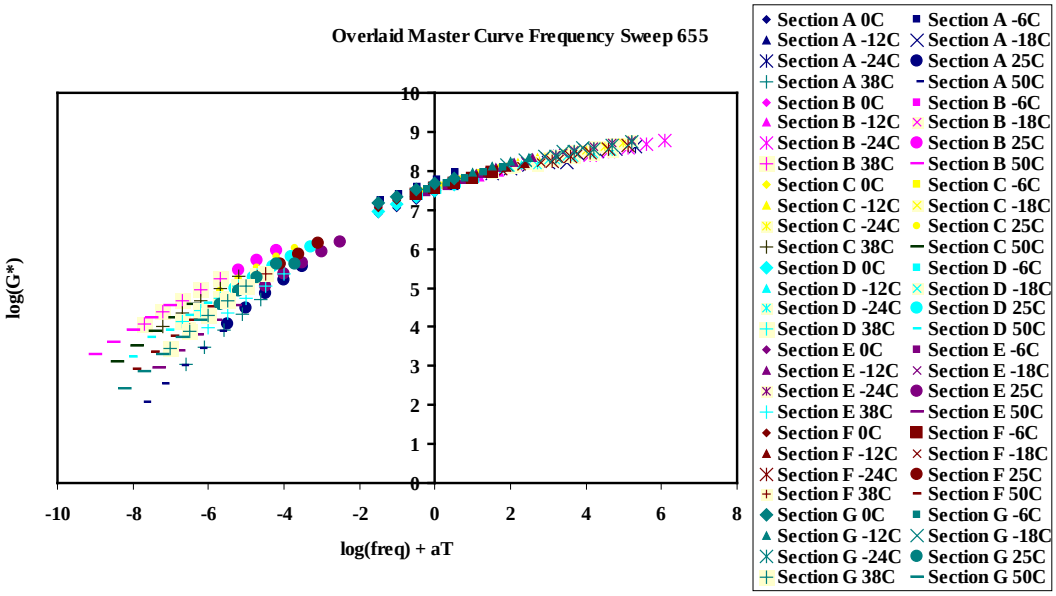

Figure 44. Overlaid frequency sweep master curve 655 field aged.

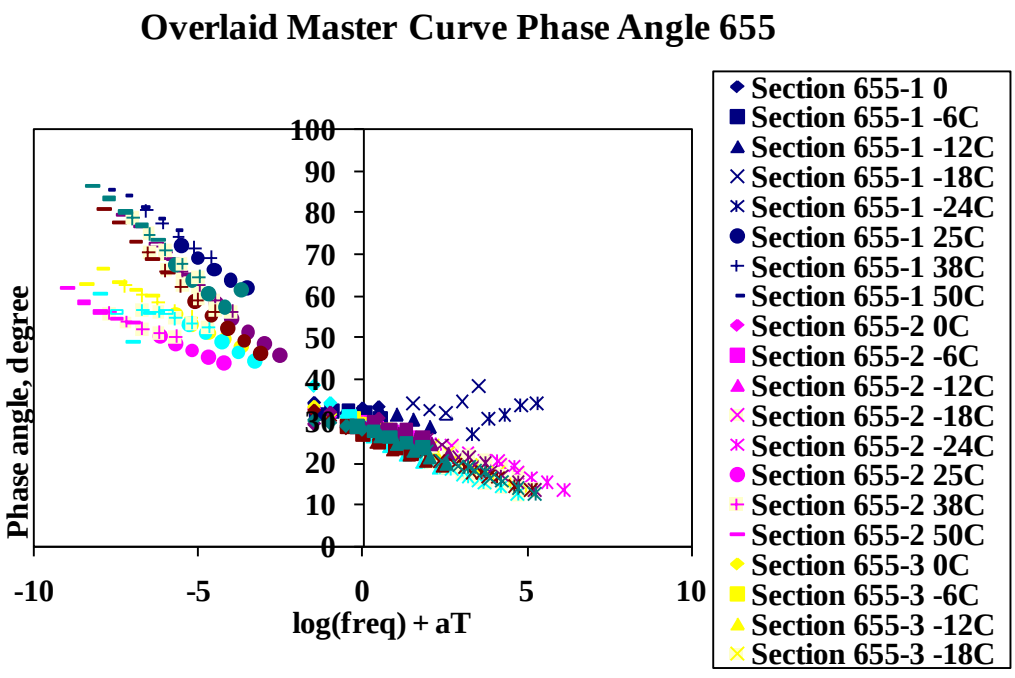

Figure 45. Overlaid phase angle master curve 655 field aged.

6.1.4 Cross-Sectional Results

For further comparison of the test sections, Black space diagrams and Cole-Cole plots were generated at -12°C, 0°C and 25°C shown in Figures 46-51. At -12°C, it can be seen that Section 655-1 has the greatest phase angle in the Black space diagram shown in Figure 46 and the greatest loss modulus in the Cole-Cole plot shown in Figure 49. Section 655-5 demonstrates the second greatest phase angle and loss modulus. Section 655-3 exhibits mid-range phase angle in the Black space diagram and loss modulus in the Cole-Cole plot. Section 655-2 and 655-4 demonstrate mid-range phase angle and loss modulus. The results show sections 655-6 and 655-7 have the smallest phase angle in the Black space diagram and loss modulus in the Cole-Cole plot. At 0°C, Section 655-1 shows greater phase angle in the Black space diagram shown in Figure 47 and high loss modulus in the Cole-Cole plot shown in Figure 50 while Section 655-5 showed mid-range phase angle and loss modulus. Section 655-4 showed mid-range phase angle and loss modulus. The lowest phase angle and loss modulus were observed for Section 655-6. Mid-range phase angle is seen in the Black space diagram and mid-range loss modulus is seen in the Cole-Cole plot for Section 655-2. Sections 655-3 and 655-7 show mid-range phase angle and loss modulus in the Black space diagram and Cole-Cole plot. At 25°C, Section 655-1 shows greater phase angle and loss modulus while Section 655-5 shows mid-range phase angle in the Black space diagram shown in Figure 48 and mid-range loss modulus in the Cole-Cole plot shown in Figure 51. Sections 655-2 and 655-4 demonstrate the smallest phase angles and loss modulus while Sections 655-6 and 655-7 show greater phase angles in the Black space diagram and higher loss modulus in the Cole-Cole plot. Mid-range values for phase angle and loss modulus were recorded for Section 655-3. The ranking of phase angle and loss modulus for section 655 are also summarized in table 8.

Table 8. The Ranking of Phase Angle and Loss Modulus for Section 655

Temperature	Ranking of Phase Angles at Respective Temperature	Ranking of Loss Modulus at Respective Temperature
-12.5(±0.5) ºC	655-1>655-5>655-3≈655-2≈655-4>655-6≈655-7	655-1>655-5>655-3≈655-2≈655-4>655-6≈655-7
0.0(±0.5) ºC	655-1>655-5>655-4≈655-2≈655-3≈655-7>655-6	655-1>655-5≈655-4≈655-2≈655-3≈655-7>655-6
25.0(±0.5) ºC	655-1>655-5≈655-3≈655-7≈655-6>655-2≈655-4	655-1>655-5>655-3≈655-7≈655-6>655-2≈655-4

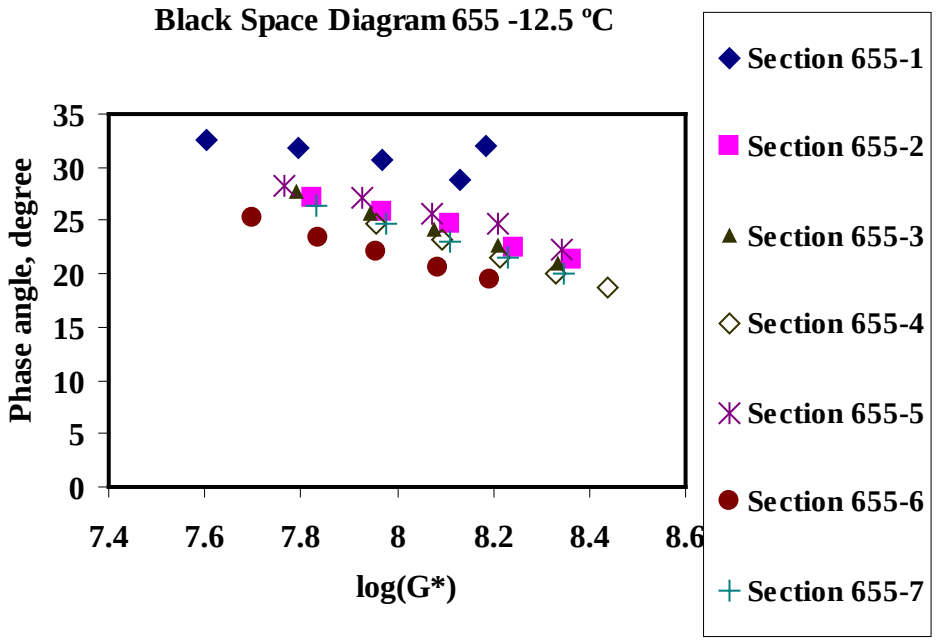

Figure 46. Black space diagram at -12.5ºC field aged.

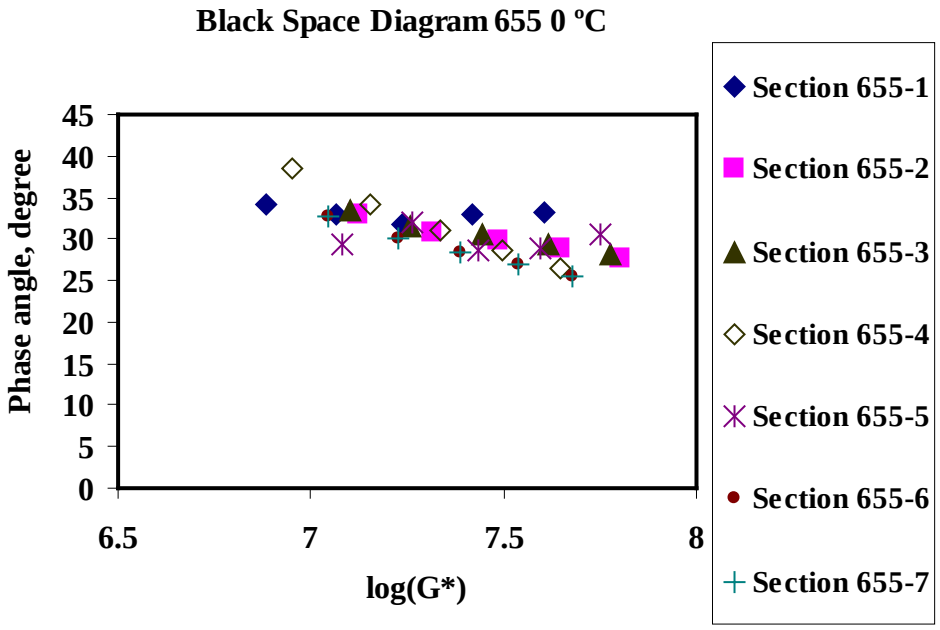

Figure 47. Black space diagram 0 ºC field aged.

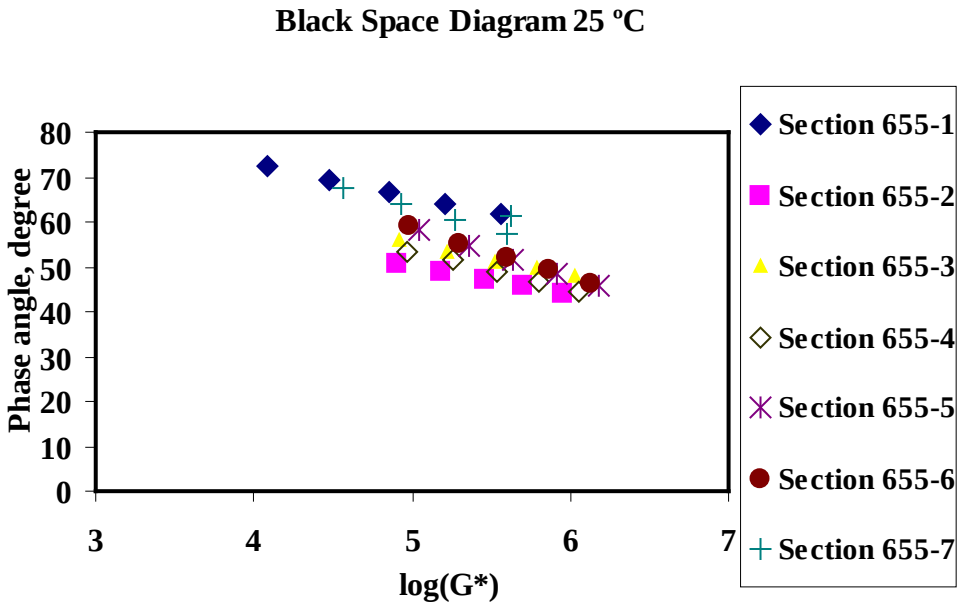

Figure 48. Black space diagram 25 ºC field aged.

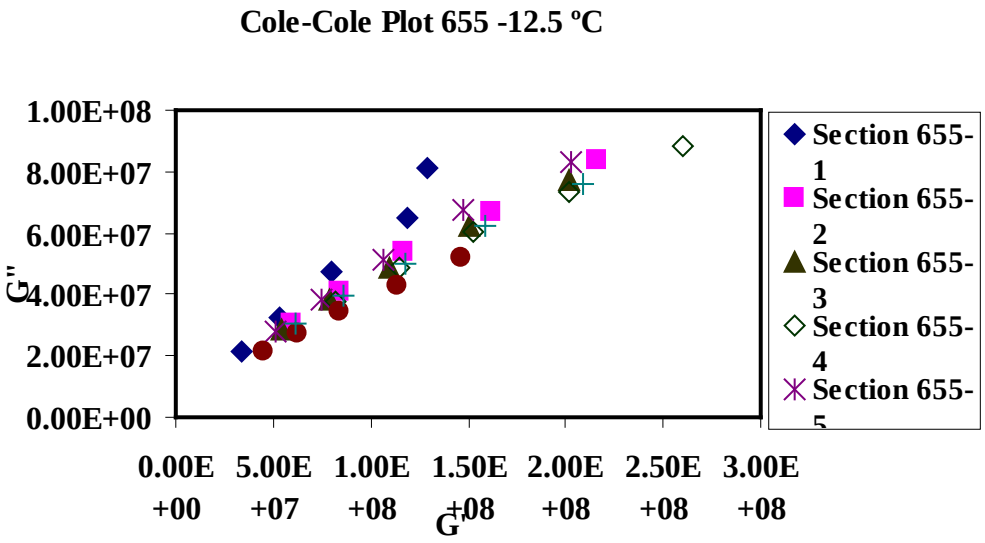

Figure 49. Cole-Cole plot at -12.5 ºC field aged.

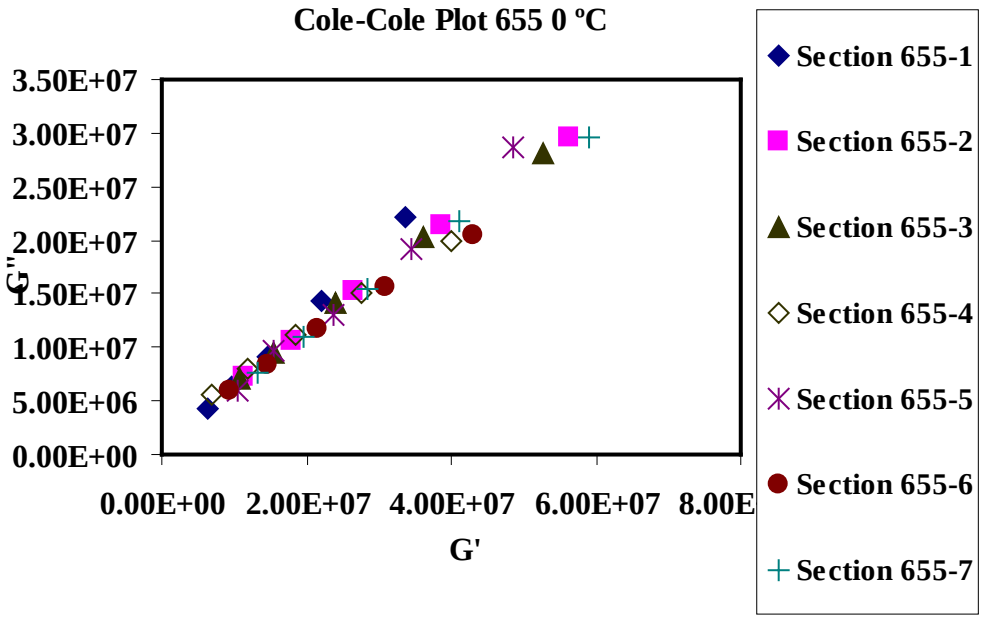

Figure 50. Cole-Cole plot at 0 ºC field aged.

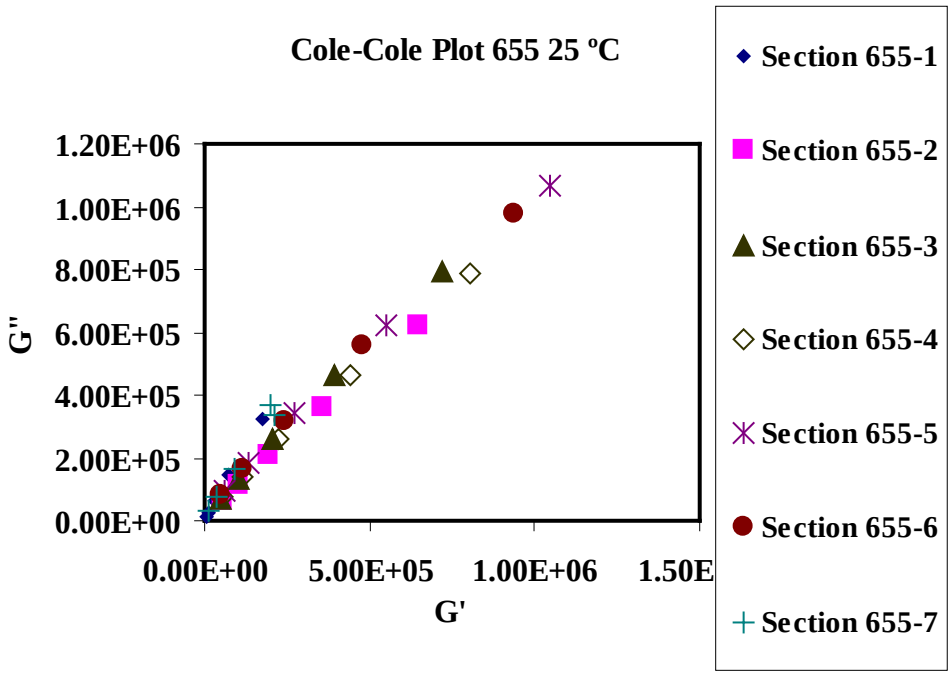

Figure 51. Cole-Cole plot at 25 ºC field aged.

6.1.5 Laboratory-Aged Material

Black space diagrams and master curve frequency sweep of the laboratory aged material are shown in Appendices 17-23. Section 655-1 seems to be rheologically simple as the Black space diagram shown in Figure 1 of Appendix 17 is a smooth curve with no jagged outliers or discontinuities. On the other hand, the Black space diagram for Section 655-2 shown in Figure 2 of Appendix 17 does not show a smooth continuous curve and may be rheologically complex. Relatively smooth curves can also be seen for Sections 655-3 and 655-7 in the Black space diagrams shown in Figures 1 and 2 of Appendix 18, respectively. From this it can be seen that these asphalts are rheologically simple. Discontinuities are observed in the Black space diagrams for Sections 655-4 and 655-5 shown in Figures 1 and 2 of Appendix 19, respectively

demonstrating rheologically complex materials. The Black space diagram for Section 655-6 appears to be fairly smooth with the exception of the outliers at 0ºC shown in Figure 1 of Appendix 20. The master curve frequency sweeps for all test sections shown in Appendix 20-22 show smooth, highly correlated curves.

For comparison to the field aged results, cross-sectional Black space diagrams and Cole-Cole plots for the laboratory aged material were produced at 0ºC and 25ºC. At 0ºC, Sections 655-1 and 655-5 have greater phase angles shown in Figure 1 of Appendix 23. Section 655-2 and 655-6 show the smallest phase angle. Sections 655-3, 655-4 and 655-7 all show mid-range phase angle.

At 25ºC, Section 655-7 shows the greatest phase in the Black space diagram as can be seen in Figure 2 of Appendix 23. Sections 655-1, 655-3 and 655-5 also show moderate to large phase angles in the Black space diagram. Sections 655-2 and 655-6 demonstrate the smallest phase angles in the Black space diagram.

For comparison to the field aged results, cross-sectional Cole-Cole plots for the laboratory aged material was produced at 0ºC and 25ºC. At 0ºC, Sections 655-1 and 655-5 have greater high loss modulus shown in Figure 3 of Appendix 23. Section 655-2 and 655-6 show the smallest loss modulus. Sections 655-3, 655-4 and 655-7 all show mid-range loss modulus. At 25ºC, Section 655-7 shows the greatest high loss modulus in the Cole-Cole plot as shown in Figure 4 of Appendix 23. Sections 655-1, 655-3 and 655-5 also show moderate to large phase angles in the loss modulus in the Cole-Cole plot. Sections 655-2 and 655-6 demonstrate the smallest loss modulus in the Cole-Cole plot.

Table 9. The Ranking of Phase Angles and Loss Modulus at Respective Temperature

Temperature	Ranking of Phase Angles at Respective Temperature	Ranking of Loss Modulus at Respective Temperature
0.0(±0.5) ºC	655-1>655-5>655-3 ≈655-4≈655-7>655-6≈655-2	655-1>655-5>655-3 ≈655-4≈655-7>655-6≈655-2
25.0(±0.5) ºC	655-7> 655-3≈655-1≈655-4≈655-5 > 655-2 ≈655-6	655-1>655-5>655-3 ≈655-4≈655-7> 655-6≈655-2

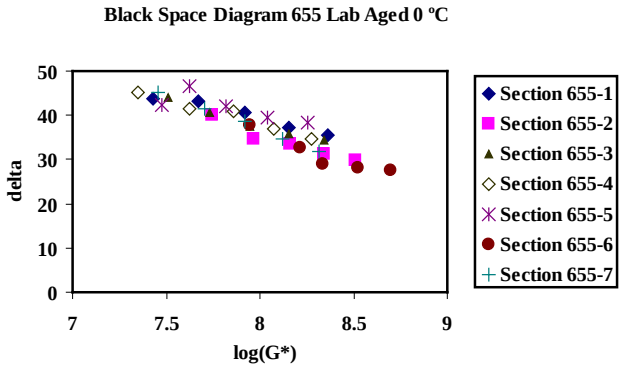

Figure 52. Black space diagram 0 ºC laboratory aged.

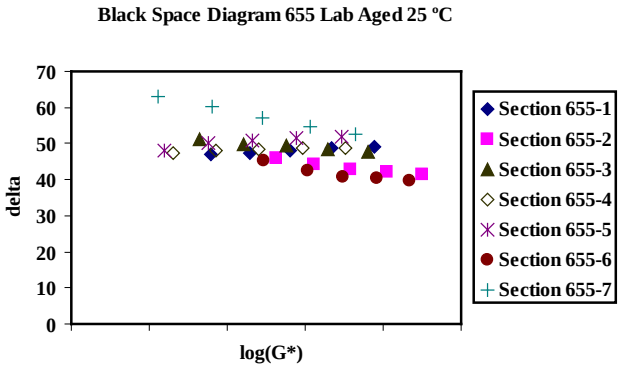

Figure 53. Black space diagram 25 ºC laboratory aged.

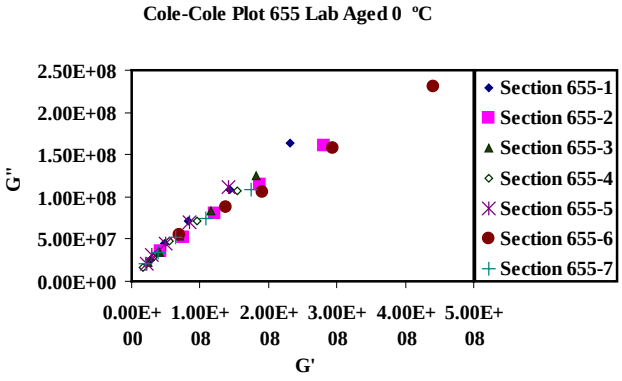

Figure 54. Cole-Cole plot at 0 ºC laboratory aged.

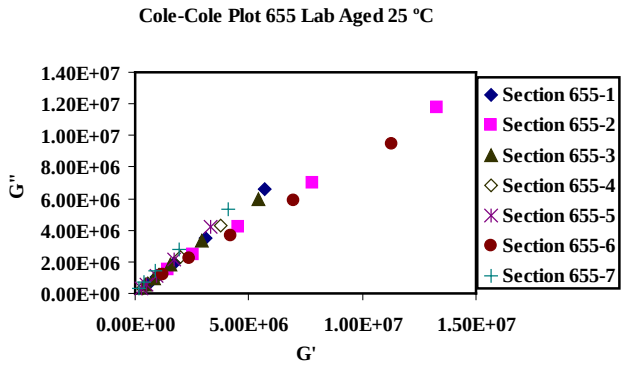

Figure 55. Cole-Cole plot at 25 ºC laboratory aged.

6.2 Discussion

6.2.1 Reversible Ageing of Binders at Low Temperatures

Past research of reversible ageing of binders at low temperature has shown that all binders lose a considerable amount of performance during cold storage. In particular, binders that provide superior performance in field analysis are linked to low tendency for reversible ageing during cold storage. It has also been observed that air-blown asphalts exhibit a strong tendency to age harden during cold storage.[70] From the results, it can be seen that Sections 655-2 and 655-3 did not perform well in the field analysis and show decreased phase angles after 24 hours of cooling compared to 1 hour of cooling. These results confirm the conclusions of past research. Sections 655-1 and 655-5 performed best in the field analysis and show increased phase angle after 24 hours of cooling compared to 1 hour of cooling. It is expected that these samples show low tendency for reversible ageing during cold storage and that they would perform better. Sections 655-6 and 655-7 showed moderate cracking in the field analysis but the results did not show considerable differences in the phase angle between 1 hour and 24 hours of cooling. As these test sections did not perform exceedingly well in field analysis it was expected that greater reversible ageing would have been observed during cold storage. Section 655-4 performed worst in the field analysis showing severe cracking beyond repair. However, this test section did not show any signs of reversible ageing after cold storage showing closely the same phase angle in both the Black space diagram after 1 hour and 24 hours of cooling. Both Sections 655-2 and 655-6 were oxidized prior to paving. However, only Section 655-2 demonstrated a strong tendency for reversible ageing during cold storage. Many asphalt binders undergo structural changes at low temperatures that could result in deteriorated performance although the molecular events are poorly understood. Some factors that are thought to play roles in the deterioration of properties when binders are stored for extended periods at low temperatures include wax crystallization, free

volume collapse, asphaltene aggregation, and perhaps other interactions.[70] The results show that structural changes during cold storage may have occurred to affect the performance of the binders. In the case of Sections 655-1 and 655-5, the changes might have even positively influenced the performance. However, no differences in behavior were observed for many of the test sections. Perhaps greater prevalence of reversible ageing might be observed for all test sections if the samples were compared after a longer period of cooling such as 72 hours instead of 24 hours or at lower temperatures.

6.2.2 Viscoelastic Behaviour and Performance

The expected viscoelastic behavior is that asphalts that perform better in field analysis exhibit greater phase angles relative to the other test sections and that asphalts that perform poorly have smaller phase angles. It can be seen that Section 655-1 performed best in the field analysis showing no cracks and is in almost perfect condition. In the field aged results Section 655-1 demonstrated a greater phase angle relative to the other test sections at -12ºC, 0ºC and 25ºC. In the laboratory aged results a greater phase angle was observed at 0ºC, however, a smaller phase angle was observed compared to the other asphalts at 25ºC. The results for Section 655-1 were consistent with the expected rheological behavior with the exception of the laboratory results at higher temperature. Section 655-2 performed poorly in the field analysis demonstrating considerable cracking. At higher temperatures in the field aged results, 0ºC and 25ºC, Section 655-2 showed a smaller phase angle relative to the other asphalts. However, at lower temperature Section 655-2 demonstrated a relatively greater phase angle compared to the other test sections. In the laboratory aged results a small phase angle was observed for Section 655-2 at both 0ºC and 25ºC. With the exception of the field aged results at lower temperature, the results for Section 655-2 were consistent with the expected rheological behavior. Moderate cracking was observed for Section 655-3 in the field analysis. In both the field aged and laboratory aged material results

for all temperatures mid-range phase angles were observed for Section 655-3. These results were consistent with the expected rheological behavior. Section 655-4 performed the worst in field analysis showing severe cracking beyond repair. Lower phase angles were observed for the field aged material at -12ºC and 25ºC. However, mid-range phase angle was observed for the field aged material at 0ºC and the laboratory aged material at both 0ºC and 25ºC. These results were not consistent with the expected rheological behavior. This test section performed significantly more poorly than the other test sections, however, the results did not show considerable differences in the phase angle compared to the other test sections. Section 655-5 also performed very well with little cracking observed in the field analysis. For the field aged material at -12ºC and 0ºC a greater phase angle was observed relative to the other asphalts. However, at the higher temperature, a smaller phase angle was observed for this section. For the laboratory aged results greater phase angles were also observed for Section 655-5. With the exception of the field aged results at 25ºC, these results were consistent with the expected rheological behavior. Section 655-6 performed moderately well showing some cracking in the field analysis. However, the results show very small phase angle in both the field aged results at -12ºC and 0ºC and laboratory aged results at 0ºC and 25ºC. However, a greater phase angle was observed for the field aged results at 25ºC. These results were not consistent with the expected rheological behavior. Section 655-7 also demonstrated moderate cracking in the field analysis. However considerably smaller phase angles were observed for the field aged material at -12ºC and 0ºC while a considerably greater phase angle was observed for Section G at 25ºC. In the laboratory aged results Section 655-7 demonstrated a smaller phase angle at 0ºC but a considerably greater one at 25ºC. These results were also not consistent with the expected rheological behavior. From the results it can be seen that binders chemically harden considerably faster in the field than what is achieved through laboratory ageing protocol. It can also be seen that the low temperature phase angle appears to be

a reasonable indicator of performance. However it should be used in conjunction with other test methods as a measurement for performance.

6.2.3 PG Grade and Performance

The low temperature PG grade value was of particular interest for this study with the application to road performance in Ontario because it represents the lowest temperature that the asphalt is expected to perform. It was expected that asphalts with a greater low temperature value would perform better in the field and demonstrate a greater phase angle at lower temperatures. Section 655-1 had the lowest low temperature PG grade value of -37ºC and performed best in the field analysis showing no cracks and was in almost perfect condition. The results show that this asphalt also demonstrated the greatest phase angle relative to the other asphalts in the field aged results at -12ºC. The results were consistent with the expected performance of this test section. Section 655-3 had the next lowest low temperature PG grade value of -36ºC. However, this section showed moderate cracking in the field analysis and demonstrated a mid-range phase angle in the field aged results at -12ºC. These results were not consistent with the expected performance of this test section. The remaining test sections all had a low temperature PG grade value of -35ºC. Although they were all expected to perform relatively equally at lower temperatures, differences in their performances were observed. Section 655-5 demonstrated a greater phase angle than the other test sections in the field aged results at -12ºC and also performed significantly better than the other test sections in the field analysis showing almost no cracks. Sections 655-2 and 655-4 performed very poorly in field analysis showing significant cracking relative to the other test sections. However, the low temperature PG grade value was the same as other test sections that performed significantly better. They also demonstrated mid-range to greater phase angle in the field analysis at -12ºC. These results were not consistent with the expected performance of these

test sections. Conversely, Sections 655-6 and 655-7 had the same low temperature PG grade value and demonstrated moderate cracking in the field analysis. These test sections also showed the lowest phase angle relative to the other test sections in the field aged results at -12ºC. These results were also not consistent with the expected results for the performance of these test sections. Based on the results, it can be seen that the PG grade is not a good measure for the low temperature cracking behavior of asphalt materials. The findings of this study confirm the results of the Lamont trial as differences in performance were observed for binders of nearly the same low temperature PG grade.[71]There is need for investigation of improved low temperature asphalt binder specification methods to determine the expected field performance of asphalts.

6.2.4 Asphalt Modifier and Performance

Section 655-1 performed best seen in almost perfect condition with cracking severity of 10 m/150 m as shown in field analysis. Section 655-1 was modified with reactive ethylene-butyl acrylate-glycidyl methacrylate terpolymer (RET) and polyphosphoric acid (PPA). The use of RET in conjunction with PPA has proven an effective binder for asphalt modification shown by superior performance of this test section in field analysis. There is no evidence that PPA has affected the low temperature performance of the asphalt cement while RET has effectively prevented the phase separation of the polymer and the asphalt. Sections 655-2 and 655-6 were both oxidized prior to paving and demonstrated cracking severities of 233 m/150 m and 80 m/150 m, respectively in the field analysis. Other factors may have contributed to the significantly poorer performance of Section 655-2 compared to Section 655-6. Sections 655-3, 644-4 and 655-7 were found to contain zinc as detected by X-ray fluorescence (XRF) and traces of phosphorous as detected by nuclear magnetic resonance (NMR). It was found that waste engine oil had been added to these sections. The concentration of used oil flux was around 15 % for the Section 655-4 and this section performed the worst in the field analysis demonstrating cracking severity of 437

m/150m. However, the concentration of used oil flux was around 8-10 % for section 655-3 and 655-7, 655-7 performed lightly better than section 655-3 with cracking severity 93 m/150 m and 233 m/150 m, respectively. It is known that iron and other metals catalyze the decomposition of hydroperoxides. Hence, the presence of metals in waste engine oil additive is likely to blame for an accelerated oxidative aging reaction. Further more, waste engine oils are thought to weaken the asphalt cement-aggregate interface[72], and PPA is found to lower the ductile strain tolerance[37] and, hence, these additives could therefore be blamed in large part for the poor performance of these sections.

6.2.5 Error Analysis

Possible sources of error include structural design issues, chemical ageing effects and physical and steric ageing effects. Design issues such as variations in the pavement thickness, void content and asphalt cement content could have contributed to errors in the results. However, as shown in Table 1 of Appendix 23, there was very little variation in any of the properties and were expected to contribute minimally to the affect of the results.[33] Chemical ageing effects include the tendency of each binder to chemically harden and the variability of ageing with depth in the pavement. Volatilization, oxidation and moisture damage can also be included as possible sources of chemical ageing. The degree to which the different binders suffer from physical and steric ageing may have also affected the results of the experiment. Increased cracking severity of the asphalt may have been induced by thermal, spring thaw or traffic.[61]

Chapter 7
Summary and Conclusions

Based on the materials, experimental procedures, results and discussions in this thesis, the following summary and conclusions are given:

- The current low temperature asphalt cement specification as embodied in AASHTO standard M320 needs to be improved as asphalts with the exact same AASHTO M320 grade are found to show very different field performance.
- The physical hardening aspect, which is totally missed out in AASHTO M320 is captured in LS-308. The poor performance asphalt loss more grade than the good performers in LS-308.
- Extended conditioning periods improved both accuracy and relative precision (i.e., standard deviation/range) of the investigated grading tests for thermal cracking.
- The double-edge-notched tension test results show that the relative ranking agrees reasonably well with the field performance and also provides an added layer of safeguard in a low temperature specification.
- Both the loss tangent at –10ºC and the limiting temperatures at which the loss tangent reached 0.3 after 72 h of low temperature conditioning appear to be good indicators for performance with respect to thermal cracking, however, it should not be used as a sole measurement for performance.
- Reversible aging (hardening) mechanisms (wax crystallization, asphaltene structuring/gelation, free volume collapse, etc.) are likely an important cause of premature and excessive cracking in present day asphalt pavements.
- Chemical hardening is seen to occur much faster in the field than through laboratory ageing methods.

References

(1) Hesp, S. A. M.; Soleimani, A.; Subramani, S.; Marks, P.; Philips, T.; Smith, D.; Tam, K. K. *Int. J. Pavement Eng.* **2009,** *10(3),* 209.

(2) Soleimani, A.; Walsh, S.; Hesp, S. A. M. *J. Transportation Res. Board, Transportation Res. Rec.* **2009,** 17.

(3) Committee for the Strategic Highway Research Program 2: Implementation, *Transportation Research Board* **2009**, *Special Report 296*, 9.

(4) Simon, A. M. H. Longer Lasting Roads. *http://www.nserc-crsng.gc.ca/Partners-Partenaires/ImpactStory-Reussite_eng.asp?ID=1002*. (Accessed August 2009).

(5) Delgadillo, R.; Nam, K.; Bahia, H. Rutting and Fatigue Specifications for Asphalt Binders. http://www.engr.wisc.edu/centers/wsmtl/WSMTL-WEB-pg02P-NEWS-Delgadillo.htm. *(Accessed August 2009).*

(6) Booij, H. C.; Thoone, G. P. *Rheol. Acta.* **1982,** *21*, 15.

(7) *American Society for Testing and Material D8 Standard Terminology Relating to Material For Road and Pavement* **2002**.

(8) Goring-Morris, A. N. *J. Isr. Preh. Soc.* **1991,** *24*, 77.

(9) Forbes, R. J. *Stud.Anc. Technol.* **1964,** *4,* 98.

(10) Abraham, H. In Asphalts and Allied Substances: Industrial raw materials; Van Nostrand, Prinston: New Jersy, 1961; Vol. 1.

(11) Nasir Khusrau, I. In *Dairy of a Journey Through Syria and Palestine;* PPTS, London: 1896.

(12) Pliny In *Nature History,* English translation by H. Rackham, Harvard University Press: Cambridge, Mass, 1978.

(13) Walsh, J. *Geographical Club of Philadephia Bull.* **1924,** *25*, 92.

(14) Nissenbaum, A. *Rev. Chem. Eng.* **1993,** *9*, 365.

(15) Gernsheim, H. In *The History of Photography;* Thames, H., Ed.; London, 1969.

(16) *http://www.britannica.com/EBchecked/topic/505109/road/71907/New-paving-materials*. (Accessed August 2009).

(17) Meyer, R. F.; De Witt, W. *U. S. Geo. Sur. Bull.* **1991,** *1944*, 14.

(18) *The Asphalt Handbook;* 7th Edition, Ed.; Asphalt Institute: USA, 2007.

(19) Petersen, J. C. *J. Transp. Res. Board.* **1984,** *999*, 13.

(20) Schweyer, H. E.; Chelton, H.; Brenner, H. H. *Proc. Assoc. Asphal.. Paving. Technol.* **1955,** *24*, 3.

(21) Middleton, W. R. *ACS. Symp.* **1958,** *3*, A-45.

(22) Corbett, L. W.; Swarbrick, R. E. *Pro. Am. Assoc. Asphalt. Paving. Technol.* **1958,** *27*, 107.

(23) Read, J.; Whiteoak, D. In *The Shell Bitumen Handbook, Fifth edition;* Hunter, R. N., Ed.; Thomas Telford: London, 2003; pp 29.

(24) *http://training.ce.washington.edu/PGI/*. (Accessed August 2009).

(25) Anderson, D. A.; Christensen, D. W.; Bahia, H. U.; Dongré, R.; Sharma, M. G.; Antle, C. E.; Button, J. **1994,** *Volume 3: Physical Characterization. Report SHRP-A-369.*

(26) Anderson, D. A.; Kennedy, T. W. *J. Assoc. Asphalt Paving Technol.* **1993,** *62*, 481.

(27) AASHTO M320, Standard Specification for Performance –Graded Asphalt binder, Ed.; In American Association of State Highway and Transportation Officials: Washington D.C., 2002.

(28) Ministry of Transportation of Ontario *LS-308 – Method of Test for Determination of Performance Grade of Physically Aged Asphalt Cement Using Extended Bending Beam Rheometer (BBR) Method. Revision 23 to MTO Laboratory Testing Manual* **February 2006**.

(29) Andriescu, A. Essential work of fracture approach to fatigue grading of asphalt binders. PhD. Thesis, Queen's University, Canada, 2006.

(30) Andriescu, A.; Hesp, S. A. M. *Int. J. Pavement Eng* **2009,** *10(4)*, 229.

(31) Mai, Y. W.; Wong, S. C.; Chen, H. C. In *Application of Fracture Mechanics for Characterization of Toughness of Polymer Blends, in Polymer Blends;* Paul, D. R., Bucknall, C. B., Eds.; Wiley and Sons, Inc.: 2000; Vol. 2.

(32) Luna, P.; Bernal, C.; Cisilino, A.; Frontini, P.; Cotterell, B.; Mai, Y. *Polymer*. **2003**, *44*, 1145.

(33) Bodly, T.; Andriescu, A.; Hesp, S. A. M.; Tam, K. *J. Assoc. Asphalt Paving Technol.* **2007,** *76*, 345.

(34) Ministry of Transportation of Ontario. *LS-299 – Method of Test for Asphalt Cement's Resistance to Fatigue Fracture Using Double-Edge-Notched Tension Test (DENT), Revision 23 to MTO Laboratory Testing Manual*, **February 2006.**

(35) Brule, B. Polymer-Modified Asphalt Cement Used in the Road Construction Industry: Basic Principles. In *Asphalt Science and Technology;* Usmani, A. M., Ed.; New York, Basel, Hong kong, 1997; pp 463.

(36) Anderson, K. O.; Hussain, S. R.; Jardine, K. G. *Proc. Can. Tech. Asphalt Assoc.* **1989,** *34*, 292.

(37) Kodrat, I.; Sohn, D.; Hesp, S. A. M.; *J. Transportation Res. Board, Transportation Res. Rec.* **2007,** *1998(1)*, 47.

(38) Petersen, J. C. *J. Transportation Res. Board, Transportation Res. Rec* **1984**; , 13.

(39) Anderson, D. A.; Marasteanu, M. O. *J. Transportation Res. Board, Transportation Res. Rec.***1999,** *1661*, 27.

(40) Bahia, H. U. Low Temperature Isothermal Physical Hardening of Asphalt Cements. PhD. Pennsylvania State University, State Collage, PA, 1991.

(41) Lu, X.; Soenen, P.; Redelius, P. In i*mpact of Bitumen Wax on Asphalt Performance Low-Temperature Cracking;* Proceeding of the Third Eurobitumen & Eurasphalt Congress; Vieena, Ausria, May12-14,2004; Vol. Paper50, Section 4.

(42) Hesp, S. A. M.; Iliuta, S.; Shirokoff, J. W. *Energy & Fuels.* **2007,** *21(2),* 1112.

(43) Van der Poel, C. *J. App. Chem.* **1954,** *4*, 221.

(44) Kramers, H. *Rescoconto del Gongresso dei Fisici* **1927,** *3*, 35.

(45) Schwarzl, F.; Staverman, A. J. *J. Appl. Phys.* **1952,** *23*, 835.

(46) Ferry, J. D. In *Viscoelastic Properties of Polymers;* John Wiley & Sons: New York, 1980.

(47) Pink, H. S.; Merz, R. E.; Bosniack, D. S. **1** *Proc. Assoc. Asphalt Paving Technol* **1980,** *49*, 64.

(48) Goodrich, J. L. *Proc. Assoc. Asphalt Paving Technol.* **1988,** *57*, 116.

(49) Airy, G. D.; brown, S. F. *J. Assoc. Asphalt Paving Technol.* **1998,** *67*, 66.

(50) Petersen, J. C.; Robertson, R. E.; Branthaver, J. E.; Harnsberger, P. M.; duval, J. J.; kim, S. S.; Anderson, D. A.; Christiansen, D. W.; Bahia, H. U.; Dongre, R.; Antle, C. E.; Sharma, M. G.; Button, J. W.; Glover, R. *Binder Characterization and Evaluation* **1994,** *4*, Test methods, SHRP A-370.

(51) Bahia, H. U.; Zhai, H.; Bonnetti, K., Kose, S. *J. Assoc. Asphalt Paving Technol* **1999,** *68*, 1.

(52) Anderson, D. A.; Le, H.; Marasteanu, M. O.; Planche, J.; Martin, D. *J. Transportation Res. Board, Transportation Res. Rec.* **2001,** 48-56.

(53) Shenoy, A. *J. Test. Eval.* **2002,** *30-4*, 303.

(54) Lesueur, D.; Gerard, J.; Claudy, P.; Letoffe, J.; Martin, D.; Planche, J. *J. Rheol.* **1998,** *42*, 1059.

(55) Partal, P.; Martínez-Boza, F.; Conde, B.; Gallegos, C. *Fuel.***1999,** *78*, 1.

(56) Eklind, H.; Maurer, F. H. J. *Polym. Networks Blends*. **1995,** *5*, 35.

(57) Van Gurp, M.; Palmen, J. *The Society of Rheology Newsletter.* **1998,** *67*, 5.

(58) Nakajima, N.; Harrell, E. R. In *Current Topics in Polymer Science, Volume II-Rheology and Polymer Processing/Multiphase Systems;* Utracki, L. A., Inoue, S., Eds.; Hanser: New York, 1987.

(59) Becker, M. Y.; Muller, A. J.; Rodriguez, Y. *J. Appl. Polym. Sci* . **2003,** *90*, 1772.

(60) Hesp, S. A. M.; Kodrat, I.; Scafe, D. A.; Soleimani, A.; Subramani, S.; Whitelaw, L. In *Rheological testing of asphalt cements recovered from a northern Ontario pavement trial;* Santagata, E., Ed.; Mairepav 6 Conference; Politecnico di Torino: Italy, 2009; Vol. 1, pp 84.

(61) Iliuta, S.; Andriescu, A.; Hesp, S. A. M.; Tam, K. K. In *Improved Approach to Low-Temperature and Fatigue Fracture Performance Grading of Asphalt Cements;* Proceedings of the Canadian Technical Asphalt Association; 2004; Vol. 49, pp 123-158.

(62) MeGennis, R. B.; Shuler, S.; Bahia, H. U. *"Background of Superpave® Asphalt binder Test Methods"Federal Highway Administration Publications SA-94-069.* **1994**.

(63) LTPPBind® Software,Version 2.1, Federal Highway Administration, McLean, Virginia, 1999.

(64) Baskin, C. M. *Ame. Soc. Test. Mater* **1935,** *Part II, 35*, 576.

(65) Shields, B. P.; Anderson, K. O. *Proc. Can. Tech. Asphalt. Assoc.* **1964,** *IX*, 209.

(66) Rader, L. F.; Ochalek, R. T. *In A Proposed Method for Testing the Physical Properties of Asphalt Paving Mixtures at Low Temperatures Los Angeles;* Symposium on the Science of Asphalt in Construction, Division of Petroleum Chemistry, American Chemical Society; Los Angeles, 1971; pp D126-D135.

(67) Van de Ven, M. F. C.; Van Assen, E. J. , *Review of the South African Bitumen Specification to Take Cognisance of Compositional Balance Relative to Long Term Behaviour,CR-96/034, CSIR, Pretoria,March 1996*.

(68) Isacsson, U.; Zeng, H. *J. Mater. Sci.***1998,** *33*, 2165.

(69) Barth, E. J. In *Asphalt Science and Technology;* Gordon Breach Science Publishers: 1962.

(70) Yee, P.; Aida, B.; Hesp, S. A.,M.; Marks, P.; Tam, K. K. *J. Transportation Res. Board, Transportation Res. Rec*, **2006,** *1962*, 44-51.

(71) Zhao, M. O.; Hesp, S. A. M. *Int. J. Pavement Eng* **2006,** *3*, 199.

(72) Villaneuva, A.; Zanzotto, L. *Can. J. Civ. Eng.* **2008,** *35*, 148.

Appendix1. Section 655-4, 655-6 Torsion Bar 1hr and 24hr Cooling at -20ºC Field Aged

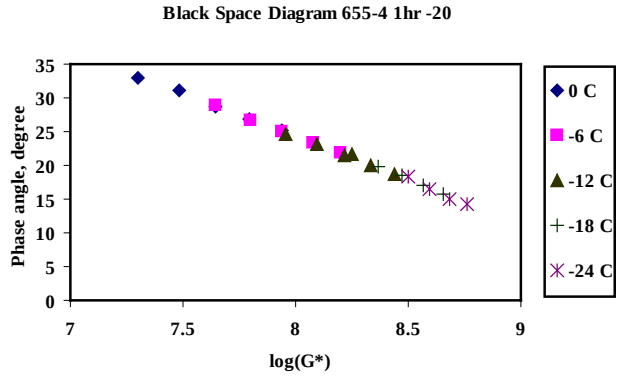

Figure 1. Black Space Diagram 655-4 1hr -20ºC

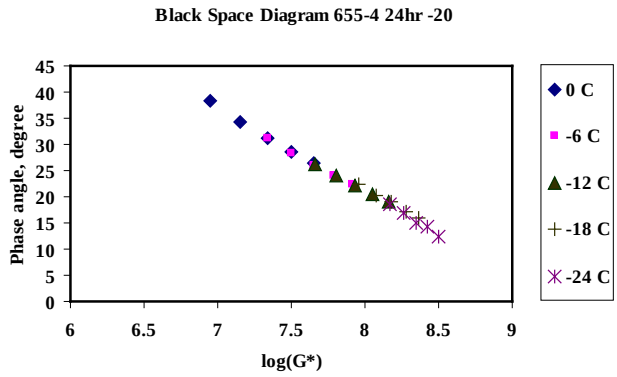

Figure 2. Black Space Diagram 655-4 1hr -20ºC

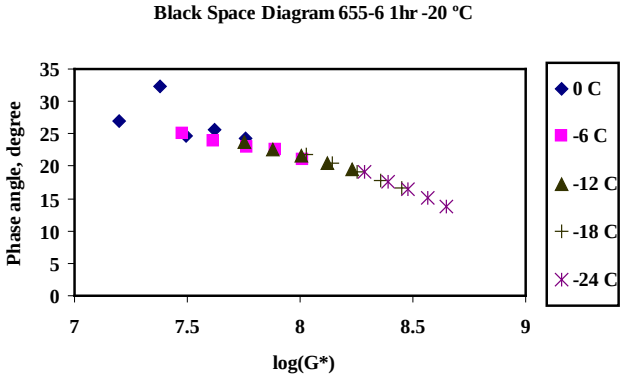

Figure 3. Black Space Diagram 655-6 1hr -20ºC

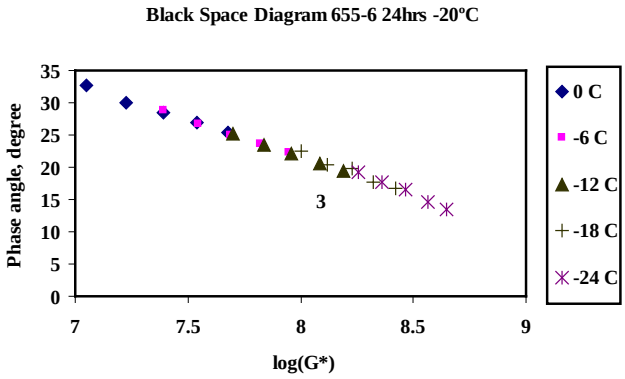

Figure 4. Black Space Diagram 655-6 1hr -20ºC

Appendix 2. Section 655-7 Torsion Bar 1hr and 24hr Cooling at -20ºC Field Aged

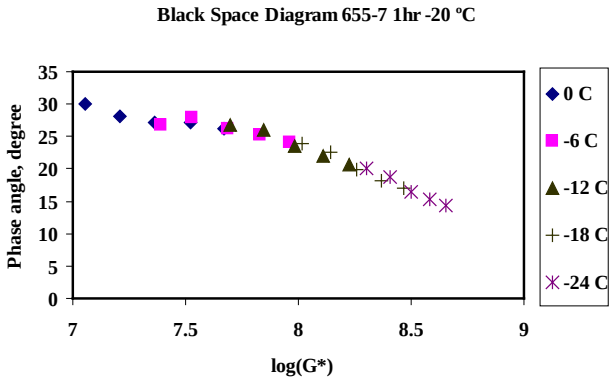

Figure 1. Black Space Diagram 655-7 1hr -20ºC

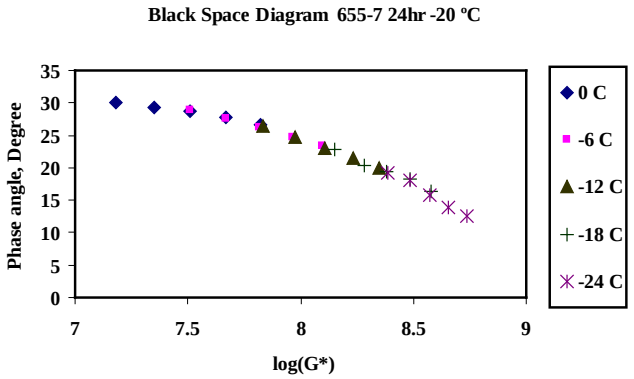

Figure 2. Black Space Diagram 655-7 1hr -20ºC

Appendix3. Section 655-2, 655-3 Torsion Bar 1hr and 24hr Cooling at -20ºC Field Aged

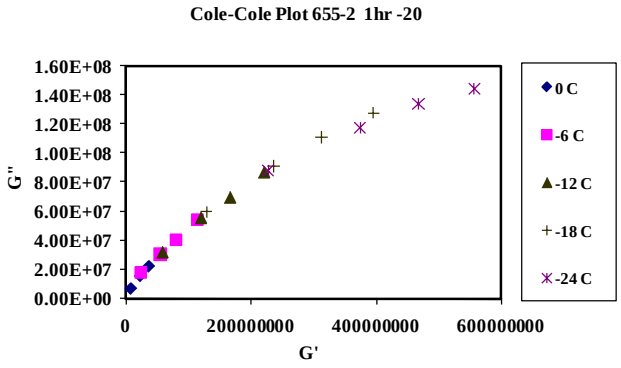

Figure 1. Cole-Cole Plot 655-2 24hr -20ºC

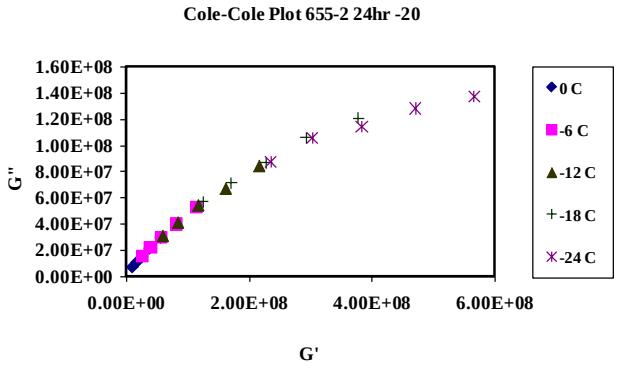

Figure 2. Cole-Cole Plot 655-2 24hr -20ºC

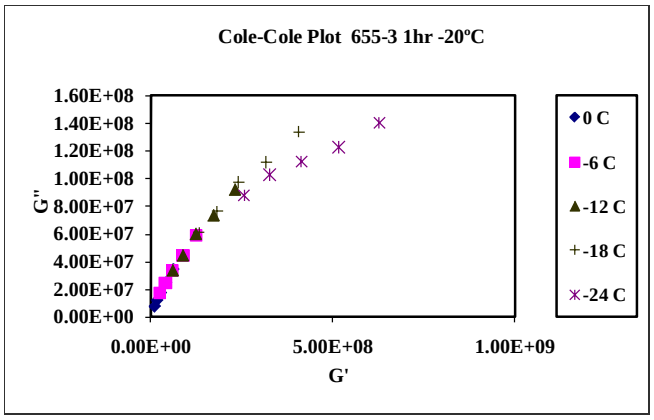

Figure 3. Cole-Cole Plot 655-3 1hr -20ºC

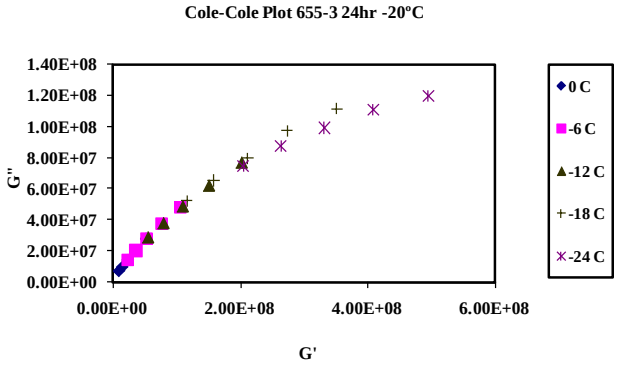

Figure 4. Cole-Cole Plot 655-3 24hr -20ºC

Appendix4. Section 655-6, 655-7 Torsion Bar 1hr and 24hr Cooling at -20ºC Field Aged

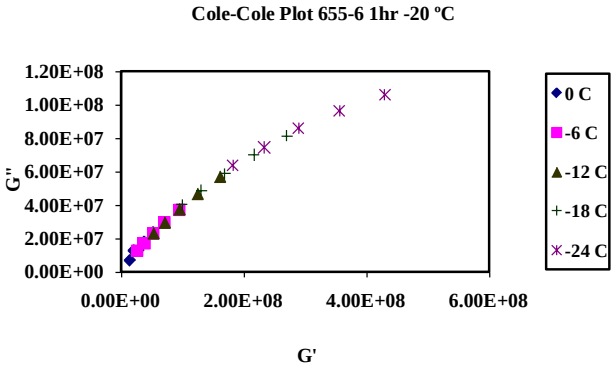

Figure 3. Cole-Cole Plot 655-6 1hr -20ºC

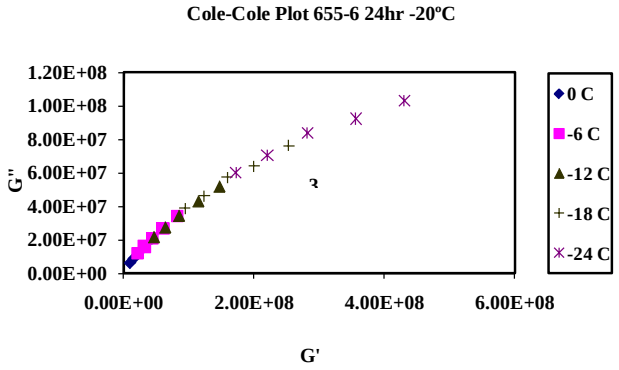

Figure 3. Cole-Cole Plot 655-6 24hr -20ºC

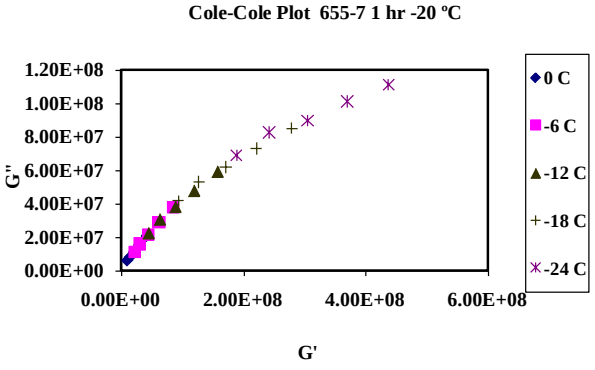

Figure 3. Cole-Cole Plot 655-7 1hr -20ºC

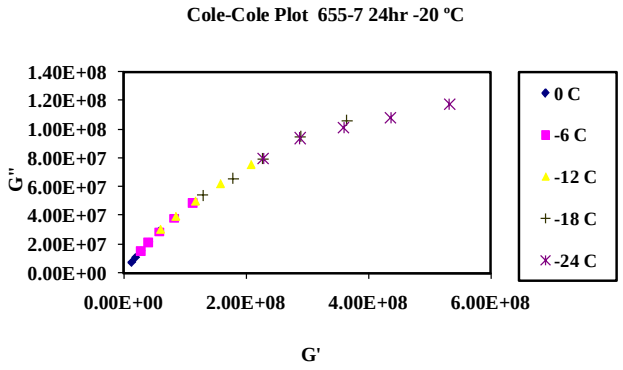

Figure 3. Cole-Cole Plot 655-7 24hr -20ºC

Appendix 5. Section 655-4 Torsion Bar 1hr and 24hr Cooling at -20ºC Field Aged

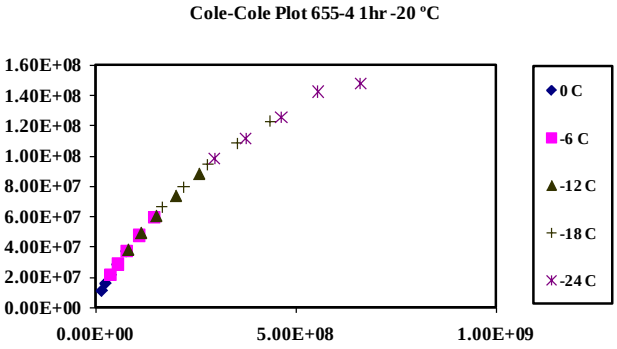

Figure 3. Cole-Cole Plot 655-4 1hr -20ºC

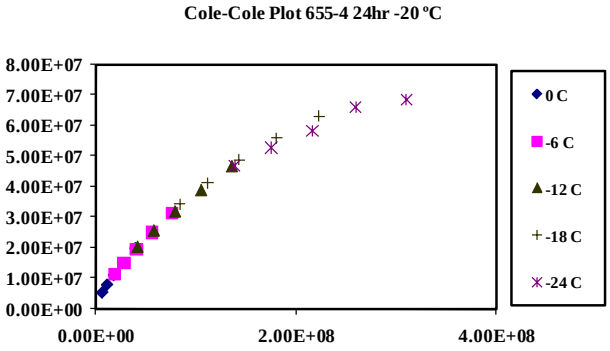

Figure 3. Cole-Cole Plot 655-4 24hr -20ºC

Appendix 6. Section 655-1 Compiled Torsion Bar 24hr -20ºC and Parallel Plate Field Aged

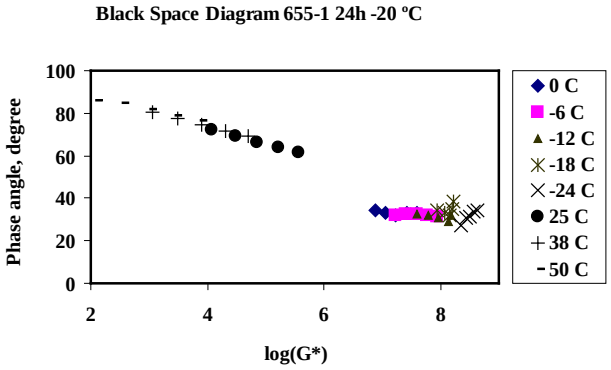

Figure 1. Black Space Plot 655-1

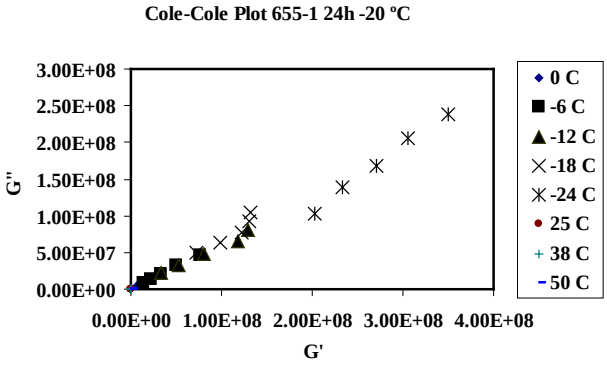

Figure 2. Cole-Cole Plot 655-1

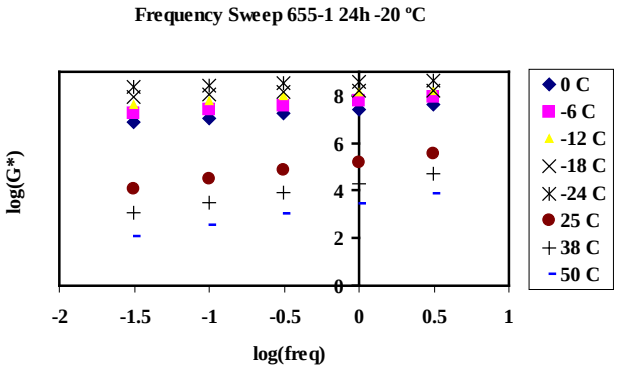

Figure 3. Phase Angle 655 -1

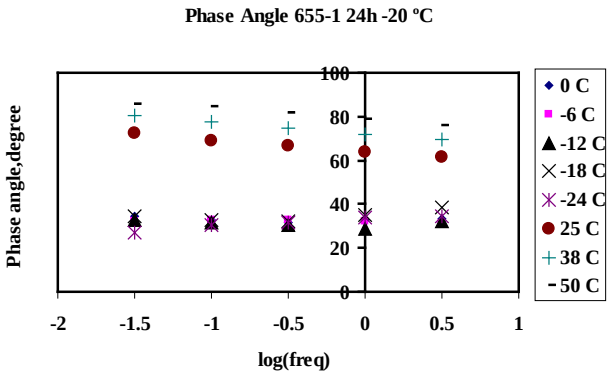

Figure 4. Phase Angle 655 -1

Appendix 7. Section 655-1, 655-2 Compiled Torsion Bar 24hr -20ºC and Parallel Plate Field Aged

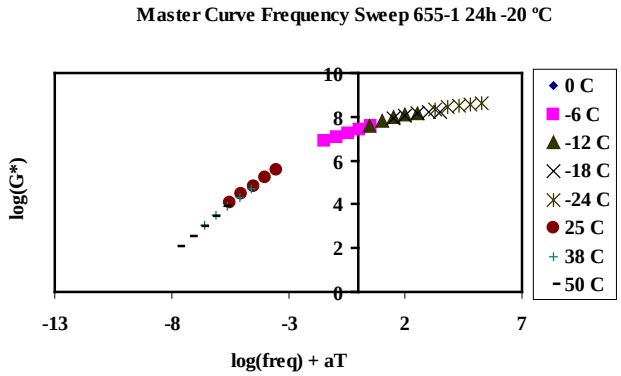

Figure 1. Master Curve Frequency Sweep 655-1

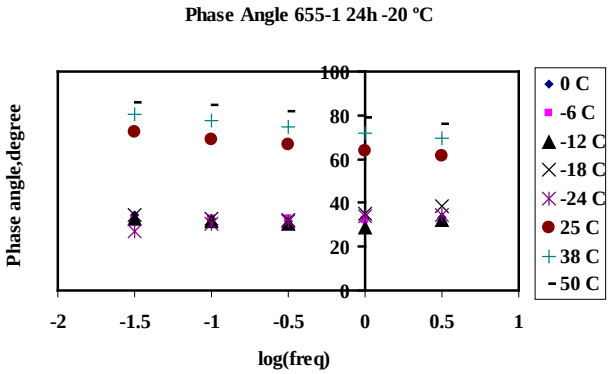

Figure 2 Phase Angle 655-1

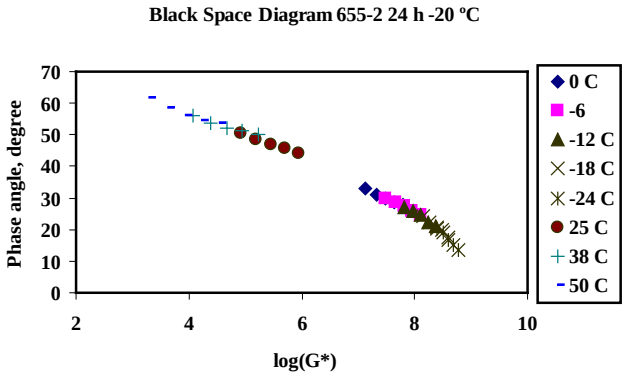

Figure 3. Black Space Diagram 655-2

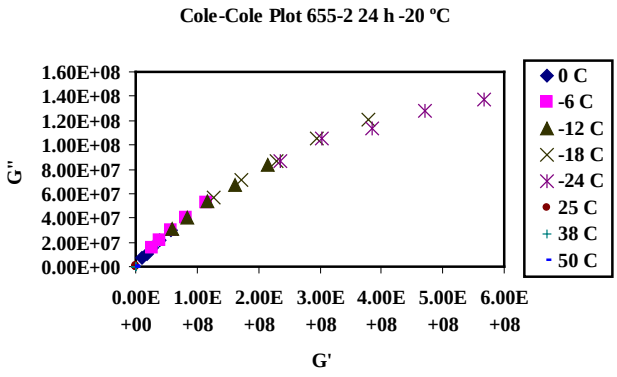

Figure 4. Cole-Cole Plot 655-2

Appendix 8. Section 655-2 Compiled Torsion Bar 24hr -20ºC and Parallel Plate Field Aged

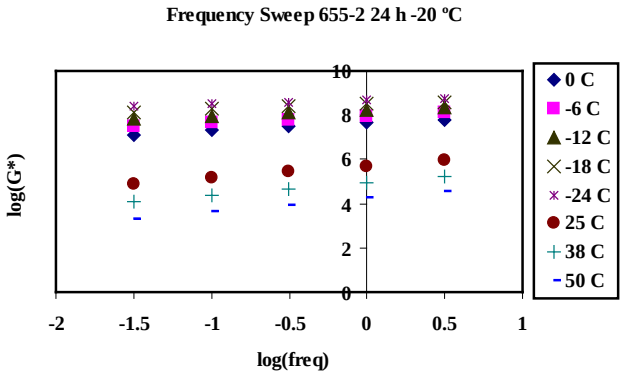

Figure 1. Frequency Sweep 655-2

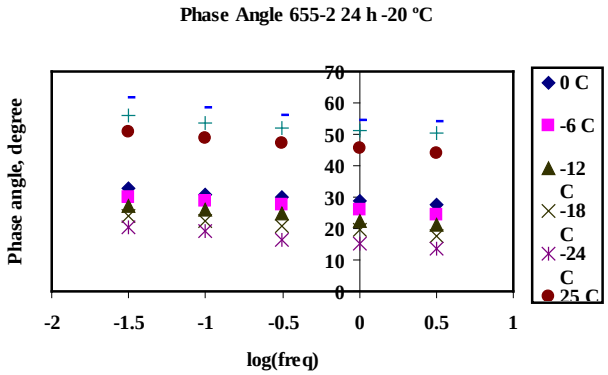

Figure 2. Phase Angle 655 -2

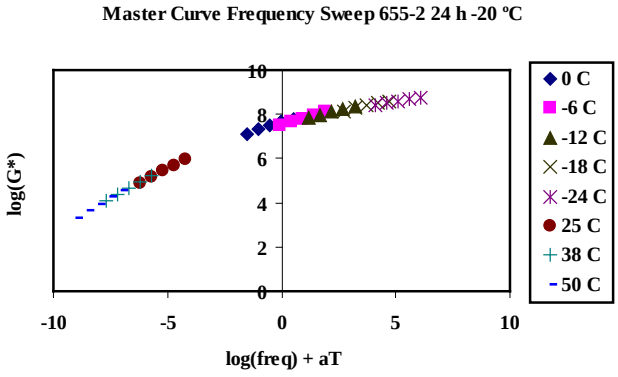

Figure 3. Master Curve Frequency Sweep 655-2

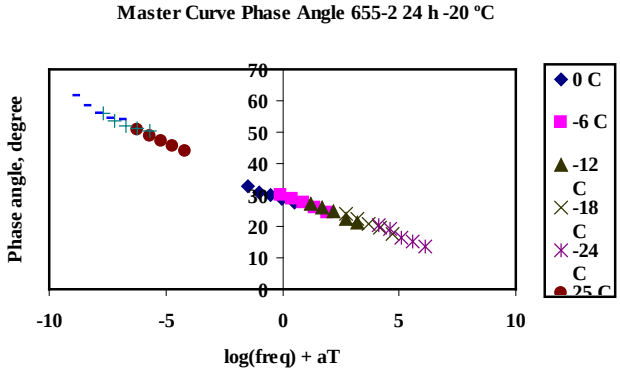

Figure 4. Master Curve Phase Angle 655 -2

Appendix 9. Section 655-3 Compiled Torsion Bar 24hr -20ºC and Parallel Plate Field Aged

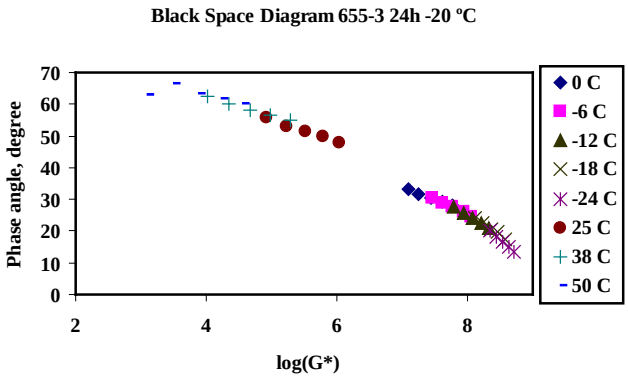

Figure 1. Black Space Diagram 655-3

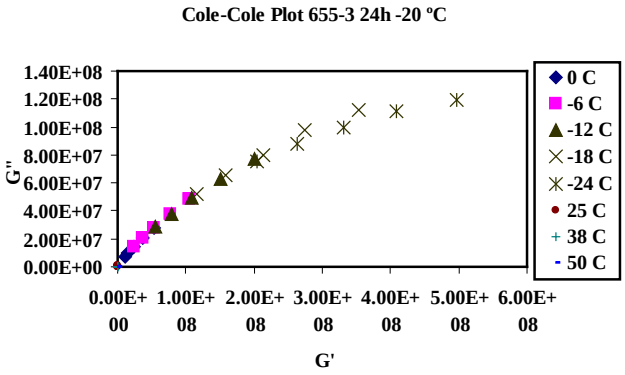

Figure 2. Cole-Cole Plot 655-3

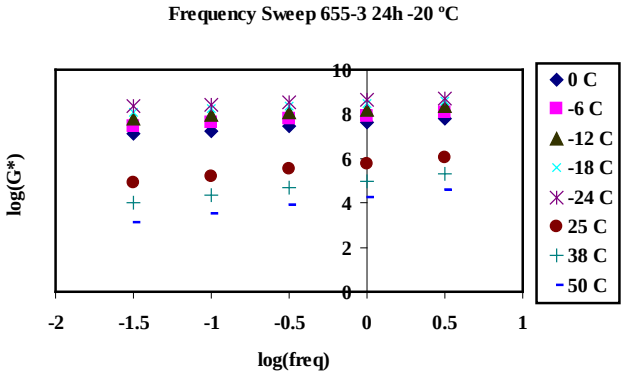

Figure 3. Frequency Sweep 655-3

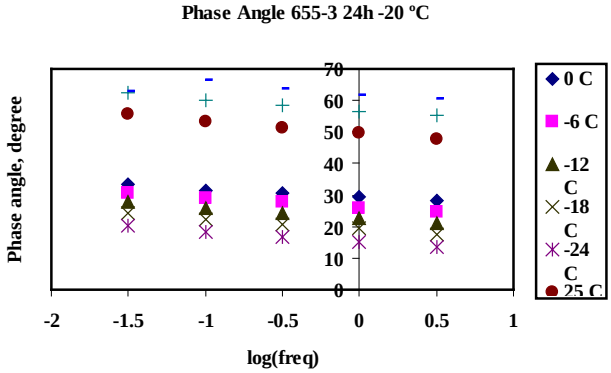

Figure 4. Phase Angle 655 -3

Appendix 10. Section 655-3, 655-4 Compiled Torsion Bar 24hr -20ºC and Parallel Plate Field Aged

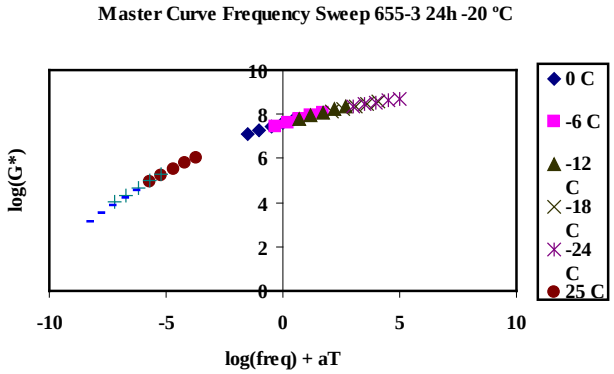

Figure 1. Master Curve Frequency Sweep 655-3

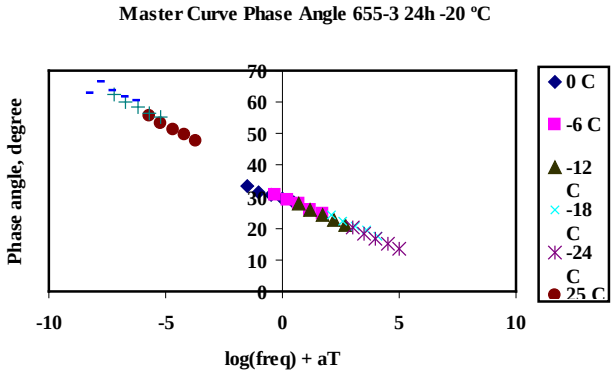

Figure 2. Master Curve Phase Angle 655 -3

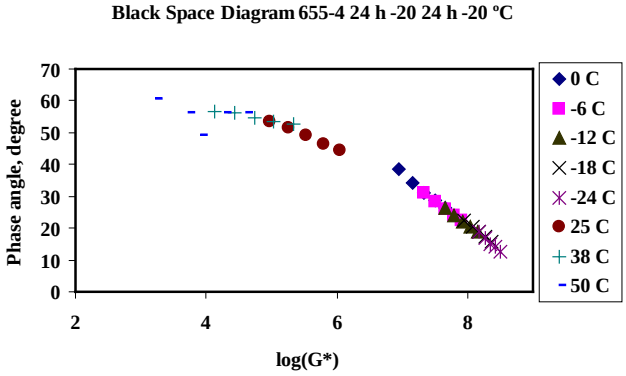

Figure 3. Black Space Diagram 655-4

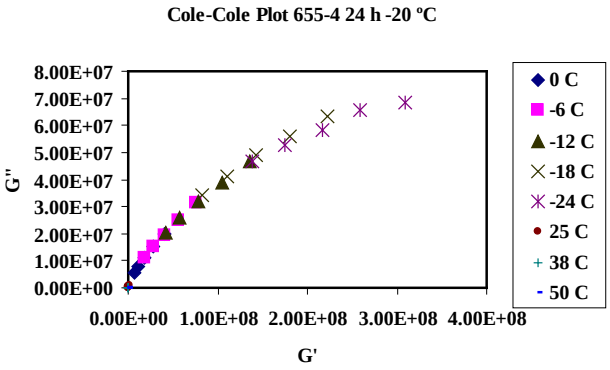

Figure 4. Cole-Cole Plot 655-4

Appendix 11. Section 655-4 Compiled Torsion Bar 24hr -20ºC and Parallel Plate Field Aged

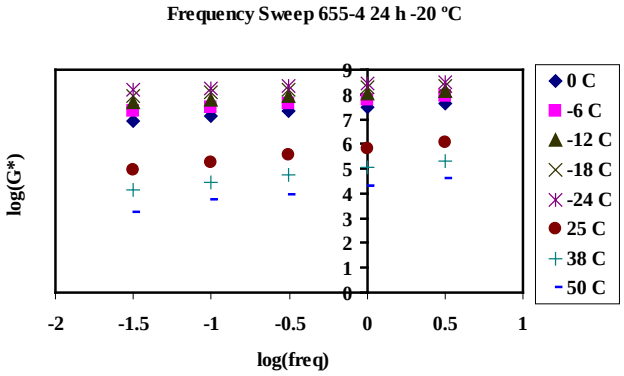

Figure 1. Frequency Sweep 655-4

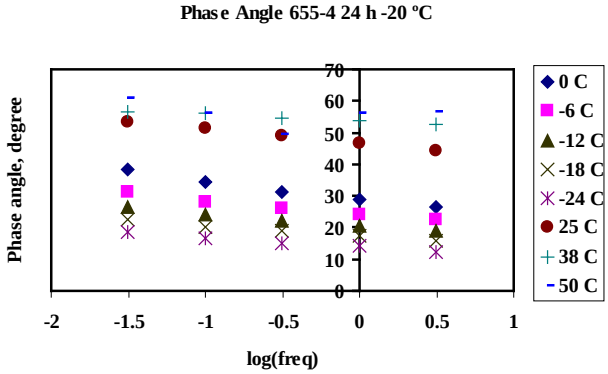

Figure 2. Phase Angle 655-4

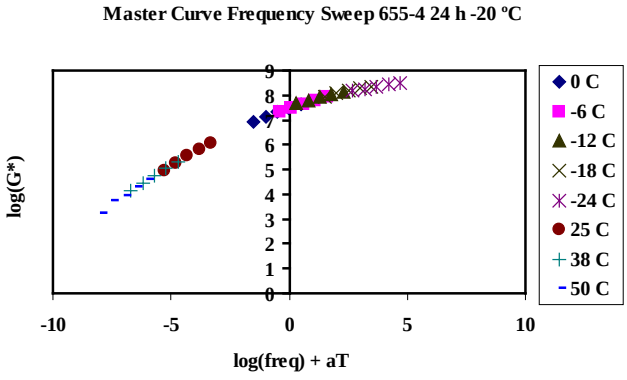

Figure 3. Master Curve Frequency Sweep 655-4

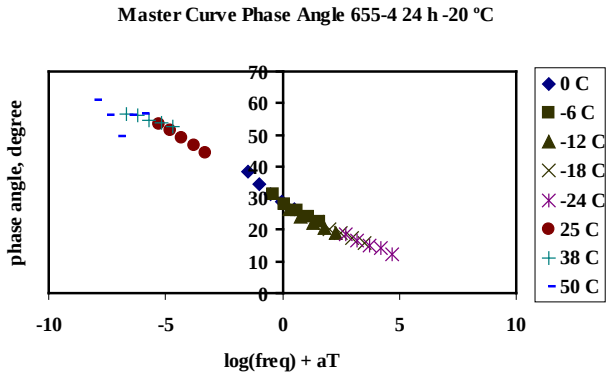

Figure 4. Master Curve Phase Angle 655-4

Appendix 12. Section 655-5 Compiled Torsion Bar 24hr -20ºC and Parallel Plate Field Aged

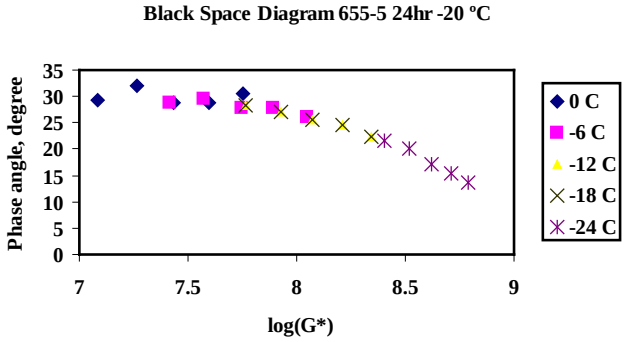

Figure 1. Black Space Diagram 655-5

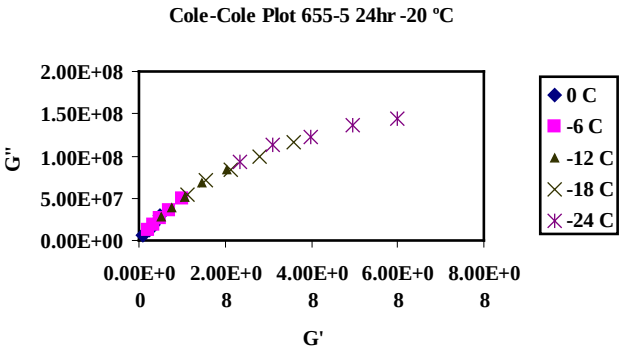

Figure 2. Cole-Cole Plot 655-5

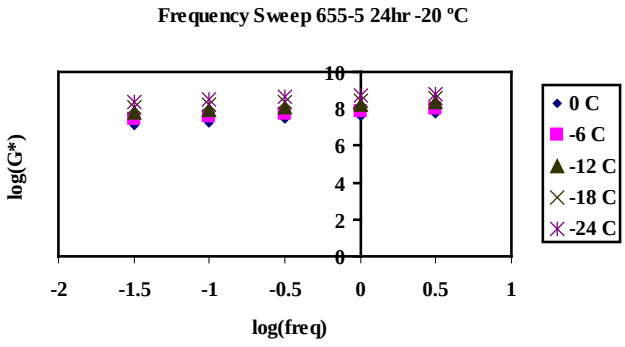

Figure 3. Frequency Sweep 655-5

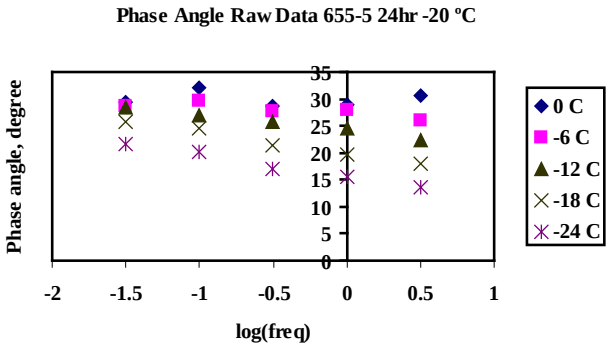

Figure 4. Phase Angle 655-5

Appendix 13. Section 655-5, 655-6 Compiled Torsion Bar 24hr -20ºC and Parallel Plate Field Aged

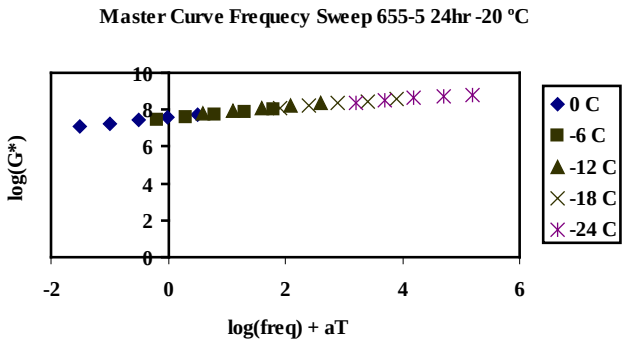

Figure 1. Master Curve Frequency Sweep 655-5

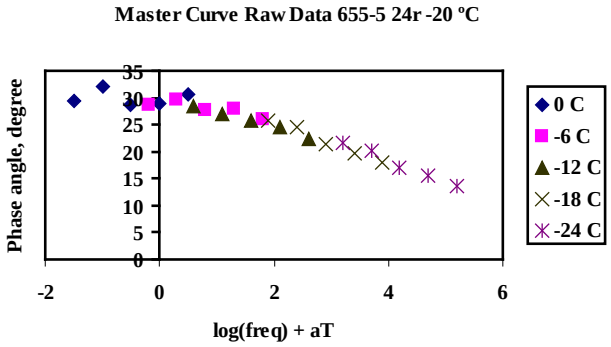

Figure 2. Master Curve Phase Angle 655-5

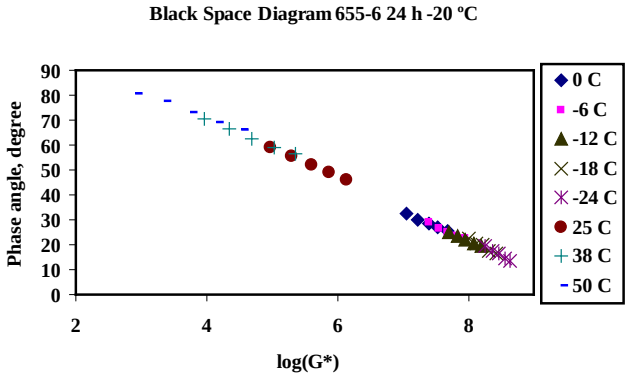

Figure 3. Black Space Diagram 655-6

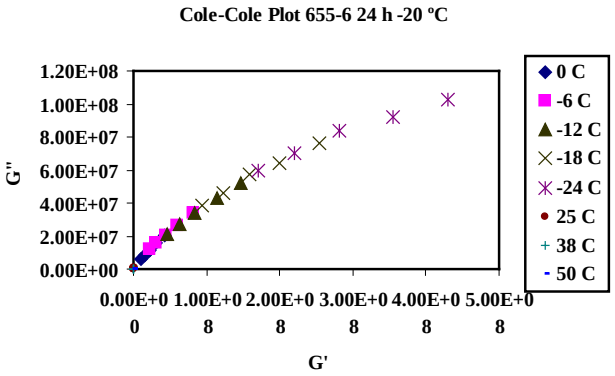

Figure 4. Cole-Cole Diagram 655-6

Appendix 14. Section 655-6 Compiled Torsion Bar 24hr -20ºC and Parallel Plate Field Aged

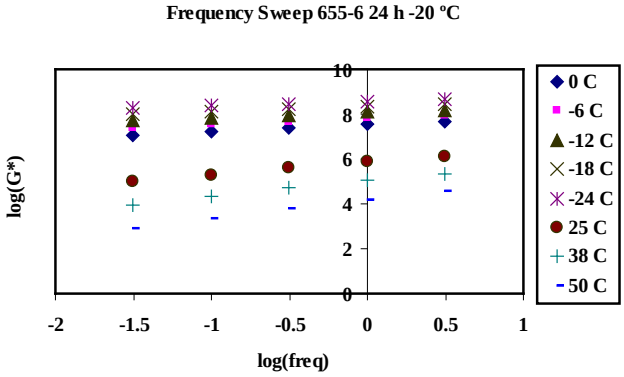

Figure 1. Frequency Sweep 655-6

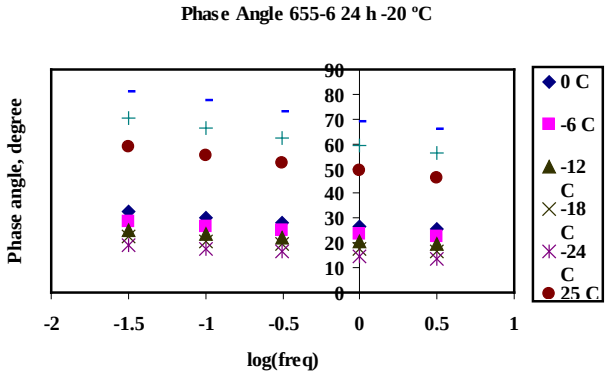

Figure 2. Phase angle 655-5

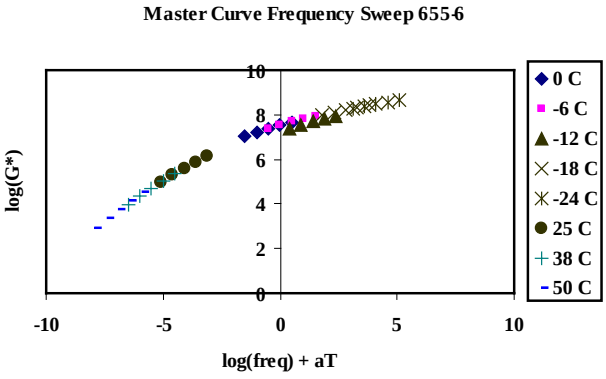

Figure 3. Master Curve Frequency Sweep 655-6

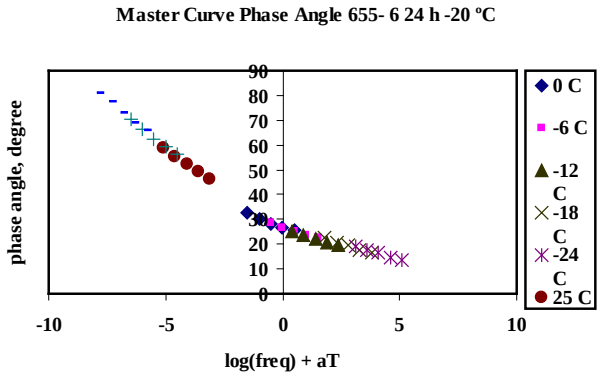

Figure 4. Master Curve Phase Angle 655-6

Appendix 15. Section 655-7 Compiled Torsion Bar 24hr -20ºC and Parallel Plate Field Aged

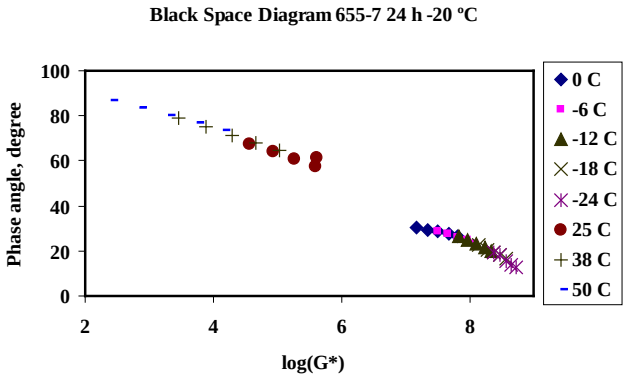

Figure 1. Black Space Diagram 655-7

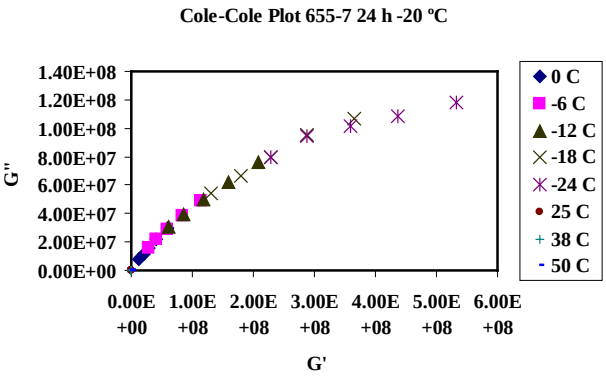

Figure 2. Cole-Cole Diagram 655-7

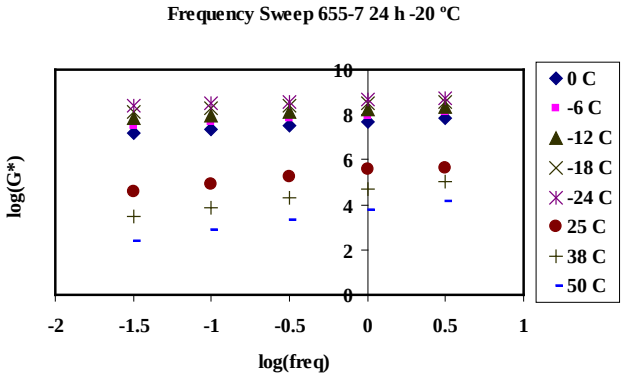

Figure 3. Frequency Sweep 655-7

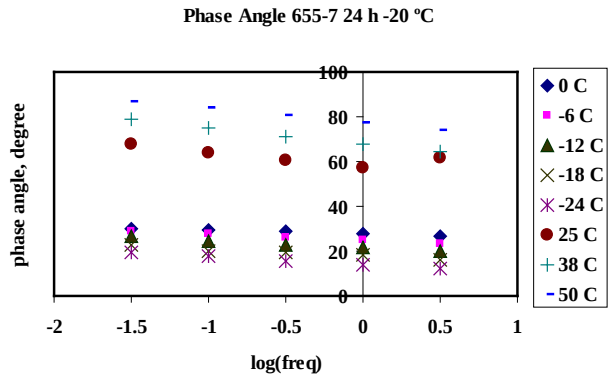

Figure 4. Phase angle 655-7

Appendix 16. Section 655-7 Compiled Torsion Bar 24hr -20ºC and Parallel Plate Field Aged

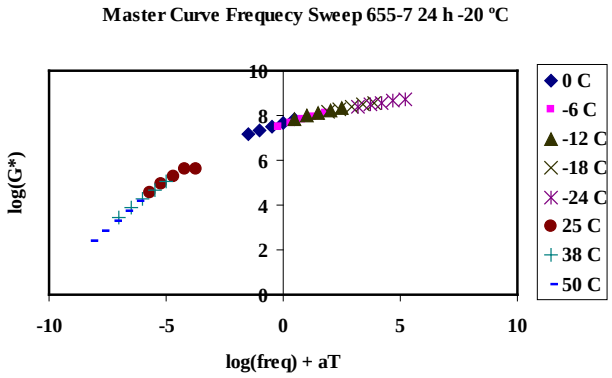

Figure 1. Master Curve Frequency Sweep 655-7

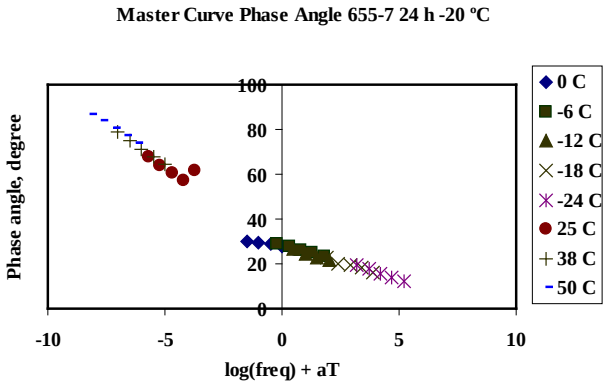

Figure 2. Master Curve Phase Angle 655-7

Appendix 17. Black Space Diagrams Laboratory Aged

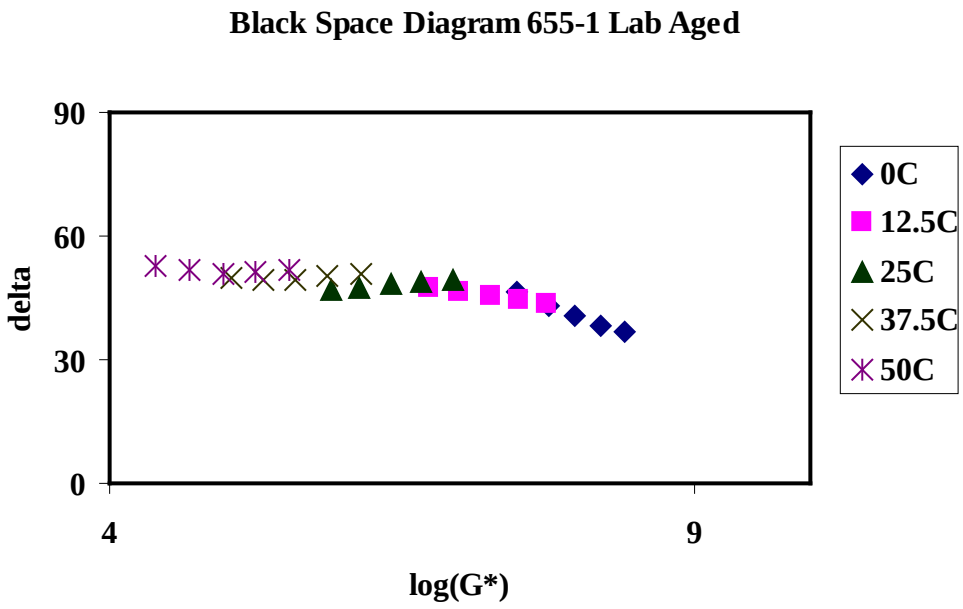

Figure 1. Black Space Diagram 655-1 Lab Aged

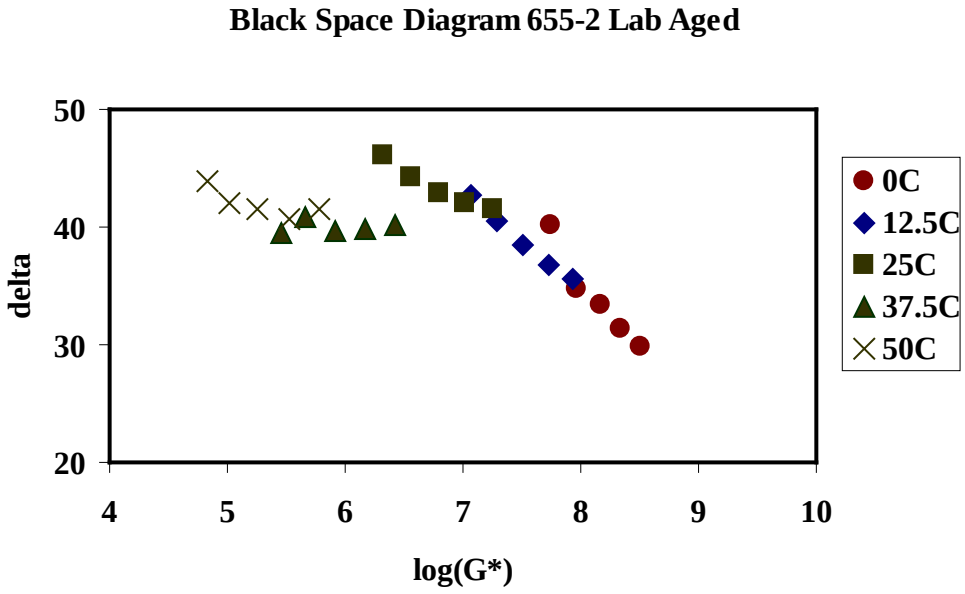

Figure 2. Black Space Diagram 655-2 Lab Aged

Appendix 18. Black Space Diagrams Laboratory Aged

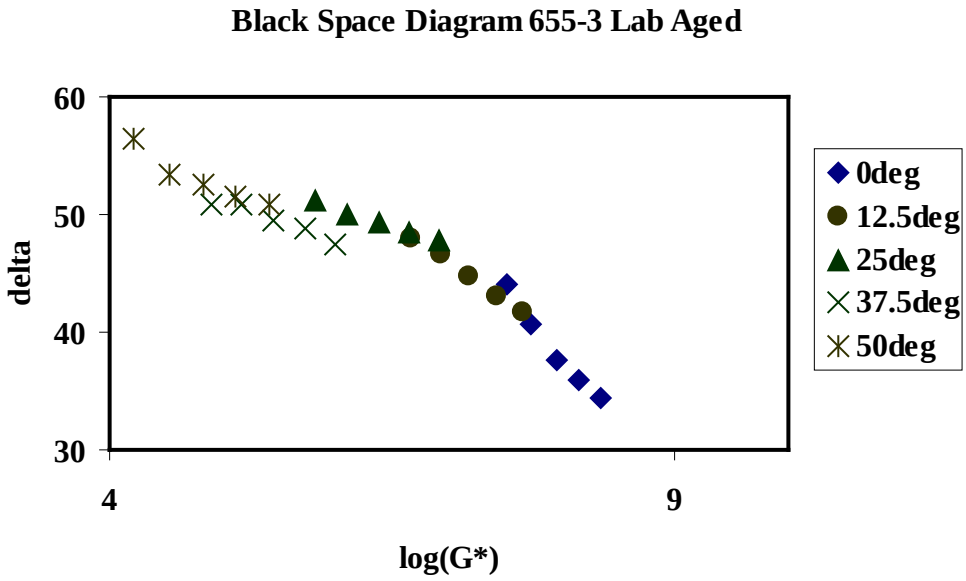

Figure 1. Black Space Diagram 655-3 Lab Aged

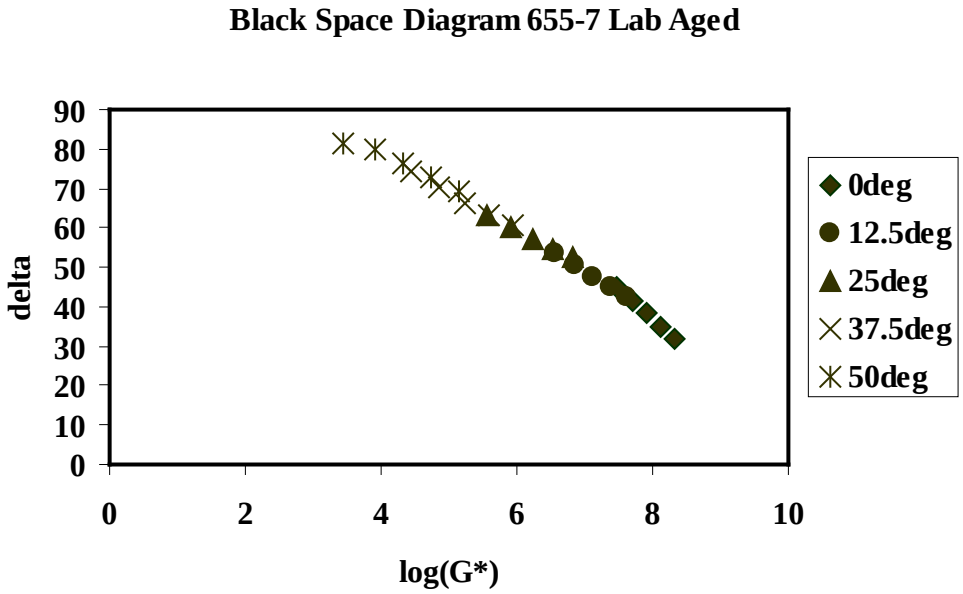

Figure 2. Black Space Diagram 655-4 Lab Aged

Appendix 19. Black Space Diagrams Laboratory Aged

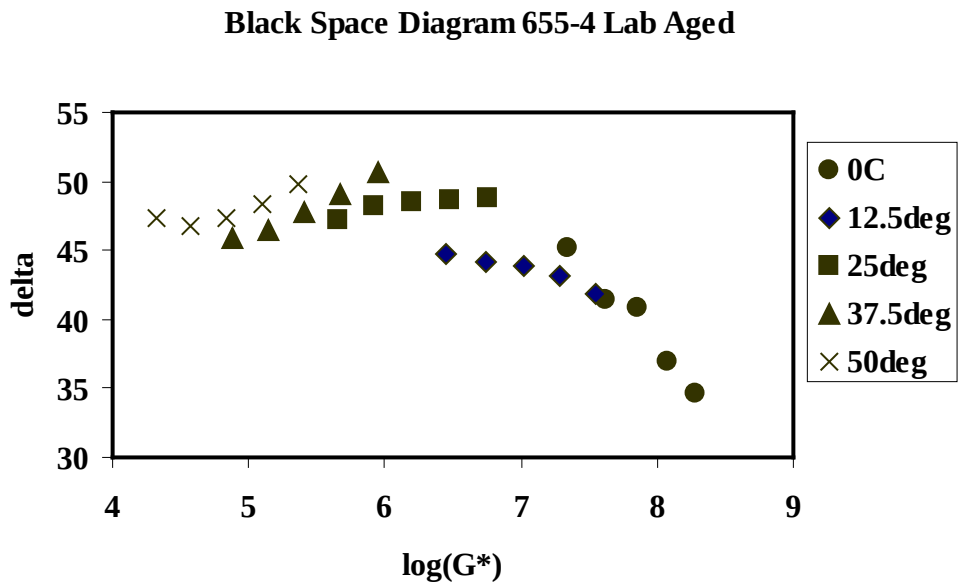

Figure 1. Black Space Diagram 655-5 Lab Aged

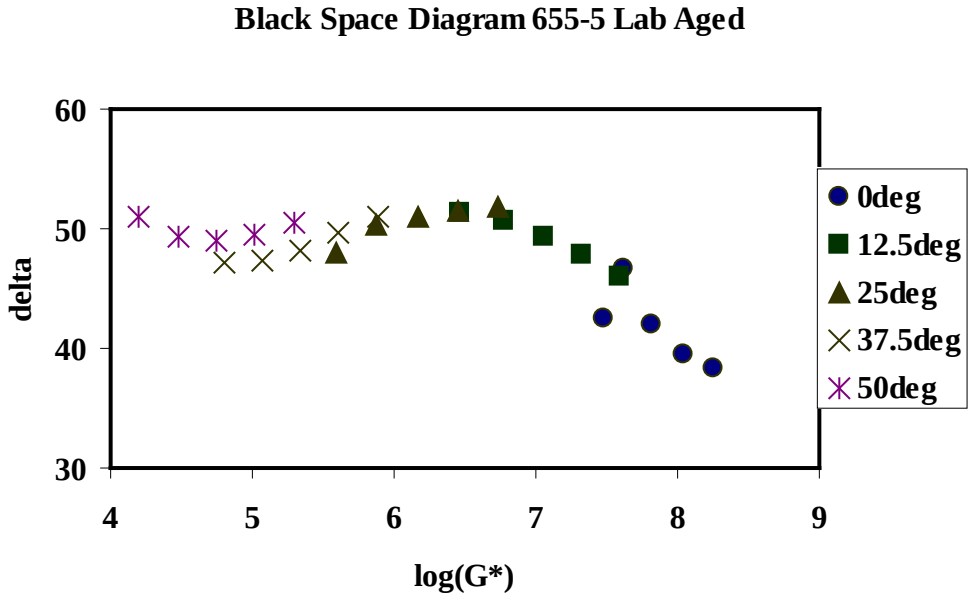

Figure 2. Black Space Diagram 655-6 Lab Aged

Appendix 20. Black Space Diagrams Laboratory Aged

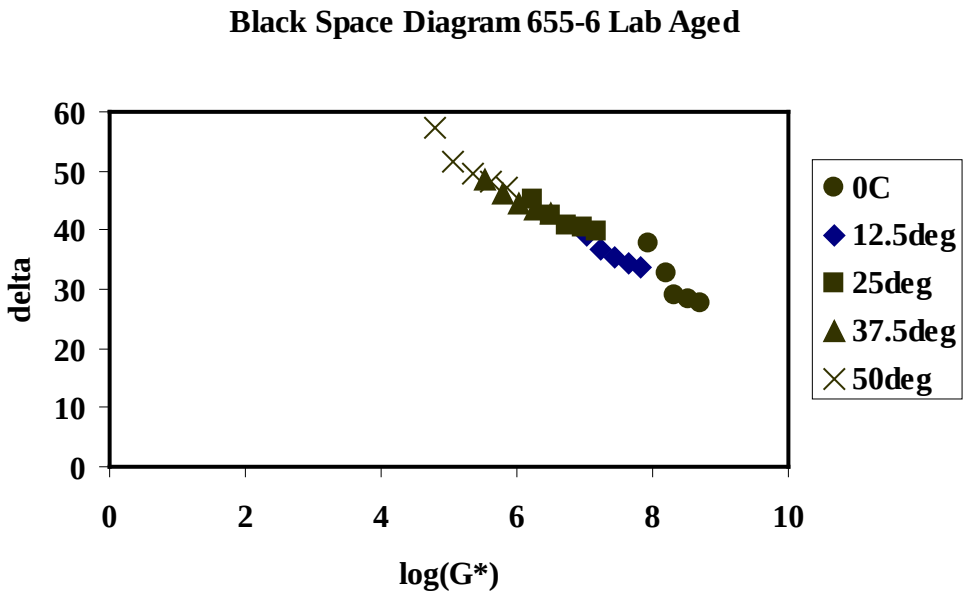

Figure 1. Black Space Diagram 655-7 Lab Aged

Appendix 21. Master Curve Frequency Sweep Plot Laboratory Aged

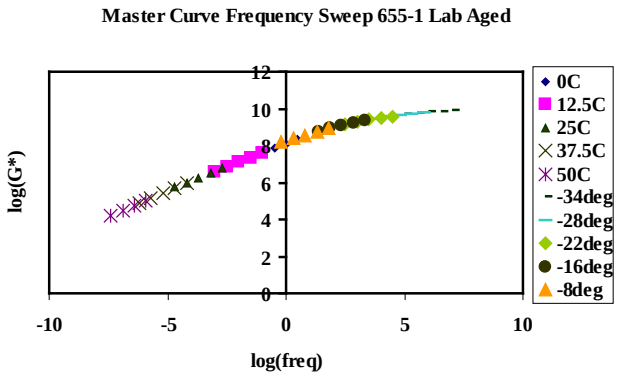

Figure1. Master Curve Frequency Sweep 655-1 Lab Aged

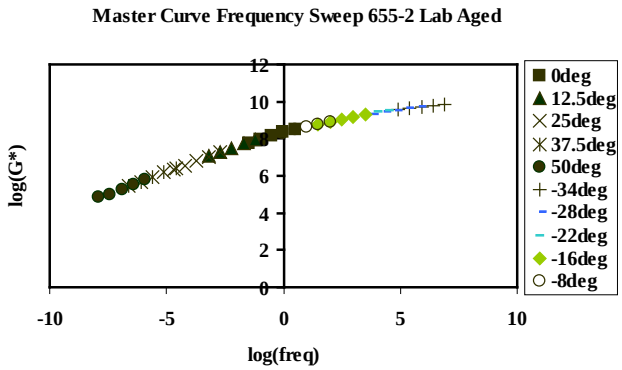

Figure2. Master Curve Frequency Sweep 655-2 Lab Aged

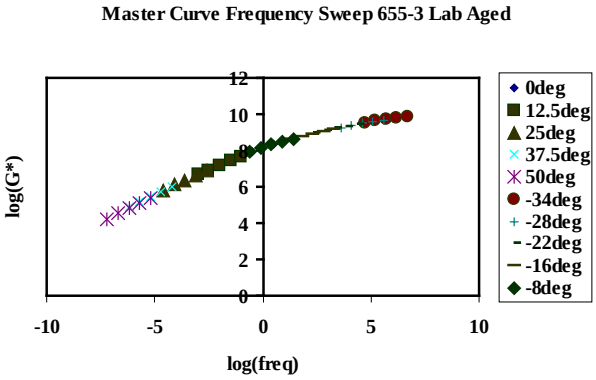

Figure3. Master Curve Frequency Sweep 655-3 Lab Aged

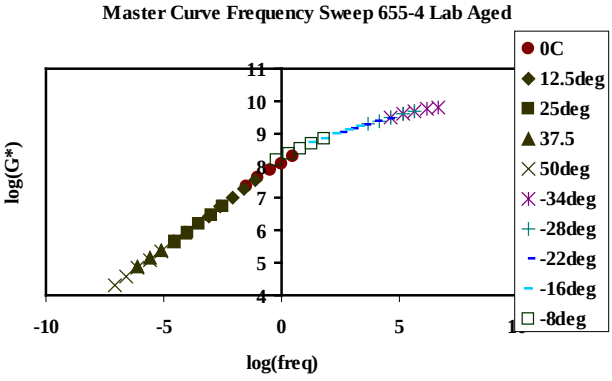

Figure 4. Master Curve Frequency Sweep 655-4 Lab Aged

Appendix 22. Master Curve Frequency Sweep Plot Laboratory Aged

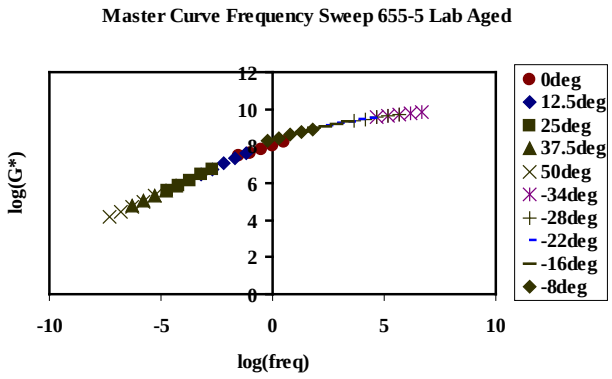

Figure1. Master Curve Frequency Sweep 655-5 Lab Aged

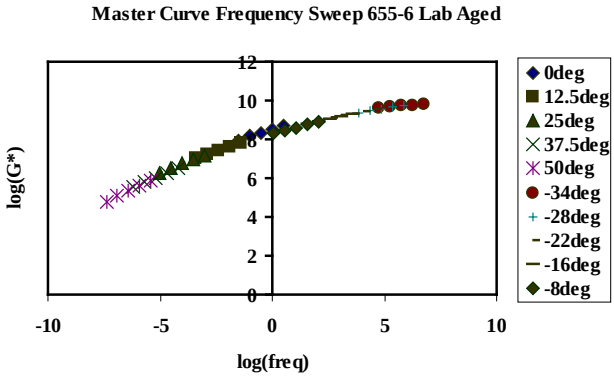

Figure2. Master Curve Frequency Sweep 655-6 Lab Aged

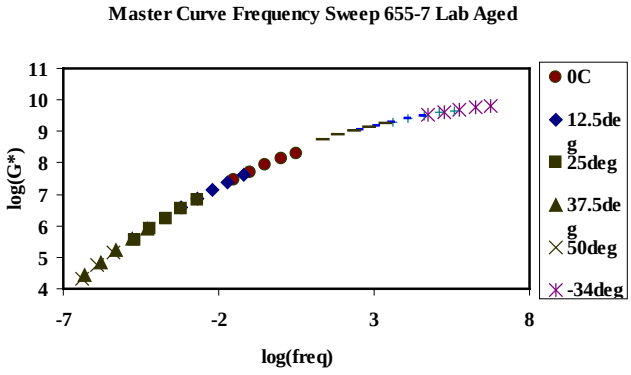

Figure3. Master Curve Frequency Sweep 655-7 Lab Aged

Appendix 23. Black Space Diagram and Cole-Cole Plot at 0ºC, and 25ºC Laboratory Aged

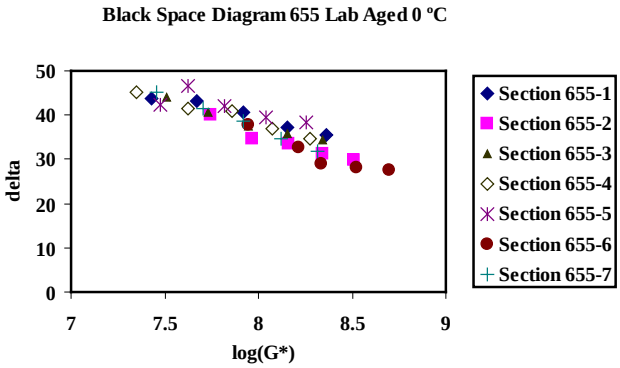

Figure 1. Black Space Diagram at 0ºC Lab Aged

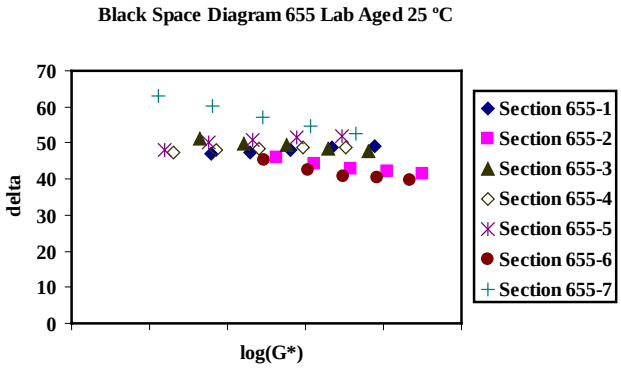

Figure 2. Black Space Diagram at 25ºC Lab Aged

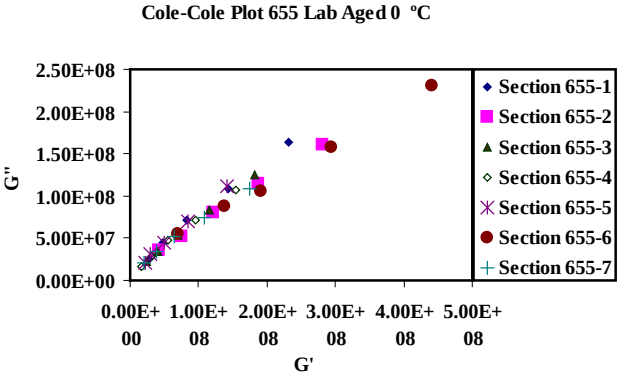

Figure 3. Cole-Cole Plot at 0ºC Lab Aged

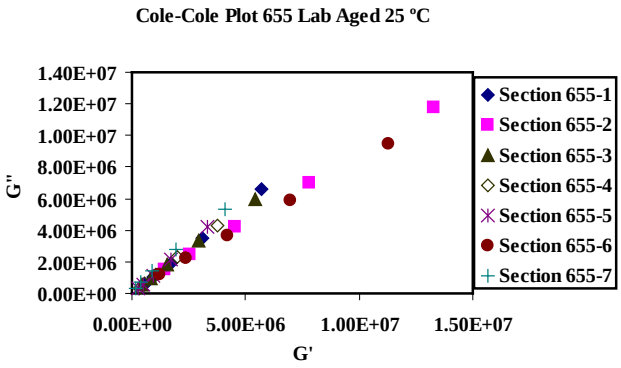

Figure 4. Cole-Cole Plot at 25ºC Lab Aged

Appendix 24. End Result Specification Findings

Table 1. End Result Specification Findings

Section	AC %	Voids %		Pavement Thickness, mm
		Plate	In Situ	
655-1	4.81	5.6	7.7	92.0
655-2	4.95	4.6	7.6	88.7
655-3	4.85	4.3	7.1	86.3
655-4	4.80	4.7	6.3	86.3
655-5	4.92	4.3	7.6	91.0
655-6	4.85	4.0	6.2	85.4
655-7	4.82	4.3	5.5	98.7
AVE ± SD	4.9 ± 0.1	4.5 ± 0.5	6.9 ± 0.9	89.8 ± 4.7